

R-05-26

Statistical model of fractures and deformations zones for Forsmark

Preliminary site description Forsmark area – version 1.2

Paul R La Pointe, Golder Associate Inc

Isabelle Olofsson, Jan Hermanson
Golder Associates AB

April 2005

Svensk Kärnbränslehantering AB

Swedish Nuclear Fuel
and Waste Management Co
Box 5864
SE-102 40 Stockholm Sweden
Tel 08-459 84 00
+46 8 459 84 00
Fax 08-661 57 19
+46 8 661 57 19



ISSN 1402-3091

SKB Rapport R-05-26

Statistical model of fractures and deformations zones for Forsmark

Preliminary site description Forsmark area – version 1.2

Paul R La Pointe, Golder Associate Inc

Isabelle Olofsson, Jan Hermanson
Golder Associates AB

April 2005

This report concerns a study which was conducted for SKB. The conclusions and viewpoints presented in the report are those of the authors and do not necessarily coincide with those of the client.

A pdf version of this document can be downloaded from www.skb.se

Executive summary

The following input data were available:

- Linked lineaments mapped over the regional model volume.
- Fracture data from outcrop mapping. Five outcrops all located inside the local model volume were available.
- Fracture data from 5 drilled boreholes and 19 percussion boreholes. All the drilled boreholes and 17 of the percussion boreholes are located inside the local model volume.

The DFN model is a “module” of the geological framework model and is developed in parallel with the deformation zone (DZ) model. The DFN model aims to describe the stochastic fractures. The output data are the geometrical properties of fractures with estimates of fracture orientation, radius distribution (size), spatial distribution and fracture intensity, and a preliminary conceptual framework that describes why and how these parameters vary throughout the site.

Open, partly open and sealed fractures are analysed separately for boreholes and outcrops. The sections identified as deformation zones in one-hole interpretation were removed from the data sets before analysis for the DFN model. In order to take into account the discrepancy of data quality offshore/onshore from the lineament mapping, only lineaments onshore were used for the DFN analysis.

One DFN conceptual model has been developed for Forsmark. Four sub-vertical fracture sets and one sub-horizontal set were identified from respectively outcrop and borehole data. For fractures in outcrops, the trace maps are also analysed in order to identify the relative chronology of the sets. The orientation of fracture sets is constant with depth, although within an individual borehole, certain sets may be present or absent over specific depth intervals. The sub-vertical fracture sets are regional lineament-related sets.

The spatial distribution model of fractures is estimated by the mass dimension calculation and through comparison of fracture intensity as a function of measured depth between the percussion boreholes. The estimates of mass dimension are given for each sub-vertical set for each outcrop. The parameters are Poissonian or in some cases show a very low fractal pattern. This is consistent with the very low correlation of fracture intensity among percussion boreholes. The patterns of zones of high and low intensity in boreholes are very difficult to trace to any other borehole, suggesting that spatial correlation is very low.

The fracture size for lineament-related sets is calculated through area-normalization of fracture trace lengths. The normalization method for Poissonian distribution models is Euclidian and directly relates the amount of fractures to the surface of the mapped area. The radius distribution estimates is Powerlaw and the parameters are given for the best fit. Upper and lower bounds are also provided in order to describe the variation of size for each fracture orientation set given the existing data. Data from outcrops and lineaments are used for the size distribution of the sub-vertical sets. The size distribution of subhorizontal fractures is very difficult to assess as the only source of information is outcrops which present a bias towards vertical fractures. Analyses of mineral fillings in subhorizontal fractures showed that epidote is identified in some fractures, which suggest that at least some of these fractures are old. In that sense the size distribution might be similar as the

one determined for the sub-vertical sets. Hence the area-normalization approach has also been applied for the sub-horizontal set using data from outcrops only. The parameters of the distribution are very similar to those obtained for the sub-vertical sets and might reinforce the hypothesis that these fractures are lineament-related as well.

Compared to version 1.1, a much larger amount of data especially from boreholes is available. Both one-hole interpretation and Boremap indicate the presence of high and low fracture intensity intervals in the rock mass. The depth and width of these intervals varies from borehole to borehole but these constant fracture intensity intervals are contiguous and present quite sharp transitions. There is not a consistent pattern of intervals of high fracture intensity at or near to the surface. In many cases, the intervals of highest fracture intensity are considerably below the surface. While some fractures may have occurred or been reactivated in response to surficial stress relief, surficial stress relief does not appear to be a significant explanatory variable for the observed variations in fracture intensity.

Data from the high fracture intensity intervals were extracted and statistical analyses were conducted in order to identify common geological factors. Stereoplots of fracture orientation versus depth for the different fracture intensity intervals were also produced for each borehole. Moreover percussion borehole data were analysed in order to identify the persistence of these intervals throughout the model volume.

The main conclusions of these analyses are the following:

- The fracture intensity is conditioned by the rock domain, but inside a rock domain intervals of high and low fracture intensity are identified.
- The intervals of high fracture intensity almost always correspond to intervals with distinct fracture orientations (whether a set, most often the NW sub-vertical set, is highly dominant, or some orientation sets are missing).
- These high fracture intensity intervals are positively correlated to the presence of first and second generation minerals (epidote, calcite).
- No clear correlation for these fracture intensity intervals has been identified between holes.

Based on these results the fracture frequency has been calculated in each rock domain for the different high and low fracture intensity intervals in order to capture the variation of this parameter in the model volume. The fracture intensity P_{32} has been derived by means of simulations for each rock domain and each fracture type, and is expressed as a mean value, and if possible standard deviation and span.

The uncertainty in the model has been quantified:

- for the different geometrical parameters by providing ranges of variations and studying relevant distribution models,
- by conducting sensitivity analysis on some input data: the effect of truncation of lineaments at the border of the regional model volume and the impact of truncation in outcrop mapping.

An alternative conceptual model is under study which is based on the identified deterministic deformation zones, and not on lineaments. An important issue using this model is the bias of information and the limited amount of structures.

The current DFN model still contains significant uncertainties which need to be resolved in order to be able to produce a final site DFN model. Three main issues are listed below:

- The definition of the subhorizontal fracture set in terms of geological processes and tectonics. The size distribution is a critical issue for the hydrogeology of the site.
- The variation of the fracture intensity by rock domain has been identified but the variation pattern and the spatial distribution within an individual domain are still sufficiently unpredictable that the fracture network permeability structure within a rock domain is uncertain from a conceptual perspective, not just a data uncertainty perspective. Moreover, many rock domains have not yet been sampled by boreholes or outcrops, and thus their fracture properties remain highly uncertain.
- Validation of the DFN models will require resolution of these two issues, and may also require the drilling of highly inclined or horizontal boreholes. Near-vertical boreholes and the mapping protocol to only map fracture traces in outcrop greater than 0.5 m make validation with the current data difficult. The scan line mapping data with a trace length truncation of only 0.2 m may provide qualitative support to smaller scale structures, but have not been analysed in this model version. However, scan line data does not provide substantial information on the spatial distribution of fractures and does not sample sub-horizontal fractures better than the outcrop data, neither does it invoke data from more rock domains.

Contents

1	Objectives and limitations	9
2	Data sources	11
2.1.1	Lineament data	11
2.1.2	Detailed fracture outcrop data	11
2.1.3	Borehole data	11
3	Software used	13
4	Modelling assumptions	15
4.1	Deformation zone model	15
4.2	Stochastic DFN model	15
4.2.1	Assumptions	15
5	Experimental procedures	17
5.1	Strategy for the analysis of the data for calculating the parameters for local site scale DFN model(s) for Forsmark 1.2	17
5.2	Set identification and orientation statistics	18
5.2.1	Set determination	18
5.2.2	Relation to lineaments	22
5.3	Size	22
5.3.1	Fracture sets not related to lineaments	22
5.3.2	Fracture sets related to lineaments	23
5.4	Intensity	27
5.4.1	Determination of geological controls on fracture intensity	28
5.5	Assessment of regional geological controls on fracturing and specification of the regional site model	29
5.5.1	Chronology of sets	30
5.5.2	Consistency of site model with tectonic and geological history	31
5.5.3	Estimation of P_{32} from P_{10} or P_{21}	32
5.6	Spatial model	33
5.6.1	Estimating a different value of P_{32} for a different value of x_p	34
6	Derivation of statistical model with properties	37
6.1	Set identification and orientation statistics	37
6.1.1	Sets	37
6.2	Estimation of fracture sizes	50
6.3	Spatial model	61
6.3.1	Intensity intervals in individual boreholes	62
6.3.2	Relation of fracture intensity and geological factors	68
6.3.3	Lateral correlation of fracture intensity	85
6.4	Intensity	91
6.5	Model validation	98
6.5.1	Procedure	98
7	Alternative model approach based on orientation and size from the deformation zone model	101
7.1	Data sources	101
7.2	Orientation of deformation zone traces	101
7.3	Size of deformation zone traces	104
7.4	Analysis of fracturing with lower truncation length (AFM100201)	104

8	Evaluation of uncertainties	105
8.1	Quantification and propagation of uncertainty	105
8.2	Unresolved aspects of uncertainty	106
9	Summary	107
9.1	Stochastic DFN model summary	107
9.2	Conclusions	109
10	References	111
Appendix 1	Sensitivity analysis	113
Appendix 2	Cross tabulation tables from statistical analyses	121
Appendix 3	Plots of TVDSS vs fracture strike	131

1 Objectives and limitations

The purpose of this report is to document the data, software, experimental methods, assumptions, results and uncertainties for the development of discrete fracture network (DFN) models for the local site domain model SDM Forsmark Version 1.2 according to the methodology described in /Munier, 2004/.

The parameters calculated for this model are presented so that they can be used for a variety of downstream models, including those pertaining to hydrological modelling and to mechanical modelling. Modelling assumptions are presented and discussed. Uncertainties related to both the conceptual model and to the data are presented, and recommendations for incorporating these uncertainties in downstream models are presented.

Section 2 describes the data used in the development of the DFN model.

Section 3 summarizes the software and the software modules used to carry out the analyses.

Section 4 lists assumptions.

Section 5 describes the experimental or analytical procedures used to analyze the data in order to calculate the fracture parameters needed for local site domain DFN modelling.

Section 6 describes the results of applying the experimental techniques described in Section 5 to the data listed in Section 2.

Section 7 describes the quantification of uncertainty and how it may be propagated to downstream models.

Section 8 indicates where additional data, studies or other activities could benefit further development of the local site scale DFN model at Forsmark.

This model is not intended to be a flow model or a mechanical model; as such, only the geometrical characterization is presented. The transmissivity properties of the fractures, or their mechanical properties are not within the scope of this report.

This model represents analyses carried out on particular data sets. If additional data are obtained, or values for existing data are changed or excluded, the conclusions reached in this report, and the parameter values calculated, may change as well.

2 Data sources

All of the data used for the development of this model are listed in this section. Outcrop and borehole data were obtained from SICADA on the 6th of July 2004 (reference: Sicada_04_162). The following files were provided in response to the data request made on the 2nd of July 2004. The lineament datafiles and GIS files for outcrops were also provided by SKB.

2.1.1 Lineament data

The following data deliveries have been utilised:

Lineament map (SDEADM.GV_FM_GEO_2079). Rock units (SDEADM.GV_FM_GEO_2074 and 2041) and rock domains (SDEADM.POS_FM_GEO_2336).

2.1.2 Detailed fracture outcrop data

The following data deliveries have been utilized:

Sprickspårsdata_forsmark.zip (SDEADM.GOL_FM_GEO_1765, 1344, 1866, 1911, 1869)

Sicada_04_162_Detailed fracture line.zip (activities.rtf, table_descriptions.txt, fracture_line_map.xls)

Sicada_04_162_Detailed fracture area.zip (activities.rtf, comments.rtf, table_descriptions.txt, fracture_area_map.xls, object_location_area_detailed_mapping.xls)

2.1.3 Borehole data

The following data deliveries have been utilised:

Sicada_04_162_Boremap.zip (Boremap_comments.rtf, p_core_loss.xls, p_rock.xls, p_rock_alter.xls, p_rock_occur.xls, p_rock_struct_feat.xls)

Sicada_04_162_Fracture data.zip (Sprickor I SICADA.doc, p_fract_core.tsv, p_fract_core.xls, p_fract_crush.xls, p_fract_sealed_nw.xls, p_freq_1m.xls, p_freq_10m.xls, p_freq_3m.xls, p_freq_4m.xls, p_freq_30m.xls, p_rqf.xls)

Sicada_04_162_Koordinater + enhålstolkning.zip (p_one_hole_interpret.xls, table_info_p_one_hole_interpret.doc, x,y,z för L=0.xls, x,y,z casing top and bottom.xls)

3 Software used

Table 3-1 lists all of the software used to carry out the calculations in this report, including their name, version numbers, modules, address of vendor and what model parameters they were used for. Modules are listed in the case where there might be ambiguity as to which options were selected. This software has not been formally validated, but has been informally checked and verified that the results appear valid for its intended use. An exception is GeoFractal, which has been validated according to ISO 9001.

Table 3-1. List of software used for this report.

Software Name	Version	Company	Modules Used	Calculation Performed
Excel 2002	(10.5815.4219) SP-2	MicroSoft Corp. www.microsoft.com	General spreadsheet operations ; no macros.	Trace length scaling calculations; general data preparation for other programs.
Analyse-It	Version 1.71 (Dec 11, 2003)	Analyse-It Software, ltd. PO Box 77, Leeds, LS12 5XA, England, UK. http://www.analyse-it.com/ telephone: +44 (0)113 229 5599	Excel add-in to perform non-parametric statistical tests and to summarize basic statistics for data.	Summary tables for fracture intensity as a function of alteration zones and rock types; variation of fracture intensity with depth.
SPSS for Windows	Version 11.0.0 (19 Sept 2001)	SPSS Inc. Headquarters, 233 S. Wacker Drive, 11th floor Chicago, Illinois 60606 http://www.spss.com/	Tabs	Contingency table analyses.
DIPS	Version 5.103 June 9, 2004	Rocscience Inc. 31 Balsam Avenue Toronto, Ontario M4E 3B5 Tel: (416) 698-8217 http://www.rocscience.com/		Orientation and display of fracture orientations; calculation of modal poles to fracture sets.
Tecplot	Version 8.0–1-0 (Feb 16, 2000)	Tecplot, Inc. (formerly Amtec Engineering, Inc.) 13920 SE Eastgate Way Suite 220 Bellevue, WA 98005 Phone: 425.653.1200 http://www/tecplot.com		Display of fracture and lineament trace maps.
GeoFractal	Version 1.2 (Build 3.21 Sept 20, 2002)	Golder Associates Inc. 18300 NE Union Hill Rd. Redmond, WA 98052 +1 425 883-0777 http://www.fracturedreservoirs.com		Mass dimension and display of fracture traces.
FRACMAN	Version 2.604	Golder Associates Inc. 18300 NE Union Hill Rd. Redmond, WA 98052 +1 425 883-0777 http://www.fracturedreservoirs.com	ISIS, FracSize	Analysis of fracture orientation statistics and size statistics for fracture sets.

Software Name	Version	Company	Modules Used	Calculation Performed
ArcView	Version 8.3	ESRI Inc http://www.esri.com	ArcMap	Visualisation of lineaments and outcrop traces.
Spheristat	Version 2	Pangea Scientific Software		Rose diagrams.
FracWorksXP	Version 4.12	Golder Associates Inc. 18300 NE Union Hill Rd. Redmond, WA 98052 +1 425 883-0777 http://www.fracturedreservoirs.com		Calculation of minimum radius value and P32 intensity for sets.

4 Modelling assumptions

4.1 Deformation zone model

The DFN model has utilised the same input data as the deformation zone model. The rock domain map (SDEADM.POS_FM_GEO_2336) has also been utilised in addition to this.

4.2 Stochastic DFN model

4.2.1 Assumptions

There are several assumptions that have been made in order to construct the stochastic DFN model for the Forsmark site. Each assumption is described below, along with its impact on the model, a rationale for why the assumption is reasonable, and recommendations for future re-evaluation of the assumption.

Assumption 1: Lineaments interpreted as deformation zone traces represent fractures.

Discussion: Much care was taken to insure that the lineaments in the delivered data set (see Section 2) were structural features likely to be fractures /Isaksson et al, 2004/, but this does not guarantee that each and every lineament trace is truly a mechanical fracture. Because of the care and protocols followed, however, it is likely that a very high proportion of the lineaments do represent mechanical fractures, and the error that may arise from considering the few data that are not fractures in orientation and size statistics is likely to be small.

Assumption 2: The length of a linked lineament or a linked fracture in outcrop is an accurate and appropriate measure of a fracture's trace length for the purpose of building a stochastic DFN model.

Discussion: This assumes that the linked lineament is a sufficiently accurate measure of a fracture's length; and that it is the appropriate one for computing size statistics. The purpose of linking lineaments is to develop a DFN model that has fracture sizes and intensities that adequately reproduce flow and transport over large and small scales simultaneously. Linking approximately straight-line individual segments into a single lineament requires consideration of several factors, such as geology, data source and resolution, and lineament geometry. Particularly where an individual lineament splits into several, or where lineaments cross, the disposition of which segments belong to which linked lineaments contains uncertainty.

Although the size model depends on the lengths of the linked lineaments and the way outcrop segments are linked, the uncertainty can be bracketed and quantified. The potential uncertainties in trace lengths at the outcrop scale are manifested (along with other uncertainties) as the variance among area-normalized frequency values for the outcrops. It is likely that the variance due to outcrop differences is greater than the uncertainty produced by the linkage algorithm, and in any case, the uncertainty is quantified by calculating an envelope of parameters for the size of a specific fracture set.

Assumption 3: Fractures in outcrop may represent the smaller portion of a population of much larger fractures if the orientation of the sets in outcrop is similar to the orientation of lineaments.

Discussion: The size calculation for lineament-related sets is based upon fitting a power law curve to lineament trace length values and outcrop trace length values. It is possible that most lineaments are actually faults, while most outcrop fractures are mostly joints, which could be in different orientations and have different size characteristics.

However, the fracturing in Forsmark is likely to be very old, and whatever the origin of the outcrop fracturing may have been, it is likely to have been re-activated many times. In this respect, large-scale lineaments may be fractures that have been more intensely re-activated because of higher stress or more focused deformation through time, and as such, share a common tectonic evolution as the outcrop fractures.

It may be worthwhile to further evaluate the fractures mapped in outcrop to determine what evidence for re-activation exists, and perhaps to construct an alternative size model based only on outcrop fractures that have clear evidence for re-activation or shear movement.

Assumption 4: Variations in fracture intensity as a function of rock type, alteration zone or other geological control can be estimated for unsampled rock units based on the inference of the controlling parameters for those units.

Discussion: Thus far, information on geological controls for fracture intensity variation suggests that lithology and alteration degree may be important controls. However, the five outcrops and limited number of boreholes have not provided data for all possible lithology/alteration degree combinations. In order to specify fracture intensity throughout the model region, it is necessary to infer similarity of unsampled rock types to sampled ones, or to adjust sampled rock types to reflect unsampled rock type characteristics. It would be useful to validate this extrapolation to unsampled rock types by acquiring data in one of these unsampled units, and comparing predictions.

5 Experimental procedures

5.1 Strategy for the analysis of the data for calculating the parameters for local site scale DFN model(s) for Forsmark 1.2

The strategy for calculating the parameter values required for the DFN focuses on first defining fracture sets, and then to calculate properties for each set. Because each set may have its own distinct parameter values, the specification of the sets impacts the uncertainty in the parameter values. For example, if all fractures were combined into a single set, the variance in parameters such as size or orientation could be quite high. The separation of the fractures into multiple sets makes it possible to reduce the parameter variance associated with each group, thereby lowering the overall variance or uncertainty in the DFN model.

After sets have been specified, it is necessary to determine the stochastic geometrical description of each set. For each set, this geometry is composed of:

- Fracture orientations, expressed as the trend and plunge of the mean pole, with variability quantified by one or more of the following models and its associated parameters: Fisher, Bivariate Fisher, Bingham, Bivariate Normal, Bootstrap.
- Fracture sizes, expressed as a size-frequency distribution following one or more of the following distributions and their associated parameters: normal, lognormal, exponential, power law (Pareto), uniform; and any minimum or maximum truncation values.
- Fracture shape.
- Fracture intensity, specified as P_{32} , the amount of fracture surface area per unit volume of rock, where surface area is measured as the area of one of the adjacent sides of a fracture.
- Fracture spatial controls. These might be such models as Poissonian, fractal, geostatistical, or more complex combinations of these processes within specific geological domains.
- Fracture terminations.

Additional parameter values may be included depending upon the model's intended use, but no additional items have been identified for this report.

The workflow for analyzing the individual borehole, outcrop and lineament data sets (Figure 5-1) is presented within its context for achieving the overall characterization objectives, which are to determine regional controls on fracture pattern geometry. In particular, the objectives are to develop a predictive algorithm to specify fracture intensity, orientation and size throughout the spatial and depth extent of the Forsmark local model domain.

The workflow diagram begins with the analysis of data sets for each individual borehole, outcrop trace map or lineament data set. These individual data sets are described as "local" in the sense that it is not initially known whether the fracture controls and geometry determined for each individual set is found elsewhere; they may not have any regional consistency among boreholes or outcrops. The results from the analyses for each borehole or outcrop are assumed to initially only represent the fracturing in the rock in the immediate proximity of the outcrop or borehole, unless comparative analysis later demonstrates that fracture orientations, geological controls on intensity, etc exhibit regional consistency.

The term, local fracture set should not be confused with the DFN model in the local model domain, which consists of the fracture model of the Forsmark region. The local DFN model is independent of whether it is composed of local fracture sets where individual borehole or outcrop data sets show little spatial consistency, regional sets, which show great spatial consistency, or some combination of regional and local sets.

The flowchart shows the components of the analysis of the local data sets. Any box that can be traced to an original input data source without connection to another data source is part of the local fracture data set analyses. For example, the chart shows that calculating the mass dimension of the trace intensity is part of the local data analysis for the outcrop trace data, but the derivation of the regional size model for lineament-related sets is not, as it relies upon the joint analysis of both the lineament and outcrop trace data sets, and whether the outcome of these analyses suggest that lineaments and smaller scale fracturing ought to be combined. In contrast, the stages in determining the possible regional controls on fracturing are based on the borehole data, as these data sets contain the most detailed geological information. Any controls identified in the borehole data set are then extended to the outcrop data to see if the controls appear to persist for these data sets as well. All of the analyses eventually flow towards the conceptual basis and parameters values for the local stochastic DFN model. This model consists of all of the pink-shaded output data sets and relations.

5.2 Set identification and orientation statistics

5.2.1 Set determination

A fracture set is essentially a group of fractures whose orientations are either similar over a large spatial domain, or else whose orientations, intensity and other properties can be closely related to geological factors in a statistically significant, predictable manner. It is not necessary that fracture orientations be invariant throughout the domain of interest; it is only necessary that they form according to the same geological factors. For example, dip parallel extension joints that form during the folding of rock will have differing orientations based upon structural position, but may be treated as a single set, despite the orientational variability, because they share a common geological origin that makes it possible to predict their orientation with a small degree of uncertainty. The fracture orientations are based on outcrop, borehole and lineament data. Fracture properties are measured in outcrop and borehole. The outcrop and lineament data are used for establishing the orientation statistics for the subvertical fracturing, since the orientation bias is minimal for these sets, while the borehole data is used for calculating orientation statistics for the subhorizontal fractures for similar reasons. The borehole data is also used as a secondary validation of the outcrop data.

The first step, as shown in the chart (Figure 5-1) is to identify statistically homogeneous subpopulations for each of the five outcrops independently of any other outcrop, each of the boreholes or lineament data set. This analysis consists of plotting fracture orientations as stereoplots of the fracture data, expressed as poles to the fracture planes, and to identify visually distinct clusters of orientations. At the same time, plots of the trace pattern are visually evaluated to determine if there might be other, less prominent sets that were visually obscured in the stereoplots due to the greater number of fractures in some sets. Stereoplots were constructed using the DIPS[®] (Table 3-1), while the trace plots were generated using GeoFractal[®] and TecPlot[®]. An example of the analysis workflow follows.

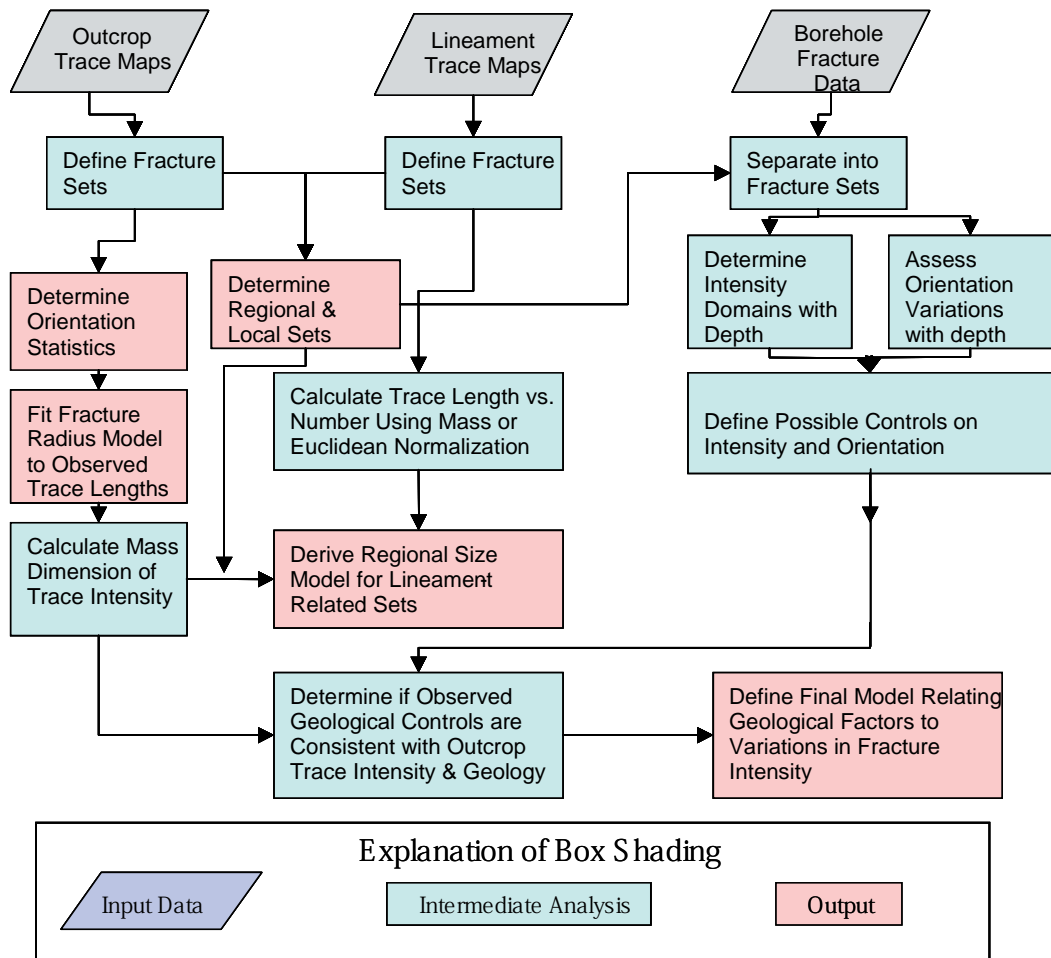


Figure 5-1. Data analysis flow chart.

Figure 5-2 shows the fracture traces measured for outcrop AFM000053, along with the stereoplot of fracture poles. The stereoplot shows two dominant, nearly vertical fracture sets: one striking north-northeast and the other striking west-northwest. However, the fracture trace pattern appears visually to contain more than two orientation sets.

For example, the west-northwest set in the stereoplot looks to range in orientation from 250 to 330°, yet the traces in that same strike range appear to consist of at least two sets. The visual display of the fracture pattern suggested a further subdivision into a east-west set, ranging from 250 to 290°, and a northwest set ranging from 290° to 330°.

When this subdivision is made, the resulting trace sets look geologically more reasonable (Figure 5-3).

The next step in the analysis of the outcrop trace data is to fit an orientation model to each identified set. This was done using the ISIS algorithm in FracMan.

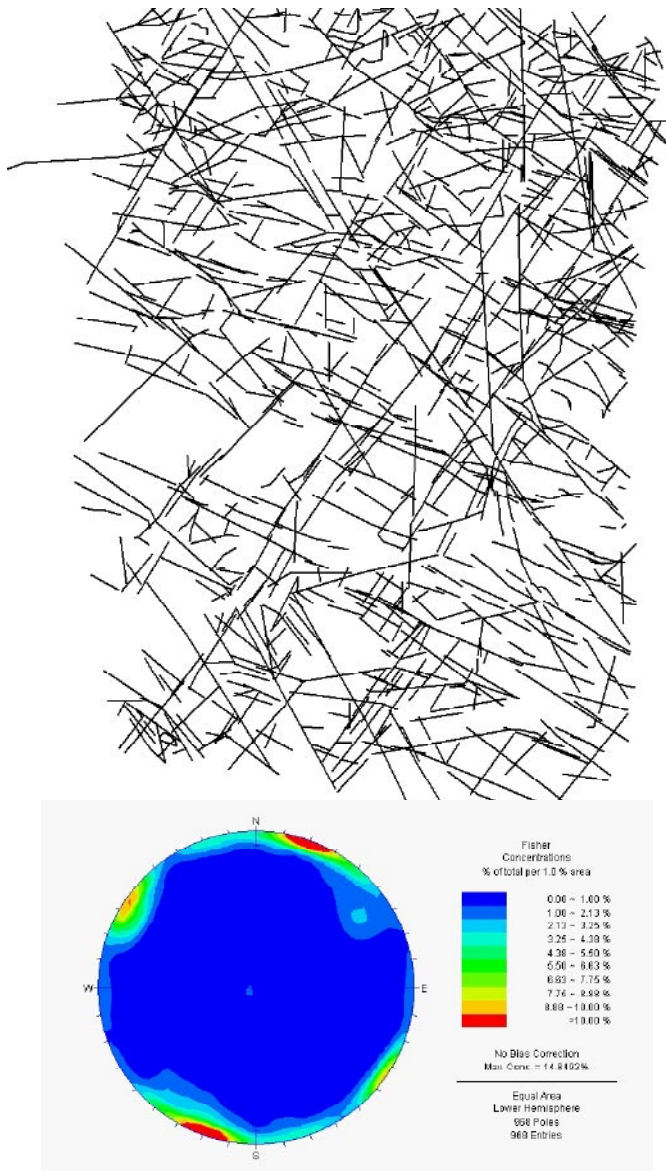


Figure 5-2. Composite stereoplot of fracture poles and fracture traces for outcrop AFM000053.

The assessment of whether the same sets are present in several outcrops relies upon the qualitative evaluation of several factors, as outlined below (Figure 5-4):

The primary observations to decide whether any sets identified in individual outcrops form part of a regional set are whether the orientations are similar AND the sets are in the same approximate chronological order; or if their orientations differ, do they still occupy about the same place in the chronological order AND can the difference in orientation be explained by changes in the lineament pattern geometry? The rationale for this decision tree is that similarity in orientation may be insufficient given the large number of sets in each outcrop. Adding the additional constraint that the set order in the relative chronology should be approximately the same helps to provide confidence that the sets in each outcrop are actually part of a regional set. On the other hand, it may be that the stress pattern has rotated slightly, so that the fracturing that was developing at a particular time actually has different orientations in different outcrops. If this were the case, then it would be expected that the relative set chronology would be very similar, and that the orientations would reflect the difference in the orientations of the lineament pattern near the outcrop.

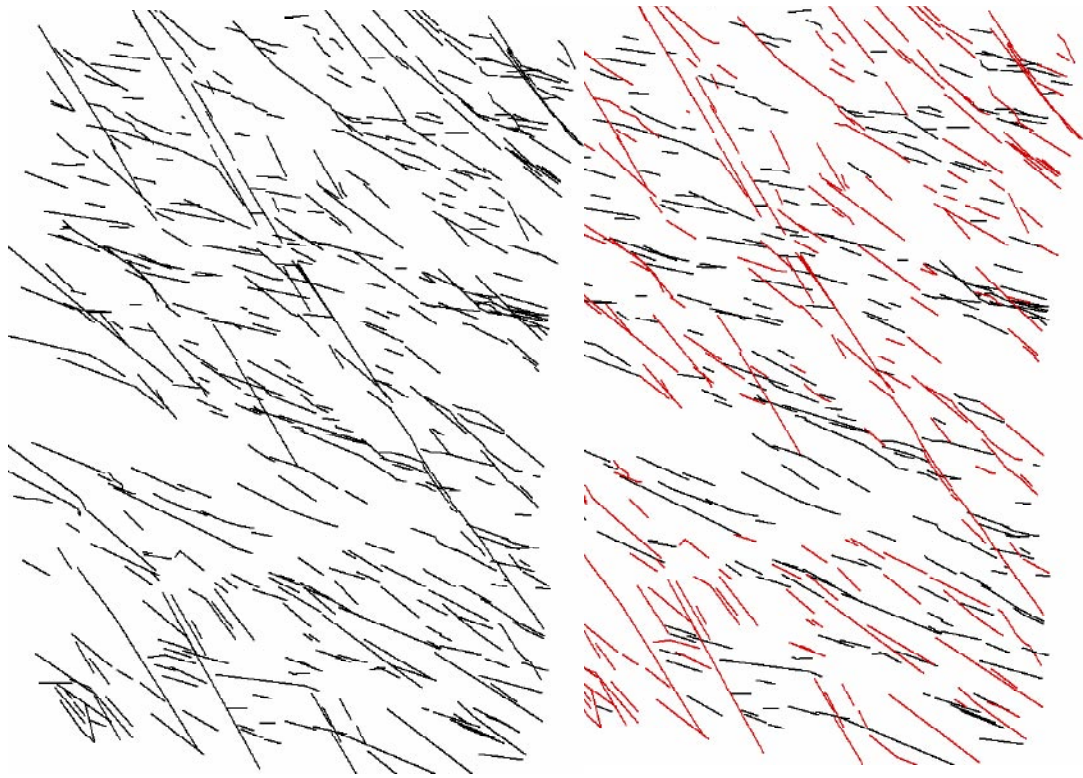


Figure 5-3. Example of refining set definitions from stereoplots by means of trace maps (ASM000053).

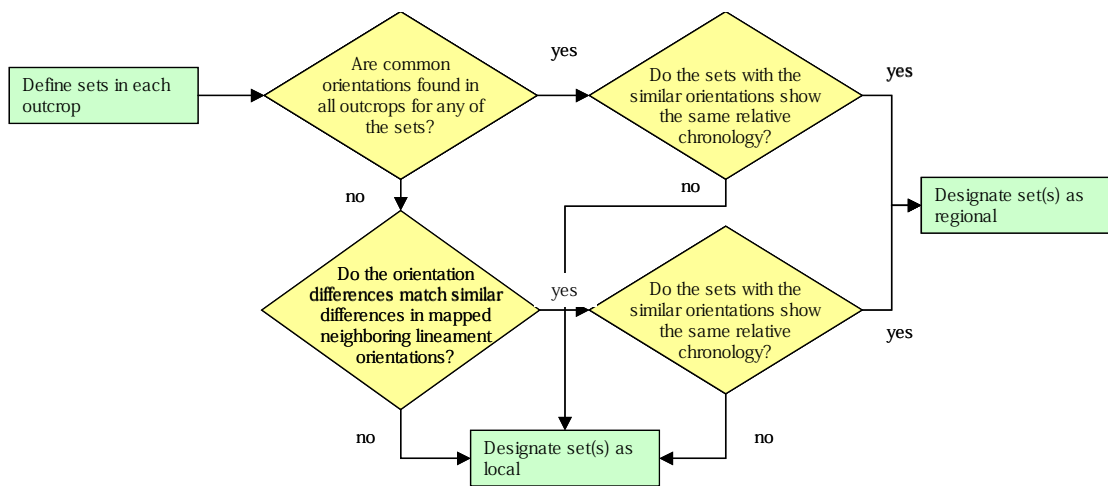


Figure 5-4. Decision tree for identifying sets identified in separate outcrops as belonging to a regional fracture set.

5.2.2 Relation to lineaments

The lineament trace map presented in Figure 6-5 suggests that lineament pattern geometry may change spatially within the local model domain under study. If fractures found in outcrop were formed at the same time and in response to the same stress system that formed the lineaments, then it would be expected that one or more outcrop regional sets would correspond to lineaments. When fractures in outcrop show that they were among the earliest formed, and are possible old, as can be implied if they are filled with minerals possibly formed early in the history such as epidote /Munier, 1989/, then it is likely that the regional outcrop set and the corresponding lineament set are samples from a single fracture population that spans a size range from at least as small as fracture seen in outcrop, to at least as large as lineaments. These sets are termed lineament-related sets and are designated as Group 1 fractures. Figure 5-5 illustrates the decision tree for identifying lineament-related sets.

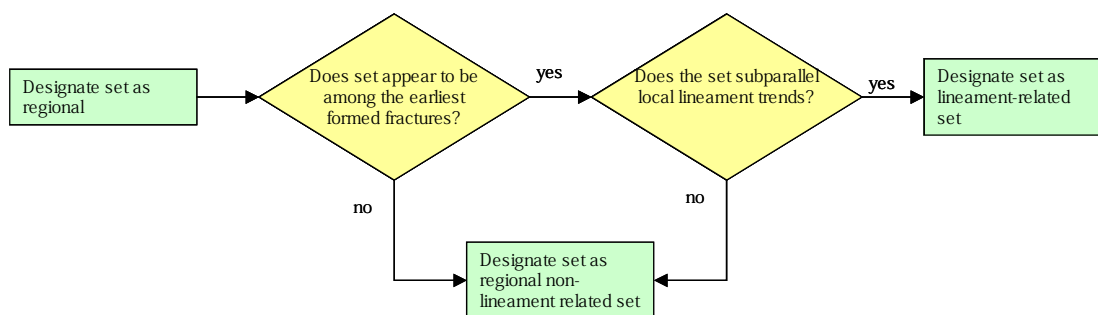


Figure 5-5. Decision tree for identifying lineament-related sets.

5.3 Size

5.3.1 Fracture sets not related to lineaments

Fracture size statistics are computed for each fracture set that varied according to whether the set was lineament-related or not. For any set identified in outcrop that is not related to a lineament set, a non-linear optimization process is used to calculate the parameters (e.g. mean, standard deviation) for a probability distribution model (e.g. lognormal) that best reproduces the observed trace length statistics. This is accomplished using the FracSize algorithm in FracMan™ Version 2.604, which is used to fit a fracture radius model to each of these sets using the orientation model derived from the ISIS analysis.

This first approach requires specification about fracture shape and orientation. As described in Section 4.2.1, it is necessary to assume that the fractures are planar, infinitely thin, circular discs, and having radii independent of position, and whose orientations conform to the orientation statistics found through the methods described in Section 5.2.

Next, a probability distribution type, for example lognormal, is selected for the fracture radius probability density function. A synthetic fracture set composed of discs with an initial “guess” of mean and standard deviation (or other appropriate parameters) is generated and intersected with a plane representing the outcrop surface. This intersection produces a set of trace lengths that can be compared with the measured trace lengths. Through a Simulated Annealing optimization routine /Press et al. 1992/, values of the mean and standard deviation are iterated until a statistically significant match is achieved. This process is repeated for several probability distribution functions, including lognormal, power law (Pareto), normal, exponential and uniform.

5.3.2 Fracture sets related to lineaments

The second method, applied to lineament-related outcrop sets, was to calculate an area-normalized trace length frequency plot. This was done by combining trace lengths from outcrop and lineaments for the same set, and fitting a scaling function to them.

In the trace length scaling analysis, the number of fractures greater than or equal to a particular trace length is plotted as a function of trace length. Since the number of fractures relates to the size of the map area, the number needs to be normalized for this effect in order to plot data gathered from different sized exposures.

A simple way to compensate for different map areas among the data sets is to divide each data set by the map area. This procedure assumes that doubling the area of the outcrop or map would lead to a doubling of the number of traces. This type of intensity scaling in which the number of fractures is directly proportional to area is Euclidean and not fractal. The manner in which the fracture intensity scales with area can be quantified by the Mass Dimension of the fracture traces (Equation 5-1). When the Mass Dimension of the traces has a value of 2.0, the intensity scales proportionately to area, and the spatial pattern of traces can be characterized by a Poissonian density function which inherently has no spatial correlation among the fractures.

It is possible that the intensity scaling of fractures is better described by a fractal model /La Pointe et al. 2002/. In this type of model, intensity varies according to:

$$N(r) = \rho \times r^{D_m} \quad \text{Equation 5-1}$$

where ρ is a constant, termed the prefactor,
 r is the radius of a circle
 D_m is the Mass Fractal dimension, and
 $N(r)$ is the number of fracture traces (partial or entire) contained within the circle of radius r .

The computation of the mass dimension can take several distinct forms, such as the scaling properties of fracture center points or random points selected along the fracture trace, of the number of traces (P_{20}) themselves, or of the P_{21} (fracture trace length per unit area) measure of fracture intensity. All are useful for certain purposes. For size-scaling analysis, the desired parameter is how the number of fractures (P_{20}) changes with scale.

The procedure for calculating the mass dimension is illustrated in Figure 5-7. The value for D_m in Equation 5-1 is equal to the slope of the line when the data are plotted on doubly logarithmic axes. The value of the prefactor is equal to the ordinate value corresponding to a circle with radius=1.0, and can be read directly from the graph. It is important to make this calculation on individual sets rather than all of the traces at once, as each set may have different scaling properties.

The methodology for analyzing the size of lineament-related fracture sets has been presented by /La Pointe, 2001/ and consists of a two-stage process. The first stage is to determine how fracture intensity for an individual fracture set scales with area. The second stage is to use this information to commensurate fracture trace data acquired over regions of different area.

The goal of this analysis is to relate the number of fractures of a given trace length measured over an area, A_i , to the number of fractures of the same size class measured over an area, A_j , of a different size. A simple way of resolving this issue is to assume that the number of fractures in a particular size class scales with area; if the area is doubled, the numbers of fractures are doubled. When the number scales linearly with area, as in this example, the scaling is termed Euclidean.

The calculation of the fractal mass dimension is used to determine whether Euclidean, Fractal or some other function best characterizes the scaling behavior of each individual lineament-related fracture set. The mass dimension exponent can vary from 2.0, which indicates Euclidean scaling, to lower values that imply that the traces scale in a fractal manner.

The procedure is to calculate and plot the cloud of mass dimension data points, as in Figure 5-7, and then compute a nonlinear least-square fit of Equation 5-1 to the locus of the mean and test for statistical significance. If the regression is found significant at the $\alpha=0.05$ level, then the regression is deemed significant and the scaling is treated as fractal. The calculations are always performed on the data set with the least censoring on the small trace end of the distribution, as censoring produces an underestimation of the number of fractures per unit area. For this reason, the mass dimensions were always calculated on the outcrop trace data rather than the lineament data.

The second stage is to use these results to combine data obtained over regions of very different area. The process is as follows:

Let the “o” subscript denote outcrop, and the “l” subscript denote lineament. Furthermore, let the variable “A” denote the area of the outcrop or lineament map, and “R” denote the radius of an imaginary circle that would have the same area as “A”. Also, let “x” represent the trace length of a fracture. Then, from Equation 5-1, it is possible to calculate the number of fracture traces that would be expected in the lineament map area based on what was measured in the outcrop area, or:

$$A_l = \pi R_l^2$$

$$\text{So } R_l = \sqrt{\frac{A_l}{\pi}}$$

$$\text{and } N(R_l) = \rho R_l^{D_m}$$

Equation 5-2

Equation 5-3 makes it possible to compensate for the difference in area by computing a normalization factor NF that is the ratio of the number of fracture traces measured in outcrop to the number estimated in Equation 5-2:

$$NF = N(R_o) / N(R_l)$$

Equation 5-3

This equation also describes how many fractures would be expected in an area of any size, for example, a reference area of 1 square meter.

It is easiest when comparing multiple data sets to reference all of them to an easily converted reference scale like the number of fractures per square meter. In this case, Equation 5-3 becomes:

$$NF_i = N(R_i) / N\left(\sqrt{\frac{1}{\pi}}\right)$$

Equation 5-4

where NF_i is the correction factor for converting the number of fractures actually measured in a domain, I, to the reference domain;
 $N(R_i)$ is the number of fracture traces measured in domain i; and
 $N(1/\pi)$ is the number of fractures estimated from Equation 5-2.

To construct the plot, the trace lengths actually measured in the domain are ordered from shortest to longest. Each trace is numbered according to its cumulative frequency. If there were 50 traces, then the shortest trace would be assigned the number 50, indicating that

there are 50 traces greater than or equal to the length of this shortest trace. The second shortest trace would be assigned the number 49, and so on through the longest trace in the data set, which would have a complementary cumulative frequency of 1. More generally, if k_i fracture traces were measured in domain I, then the shortest trace has the cumulative frequency value of k_i , and the next longest has the value of k_i-1 , and so on such that the longest trace measured has the value of 1. Next, these cumulative frequency numbers are each divided by NF_i . The values are plotted with the normalized cumulative frequency value on the ordinate (Y-axis), and the trace length value on the abscissa (X-axis) as shown in Figure 5-6.

In order to distinguish between the parameters for the various power law distributions used in this report, the following nomenclature is adopted (Table 5-1):

Table 5-1. Nomenclature used to describe power law relations in this report.

Distribution Name	Parameter 1	Parameter 2
Mass Dimension	ρ (prefactor)	D_m (mass dimension)
Cumulative number of trace lengths	t_{0n} (coefficient)	k_t (trace length exponent)
Trace length CCDF	x_{t0} (coefficient)	k_t (trace length exponent)
Radius CCDF	x_{r0} (coefficient)	k_r (radius exponent)

Note that Parameter 2 for both the cumulative number of trace lengths and the trace length CCDF are identical.

This graph shows the results of normalization of 5 outcrop sets, the lineament set, and a model fitted to the composite data.

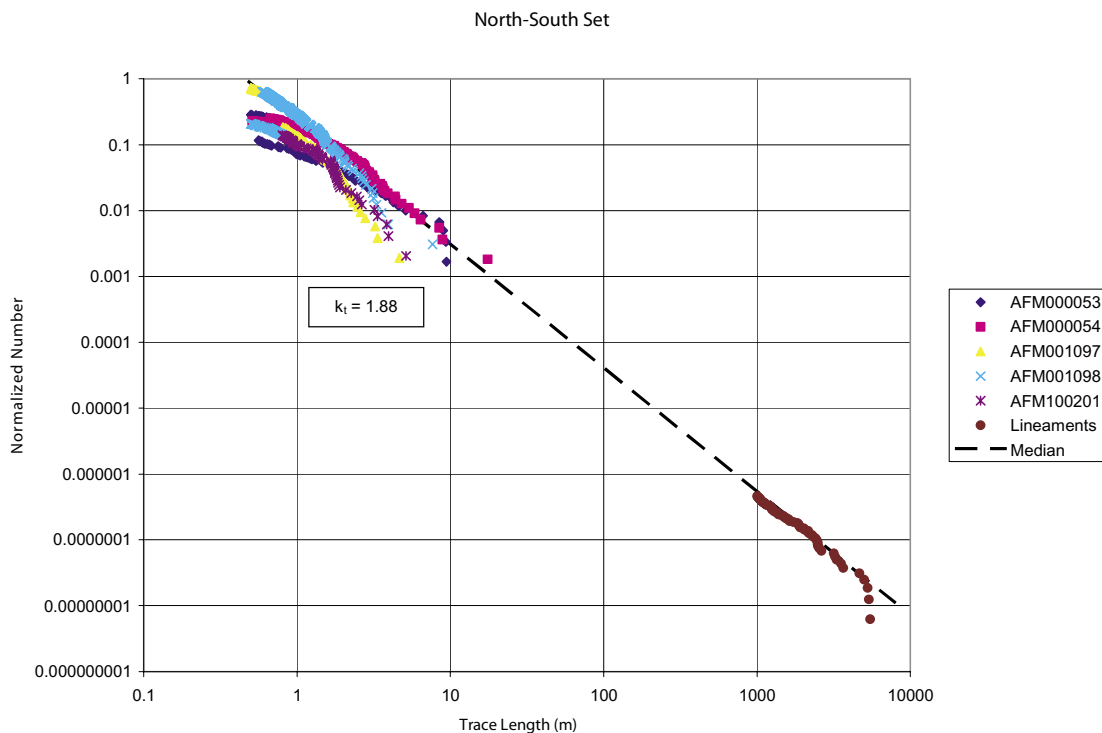


Figure 5-6. Example of trace length model estimation plot resulting from fractal mass dimension normalization of fracture intensity with area. Plot shown is for the NS lineament-related regional fracture set.

The equation of the black line shown on the figure conforms to a power law. The complementary cumulative number (CCN) plot shown in Figure 5-6 represents the number of traces, per unit area, greater than or equal to a specific trace length:

$$Number/area(x \geq t_{0n}) = \left(\frac{t_{0n}}{x} \right)^{k_t} \quad \text{Equation 5-5}$$

The value of t_{0n} corresponds to a trace length of which it is expected that there is only one of them per unit area of this length or longer. Note that the relation depicted in Figure 5-6 and does not describe a probability distribution, but rather a cumulative number distribution. The parameter k_t is the slope of the black line on Figure 5-6, and the parameter t_{0n} is the abscissa value that corresponds to the ordinate value of 1.0.

It is possible to calculate a probability distribution from the cumulative number distribution, but this requires fixing the value of x_{t0} or x_{r0} , as described in Section 5.5.3 This probability density (CCDF) function for trace lengths, which is quantified by this line, has the functional form:

$$Prob(x \geq x_{t0}) = \left(\frac{x_{t0}}{x} \right)^{k_t} \quad \text{Equation 5-6}$$

where x_{t0} is the minimum trace length;
 x is any trace length greater than or equal to x_{t0} ;
 k_t is the Trace Length Dimension, and
 $Prob(x \geq x_{t0})$ is the probability that x is greater than or equal to x_{t0} .

The value of x_{t0} is not the same as t_{0n} . x_{t0} corresponds to a minimum trace length, and is not calculated from t_{0n} . x_{r0} and x_{t0} are related, however, as are k_r and k_t /La Pointe 2002/, according to Equation 5-7:

$$k_r = k_t + 1.0$$

$$x_{r0} = x_{t0} * \frac{2}{\pi} \quad \text{Equation 5-7}$$

This equation implies that the exponent describing the radius CCDF can be calculated from the slope of the cumulative number plot by simply adding 1.0 to the slope. The values of x_{r0} or x_{t0} are not calculated from the cumulative number plot, but are based either on the minimum fracture trace or radius required in the simulation. The methods for calculating P_{32} for a specific combination of minimum size and exponent, as well as re-adjusting the P_{32} for different minimum sizes, is described in Section 5.5.3.

Note also that the shape parameter of the parent radius distribution is sometimes specified by a parameter, b , often termed the Pareto Exponent. This exponent is related to the trace dimension in Equation 5-8 as:

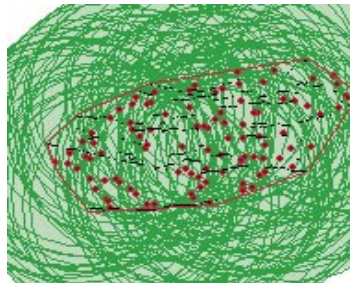
$$k_r = b - 1 \quad \text{Equation 5-8}$$

Those using results from these analyses should be aware of which convention is being used in the specification of the radius distribution model parameters in their particular application.

Also note that the parameter k_t is not the same as the mass fractal dimension, D_m ! They are, in fact, independent parameters.

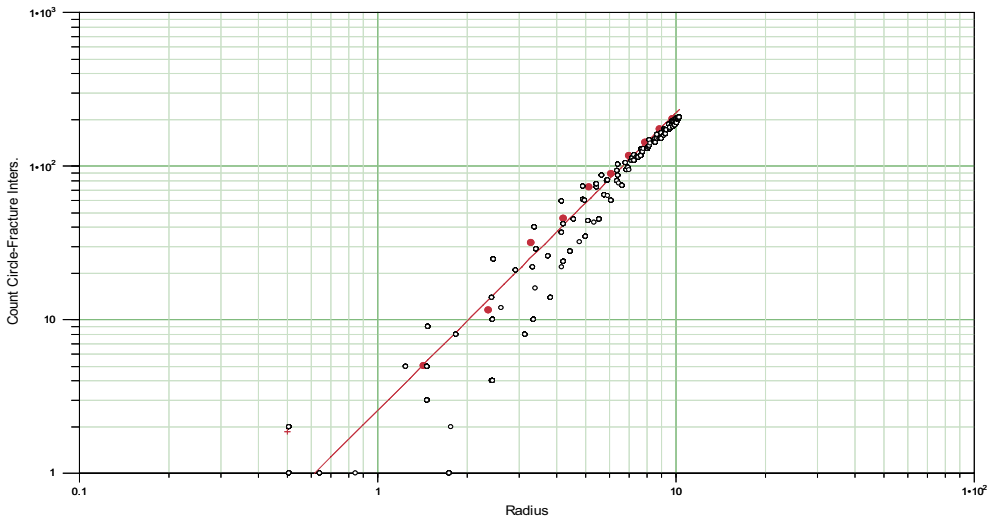
Concentric circles (dark green) are drawn around a single point (red dot), and the number of fractures within each circle as a function of the circle's radius are tabulated.

This is repeated for a number of randomly selected points within a defined data region (red line)



Red polygon defines the areal limit of the data (outcrop boundaries or other similar boundaries) outside of which no data was measured.

Mass Fractal Analysis



Results (open black circles) are plotted on doubly logarithmic axes. The mean values for this cloud of data (red solid circles) are calculated and displayed. A line is then fit to the mean values through nonlinear regression. The slope of the line is D_m , the mass dimension.

Figure 5-7. Workflow for calculating the mass dimension from maps of fracture traces.

5.4 Intensity

Fracture intensity can be quantified by several measures, including the number of fractures per unit length (P_{10}), the number of fractures per unit area (P_{20}), the amount of trace length per unit area (P_{21}), and the amount of fracture surface area per unit volume of rock (P_{32}). The parameter P_{32} is often the most useful way to describe fracture intensity in a stochastic DFN model, as it is scale- and directionally-independent. However, P_{32} is not measured in the field; usually only values of P_{10} from boreholes or P_{21} from outcrop maps are available.

Fortunately, it is possible to estimate P_{32} from either P_{10} or P_{21} through simulation.

Thus, the procedure to calculate fracture intensity involves first determining geological controls on P_{10} and/or P_{21} , and then converting these values to values of P_{32} .

5.4.1 Determination of geological controls on fracture intensity

The determination of geological controls on fracture intensity relies upon comparing fracture intensity from boreholes with borehole geology, and subsequent evaluation of possible controls with intensity variations in outcrop. The boreholes form the primary source of data since:

- 1) They provide a record of fracturing from the surface or near-surface to beyond the depth of the proposed repository;
- 2) There are large volumes of fracture data from the boreholes, leading to better statistical power for hypothesis testing;
- 3) The data encounter a wider variety of geological settings than do the outcrops.

Outcrop fracture data is much more limited. However, borehole data may be biased towards subhorizontal fracturing and hence be better suited for investigating controls on subhorizontal fracture intensity. Possible biases towards subhorizontal fracturing in boreholes was investigated by separating fractures into subhorizontal and subvertical sets, to see if there were any significant differences.

Borehole fracture intensity was measured in two ways: by plotting the average intensity over borehole intervals of fixed length; and through Cumulative Fracture Intensity (CFI) plots (Figure 5-8).

The first option consists of specifying the fixed interval length, and then dividing the number of fractures by the interval length. This method can be very sensitive to the interval length selected, and there are no simple procedures to ascertain what the most useful length might be.

The CFI plots do not have this particular limitation. These plots are constructed by sorting the fracture data by measured depth, starting either at the top or the bottom of the borehole. The depth value is the ordinate in the CFI plot. Next, the fractures are numbered from 1 to n , where n is the total number of fractures that are to be plotted. These numbers are divided by n , such that the 1st fracture has the abscissa value of $1/n$, the 2nd fracture has the value $2/n$, continuing to the last fracture, which has the value of n/n or 1. The CFI plots are chosen prior to non-cumulative plots or histograms as they represent better tools for the identification of intervals of more or less constant fracture intensity and of geological controls on intensity.

In the CFI plot, portions of the line that have constant slope indicate where the fracture intensity has a constant value. Shallow slopes indicate higher intensity, while steeper slopes indicate lower intensity. The range of depth values over which the line maintains constant slope indicate domains of constant fracture intensity. Surface stress-relief effects leading to a higher fracture intensity, for example, would manifest as a domain extending down from the surface possibly a few tens of meters, with a slope much shallower than found below in rock of similar geological character.

The intensity domains can also be compared to mapped geological factors such as lithology, alteration, mineral infilling and other variables to see if zones of consistently higher or lower intensity correspond to specific geological characteristics.

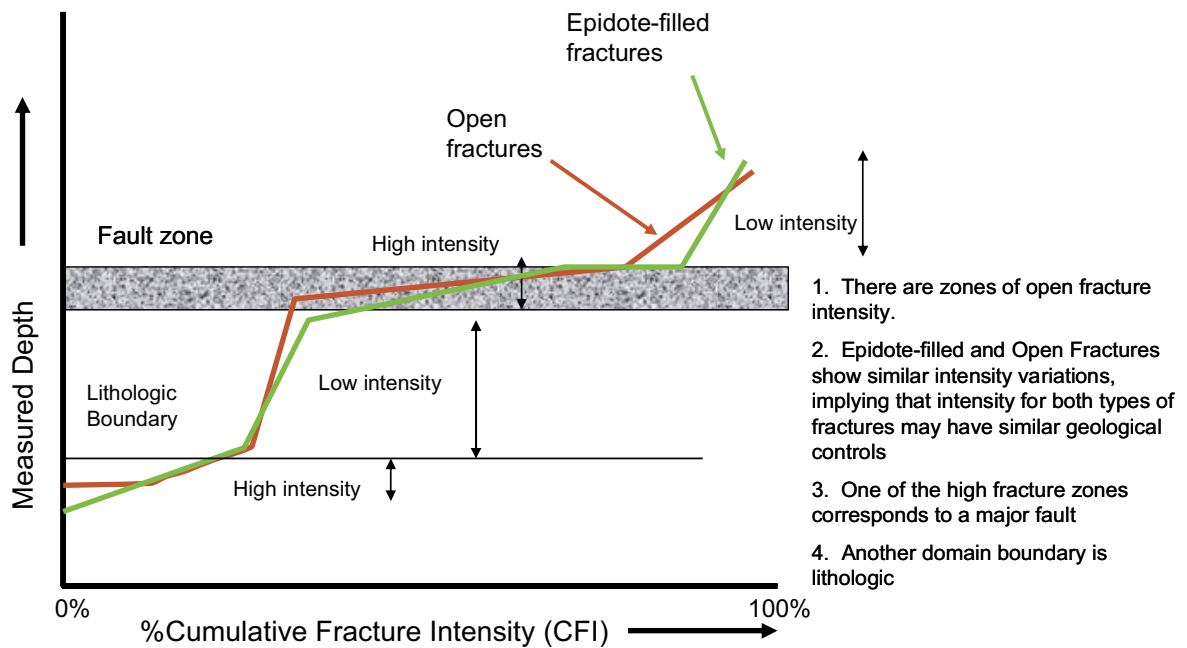


Figure 5-8. Hypothetical Cumulative Fracture Intensity (CFI) plot.

The fracture frequency analysis was carried out in two steps: superimposition of the CFI plots on graphical displays of geological variables to formulate testable hypotheses regarding possible geological controls; and statistical testing and analysis to refute or buttress the hypotheses. The statistical tests employed standard parametric and non-parametric tests of confidence intervals about the mean and median, tests to examine the similarities of means and medians among groups, and linear regression. CFI plots were constructed using Excel2000©./MicroSoft Corporation, 2000/ Statistical analyses were carried out using the Excel Add-In Analyse-It© Version 1.71 /Analyse-It Software Ltd, 2003/.

Additional analyses involved the construction of depth vs orientation plots to see if orientations and intensities remained constant throughout, or whether there are zones with distinct orientations that also corresponded to the presence or absence of a particular fracture set. Depth vs orientations plots were constructed using Excel2000©.

5.5 Assessment of regional geological controls on fracturing and specification of the regional site model

As previously described, the development of the Forsmark site model is built upon the analyses of individual local data sets from boreholes and outcrops together with regional lineament patterns. A critical question is how consistent the results are among the local data sets. For example, are the controls on fracture intensity identified in one borehole consistent with the controls identified in other boreholes and in outcrop? Do the fracture sets defined in each outcrop appear in all other outcrops, or do some outcrops have unique sets? Are any of these sets found in outcrops related to the sets identified in the lineament data? If so, is there further evidence that the outcrop and lineament data sets are size-limited subsets of single parent fracture populations whose sizes span the range from outcrop to lineament?

Once these and related questions are satisfactorily resolved, it is possible to aggregate the local data in ways that are consistent with the resolution, and summarize or re-analyze these aggregated groups of data to derive the regional site-scale fracture model parameters.

The regional consistency of geological controls is evaluated by testing the observations made in the boreholes against the observed open fracture intensity variations in the outcrops. If the same relations are found, then the confidence that the geological controls on fracture intensity are regional is increased.

5.5.1 Chronology of sets

The chronology of fracture sets is based upon three semi-quantitative parameters:

- Whether one set consistently terminates against another set;
- Whether a set that appears to be earlier based on terminations has long traces, or a set that appears to be younger has short traces; and
- Whether a set that appears to be earlier based on terminations has more uniformly or periodically distributed traces, or a set that appears to be younger exhibits spatially restricted traces.

These three observational criteria are used to classify fracture sets as early or late (or somewhere in between) in their relative formation chronology (Figure 5-9 and Figure 5-10).

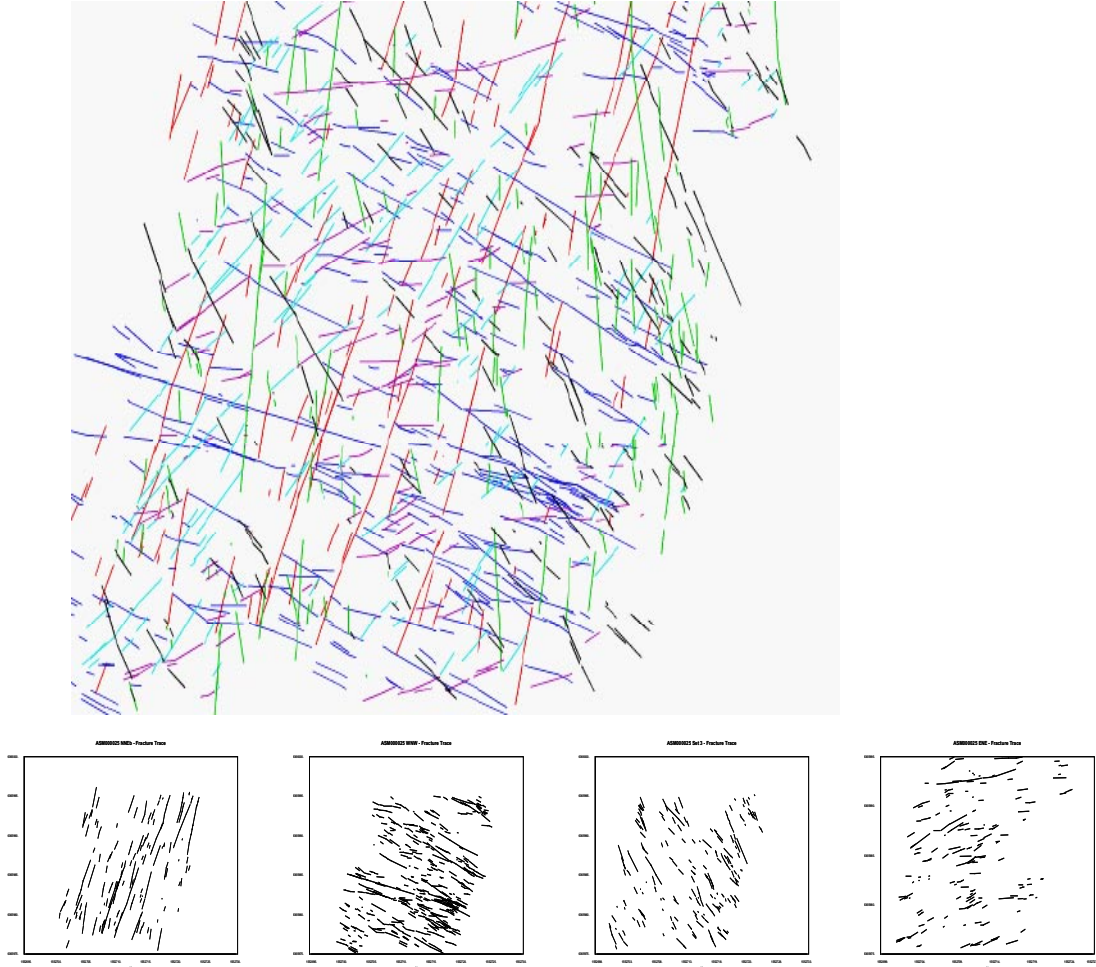


Figure 5-9. Methodology for assigning chronology to identified outcrop fracture sets.

Figure 5-9 shows an interpretation for outcrop ASM000025 in Simpevarp to illustrate the methodology. The oldest sets (shown as the leftmost two inset diagrams) have long traces that are homogeneously scattered over the outcrop. The WNW set, however, shows some indications of banding caused by its terminations against the NNE set. The sets shown in the two right-hand inset diagrams have shorter traces and show pronounced terminations against other sets, leading to much more of a banded appearance. They are also not as pervasively distributed across the outcrop. As a consequence, NNE set is interpreted to be the oldest formed, followed by the WNW, and then followed by the remaining two sets whose relative chronology is harder to distinguish.

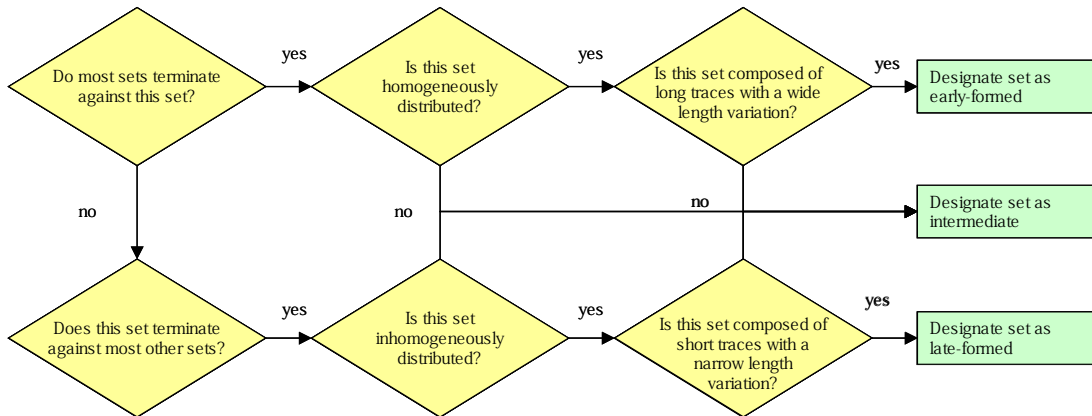


Figure 5-10. Decision tree for identifying set chronology.

5.5.2 Consistency of site model with tectonic and geological history

Confidence is improved in the regional site model if the conclusions made are consistent with what is known concerning the tectonic and magmatic history of the Forsmark region. Each identified fracture set has a relative chronology with regards to other sets, and many fractures have mineral fillings that place some limits on their time of formation. For example, epidote-filled fractures should be among the very oldest. In the Simpevarp area Munier, /Munier, 1989/, reports epidote being mobile not much later than about 1.4 bypb. The second generation of mineralization includes the only occurrence of prehnite and analcime. Laumontite occurs only in the third generation. There are also unique minerals appearing in the fourth and fifth stages, and all have been related to specific ages and tectonic events /Tullborg et al. 1996/. These tectonic events, like the Sveconorwegian collisional orogeny should have produced strongly anisotropic stresses on the rock, either creating new joints and faults in a characteristic geometrical relation to the tectonic movements, or preferentially re-activating existing joint and faults in favorable geometries, making them more prone to being infilled by minerals present during that stage of mineralization and deformation. While older fractures can also be filled with younger minerals during, the presence of early-stage mineralization suggests that such a set probably formed at an early stage. If none or only a very small percent of the fractures have early-stage mineralization, then it is more likely, though not conclusive, that this fracture set is younger.

5.5.3 Estimation of P_{32} from P_{10} or P_{21}

The approach for calculating P_{32} from P_{10} or P_{21} requires simulation. The relation between P_{32} and the measurable fracture intensity quantities is given by:

$$P_{32} = C_1 P_{10} \wedge P_{32} = C_2 P_{21} \quad \text{Equation 5-9}$$

where the constants, C_1 and C_2 depend only upon the orientation and diameter of the borehole, and the orientation distribution of the fracture set. The goal of the simulations is to estimate C_1 if borehole data are being used, and C_2 if outcrop data are used.

The first step is to create a DFN model with the same orientation statistics as the fracture set of interest. Next, a borehole or outcrop surface is inserted into the model with the same geometry as the borehole or outcrop for which actual data has been obtained (Figure 5-11). A guess for P_{32G} is made so that a statistically significant number of fractures in the simulation intersect the borehole. This results in a value of P_{10G} or P_{21G} . This computation for a specific P_{32G} is simulated as a Monte Carlo process for at least 25 realizations. The constant is estimated as:

$$E[C_1] = \frac{P_{32G}}{\langle P_{10G} \rangle} \quad \text{Equation 5-10}$$

and similarly for C_2 , where $E[]$ denotes the expected value of the quantity in brackets, and $\langle \rangle$ represents the average value of the Monte Carlo realizations.

As previously mentioned, the value of P_{32} depends upon the specified minimum size and exponent for a Power law CCDF, which is not normally the case. This is because the value of P_{32} is estimated from trace length data and traces shorter than a specified value have purposely not been measured. The P_{21} value for the outcrop represents only the trace length intensity for traces longer than the threshold, L_t . The complication arises because the amount of P_{21} that is removed by applying a threshold trace length size is sensitive to

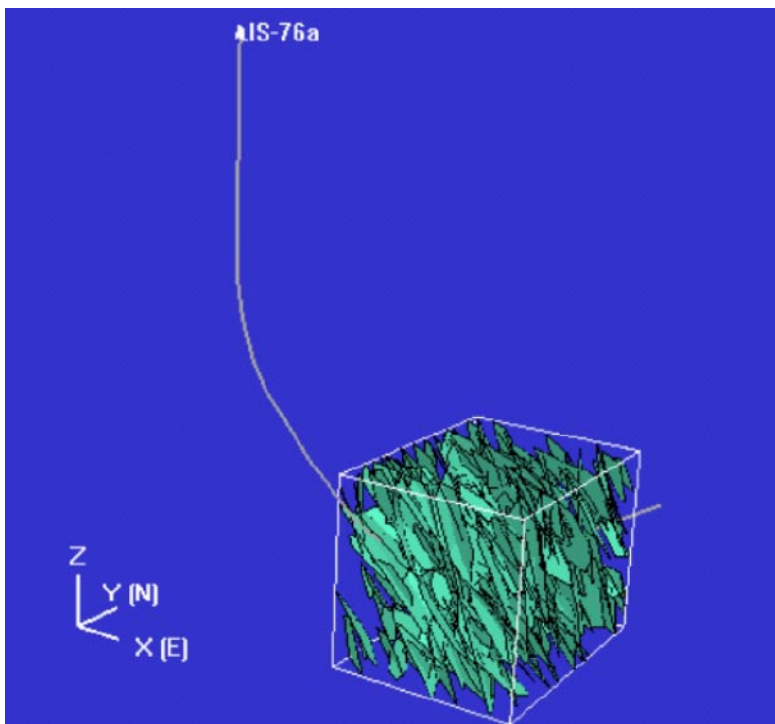


Figure 5-11. DFN simulation to estimate constant relating P_{10} to P_{32} .

the distribution form (power law, lognormal, etc), and so the form of the distribution and its specific parameters become important. If there is no sampling truncation applied, then the form of the radius distribution is not important, and the specific parameter values of the distribution are also unimportant. It is important to note that L_t is not related to x_{r0} in the discussion that follows.

For any specified value of k_r , it is possible to find a combination of x_{r0} and P_{32} that will exactly match a value of P_{21} in which the measured and simulated traces have been excluded if they are shorter than L_t . In other words, the determination of P_{32} is not unique because there are two degrees of freedom, x_{r0} and P_{32} , and only one parameter to match, the truncated value of P_{21} .

However, it is possible to introduce a second constraint to make the solution unique. In this report, the second constraint is a value of P_{10} from boreholes in the same rock domain as the outcrop. A simultaneous match to the borehole P_{10} and the outcrop P_{21} does provide a unique set of values for x_{r0} and k_r .

The procedure for obtaining this unique match is not fully automated. First, a set of values for x_{r0} and P_{32} are selected as initial guesses. A series of realizations are run using these values. A trace plane or planes, representing the approximate size, shape and orientation of the outcrops are intercepted into each DFN realization, and the resulting traces, truncated at L_t , are recorded. The mean value of the truncated P_{21} is compared to the target value of the measured P_{21} . This ratio is used to calculate the value for C_2 in Equation 5-9. The value of C_2 is then multiplied by the measured value of P_{21} from the outcrops to derive a new value of P_{32} . This process is repeated two or three times until a value of P_{32} is found that matches the truncated value of P_{32} for the specified combination of x_{r0} and k_r .

The second step is to insert the target boreholes into the DFN realizations and calculate the value of P_{10} for the simulations. If the simulation P_{10} is too low, this implies that the value of x_{r0} is probably too large. If the simulation P_{10} is too high, then the value of x_{r0} is probably too low. The value of x_{r0} is re-adjusted based on the comparison between the simulation P_{10} and the measured P_{10} . Then the entire process starts over at Step 1, with a new P_{32} being determined and tested. In practice, it takes about four or five iterations in order to simultaneously match a truncated P_{21} and a borehole P_{10} .

This process does not guarantee that the values for x_{r0} for the various sets will be the same; in fact, it is likely that they will differ, reflecting differences in both size and intensity among the sets.

The values reported in Section 6.4 are for a specific combination of k_r , x_{r0} and L_t .

5.6 Spatial model

The spatial model is defined separately from the intensity model, though it is closely related to the intensity model. The location of the fractures is specified by a combination of the intensity and spatial models. For example, certain rock types have higher mean fracture intensities than others, but within each rock unit, the fractures are distributed according to the spatial model. Likewise, fractures related to lineaments may have a zone of higher intensity around mapped lineaments, but within this zone, they may be distributed according to a Poisson process. In this context, the spatial model describes how fractures vary within spatial domains of stationary intensity.

The spatial model is determined through the calculation of the mass dimension of the number of fractures per unit area for outcrop trace data, and the number of fractures per unit length for borehole data. The calculation of the mass dimension has previously been described in Section 5.3.2.

Outcrop trace data are used for calculating the spatial model for the subvertical fracture sets, as borehole data contain a bias that makes calculations for the subvertical sets in boreholes less reliable than the outcrop calculations. Conversely, the borehole data is used to determine the spatial model for the subhorizontal sets in zones where intensity is stationary.

If the mass dimension has a value of 2.0 for trace data or 1.0 for borehole data, the fractures follow a Poisson distribution. Values less than 2.0 for trace data (less than 1.0 for borehole data) indicate a clustering process where there is some degree of spatial correlation among the locations of the fracturing. The failure of the data to approximate a straight line on the mass dimension plots indicates that the spatial model is something other than Poissonian or fractal, and needs to be further investigated using other types of calculations.

5.6.1 Estimating a different value of P_{32} for a different value of x_r .

If a different value for the minimum size is needed for a particular application, it is relatively straightforward to calculate the adjusted value of P_{32} that corresponds to this new value. If the new minimum radius size is denoted by x_1 , a new maximum radius size by x_2 , and the new adjusted value of intensity is denoted by P_{32adj} , then:

$$t(x) = \left(\frac{k_r x_{r0}^{k_r}}{x^{k_r+1}} \right) * \pi x^2 \quad \text{Equation 5-11}$$

$$T(x_1, x_2) = \int_{x_1}^{x_2} t(x) dx \quad \text{Equation 5-12}$$

or

$$T(x_1, x_2) = \frac{\pi k_r x_{r0}^{k_r}}{2 - k_r} \left[x^{2-k_r} \right]_{x_1}^{x_2} \quad \text{Equation 5-13}$$

where $t(x)$ is the fracture area density function for a fracture of radius x ;

$T(x)$ is the total area of all of the fractures;

x_1, x_2 are, respectively, any minimum and maximum radius values.

All other parameters are as previously explained.

Now these equations hold for any minimum and maximum fracture radius. Therefore, the original P_{32} for fractures with radii from x_{r0} to ∞ is:

$$T(x_r, \infty) = \frac{\pi k_r x_{r0}^{k_r}}{2 - k_r} \left[x^{2-k_r} \right]_{x_r}^{\infty} = - \frac{\pi k_r x_{r0}^{2-k_r}}{k_r - 2} \quad \text{Equation 5-14}$$

and

$$T(x_1, x_2) = \frac{\pi k_r x_{r0}^{k_r}}{2 - k_r} \left[x^{2-k_r} \right]_{x_1}^{x_2} = \frac{\pi k_r \left[x_2^{2-k_r} - x_1^{2-k_r} \right]}{k_r - 2} \quad \text{Equation 5-15}$$

The adjustment of P_{32} is the ratio of $T(x_1, x_2)$ to $T(x_{r0}, \infty)$ multiplied by the P_{32} corresponding to $T(x_{r0}, \infty)$:

$$P_{32}(x_1, x_2) = \frac{\frac{\pi k_r [x_2^{2-k_r} - x_1^{2-k_r}]}{k_r - 2}}{\frac{-\pi k_r x_{r0}^{2-k_r}}{k_r - 2}} * P_{32}(x_{r0}, \infty) = \frac{[x_1^{2-k_r} - x_2^{2-k_r}]}{x_{r0}^{2-k_r}} * P_{32}(x_{r0}, \infty) \quad \text{Equation 5-16}$$

Note that $k_r > 2.0$ for Equation 5-16 to be valid. For values of $k_r \leq 2.0$, the correction must be done empirically through DFN simulation.

6 Derivation of statistical model with properties

6.1 Set identification and orientation statistics

6.1.1 Sets

The subvertical sets were determined from the outcrop trace data and the lineament data. Figure 6-2 shows the outcrop fracture traces that were mapped and constitute the basis for analysis. Although the truncation length applied for the detailed outcrop mapping is 0.5 m there were several linked traces in the database that had linked trace lengths less than 0.5 m. These were not used in the analysis as they might be strongly underrepresented and thus create a bias, but are shown in the trace maps as they were part of the original data base.

The orientations of the traces plotted in Figure 6-2 are not uniform from outcrop to outcrop, although the pattern is typically dominated by a northeasterly trending trace set and a west-northwest to northwesterly trending trace set, sets that also stand out prominently in stereoplots (Figure 6-3). A minor north-northwest to northerly trending set is also present in all outcrops except possibly AFM001098. A very minor east-west set is present as well. There are also sub-horizontal fracture data in outcrops.

Figure 6-1 illustrates the location of the outcrops with regards to the modeled rock domains. Three outcrops, AFM000053, AFM000054 and AFM100201 are located in the rock domain RFM029, which represents the tectonic lens. The two remaining outcrops are located in two different narrow rock domains with greater deformation: AFM001097 in RFM018 and AFM001098 in RFM032. The same fracture sets are identified in the different outcrops irrespective of their location but the intensities are quite different. However significant variations in relative proportion of the different sets are also observed inside RFM029. Thus the fracture orientation sets are similar for the five mapped outcrops but the intensities are not. The differences in intensity and the identification of possible geological factors that may be associated with intensity differences is presented in Section 6.4.

The same orientation sets can be observed in open and closed fractures in outcrops, even if the relative density of the sets appears to be different (Figure 6-4).

The lineaments consist of local major and regional lineaments. One issue is the difference in coverage onshore and offshore. Figure 6-5 shows the lineaments that are primarily onshore and have a higher reliability and resolution. Figure 6-6 shows the entire lineament data, including the offshore portion to the northeast. For purposes of data analysis unless stated otherwise, the lineaments belonging to the onshore (southwestern) portion of the Forsmark lineament data set were analyzed rather than the entire set. The influence of truncation of lineaments at the model boundary and of creating a subset of data is presented in Appendix 1.

There appears to be a clear division of the lineament data into three sets (Figure 6-7), with the possibility of a fourth east-west set, although this is not so distinct in the rosette data. When the highest reliability data are plotted only (Figure 6-8), the sets become more apparent. In particular, the color-coded lineament traces (Figure 6-9 and Figure 6-10) suggest that the northwest and east-west sets are distinct, having different abutting relations and trace length distributions.

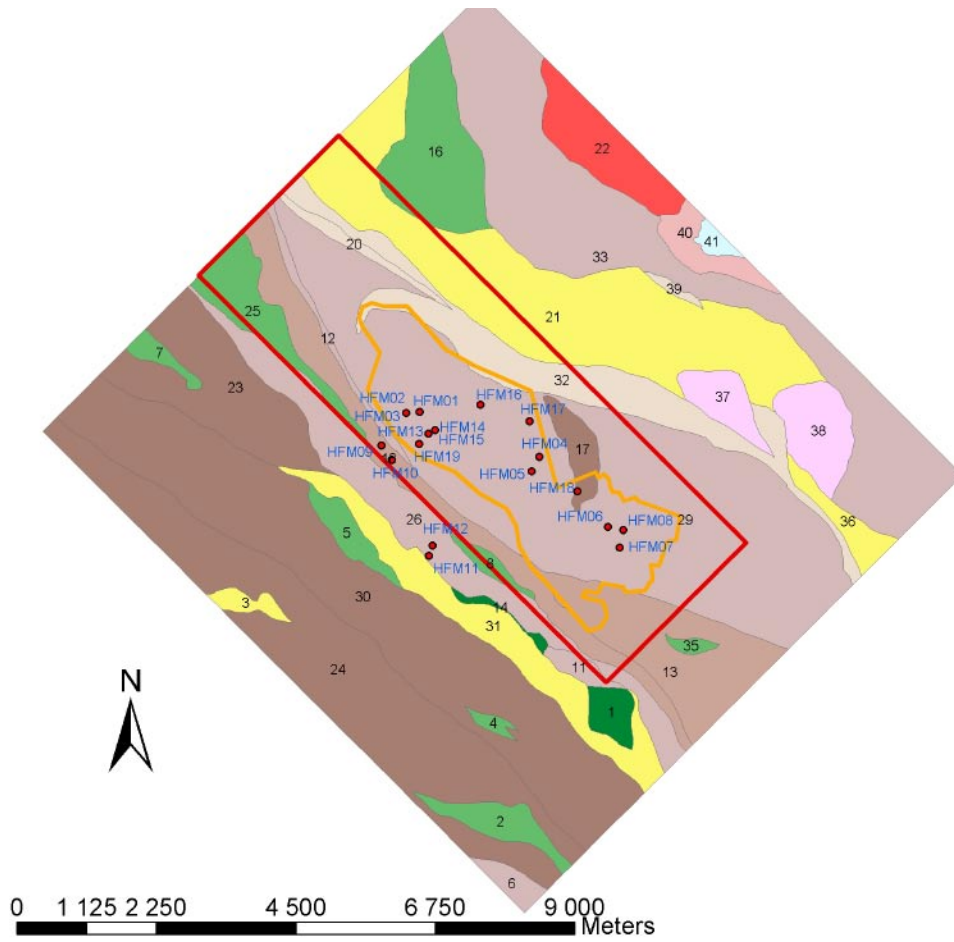


Figure 6-1. Location of the outcrops with regards to the rock domains.

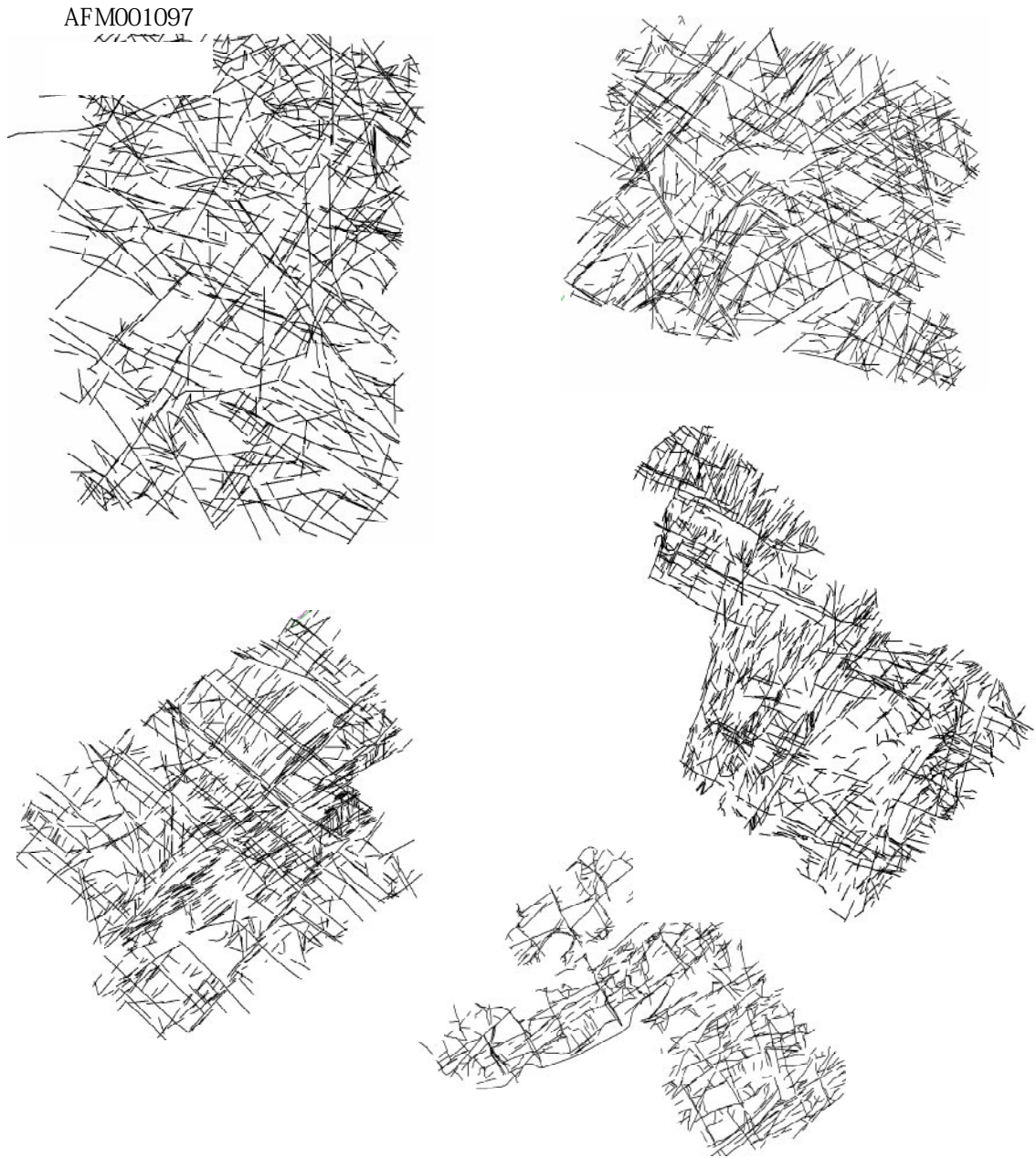


Figure 6-2. Trace maps for outcrops AFM000053, AFM000054, AFM001097, AFM001098 and AFM100201 (maps are not to scale, north is up).

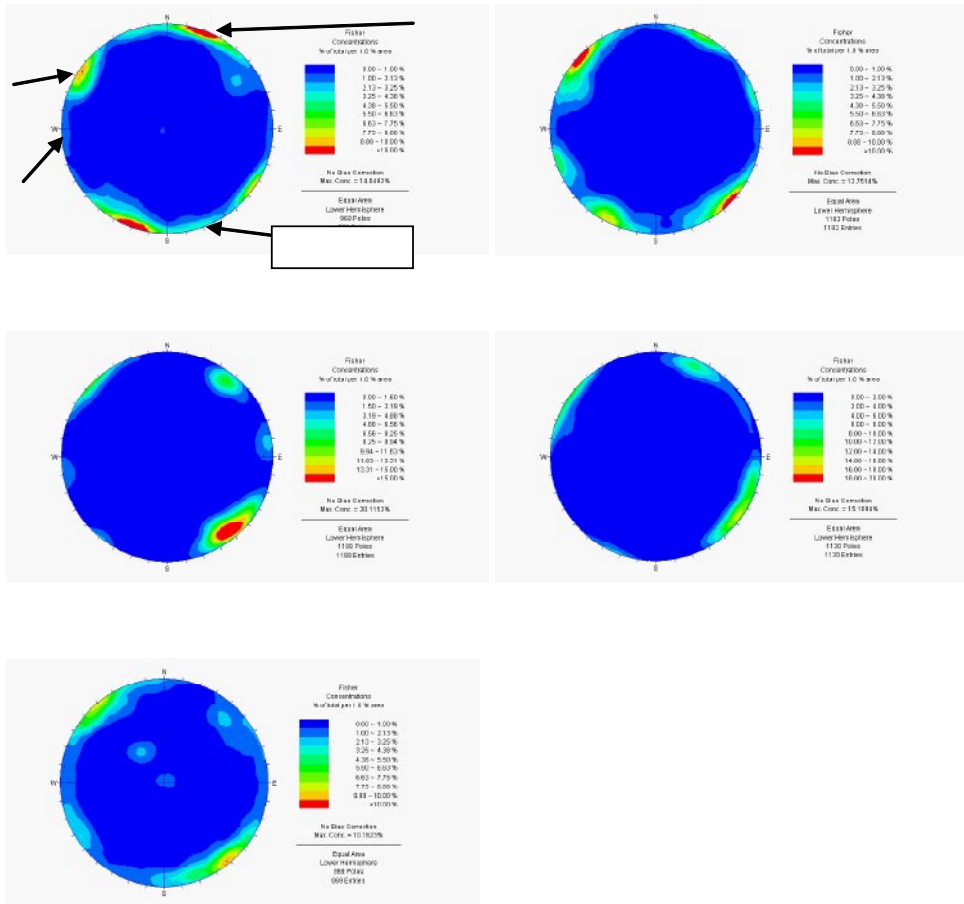


Figure 6-3. Stereoplots of poles to all fractures mapped in outcrops.

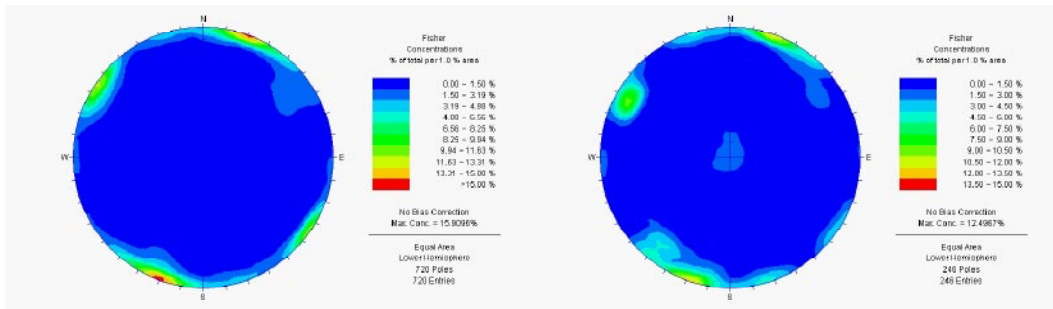


Figure 6-4. Stereoplots of poles to (a) closed and (b) open fractures mapped in outcrop AFM000053.

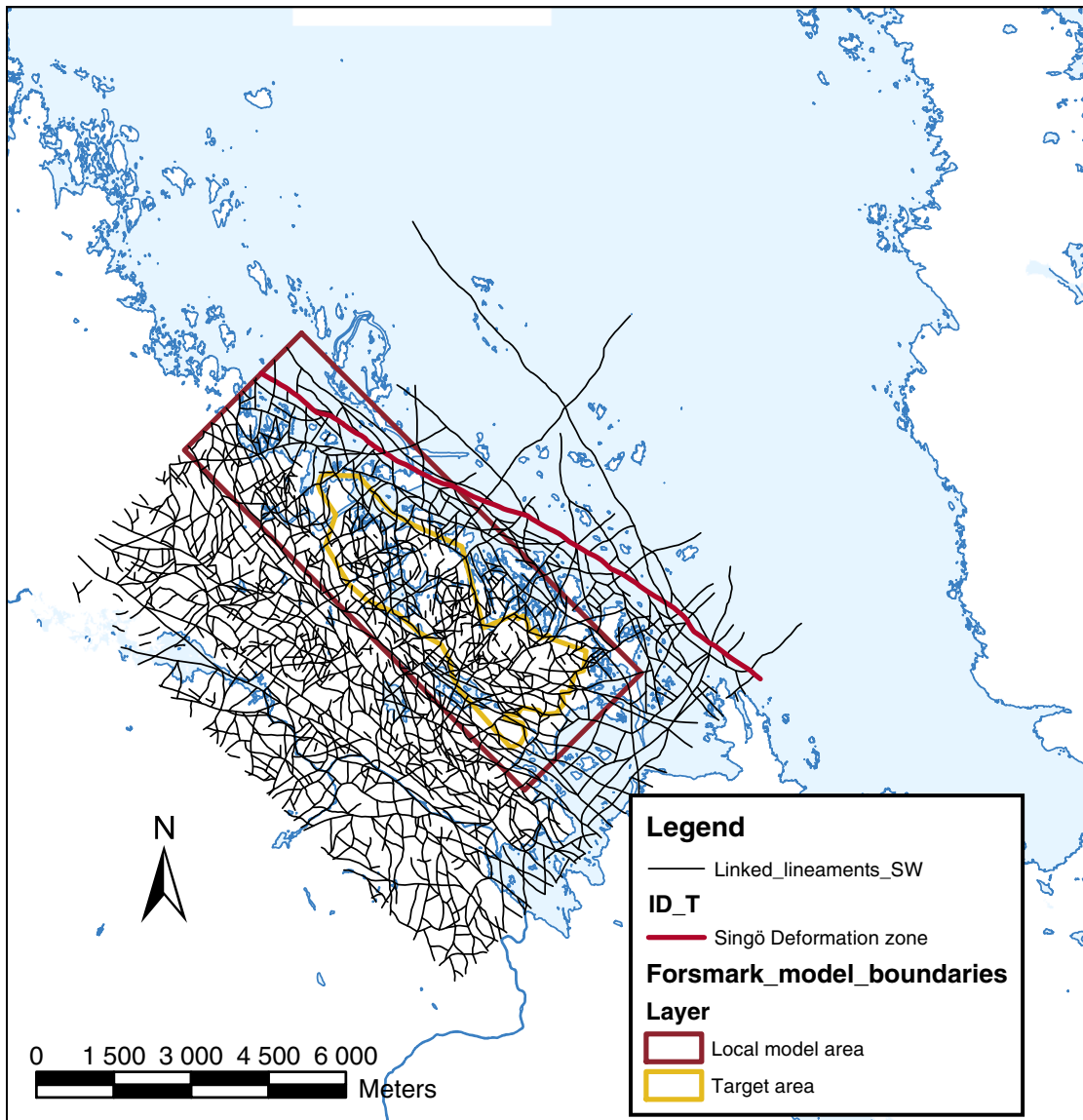


Figure 6-5. Lineament traces for the southwestern portion of the Forsmark region.

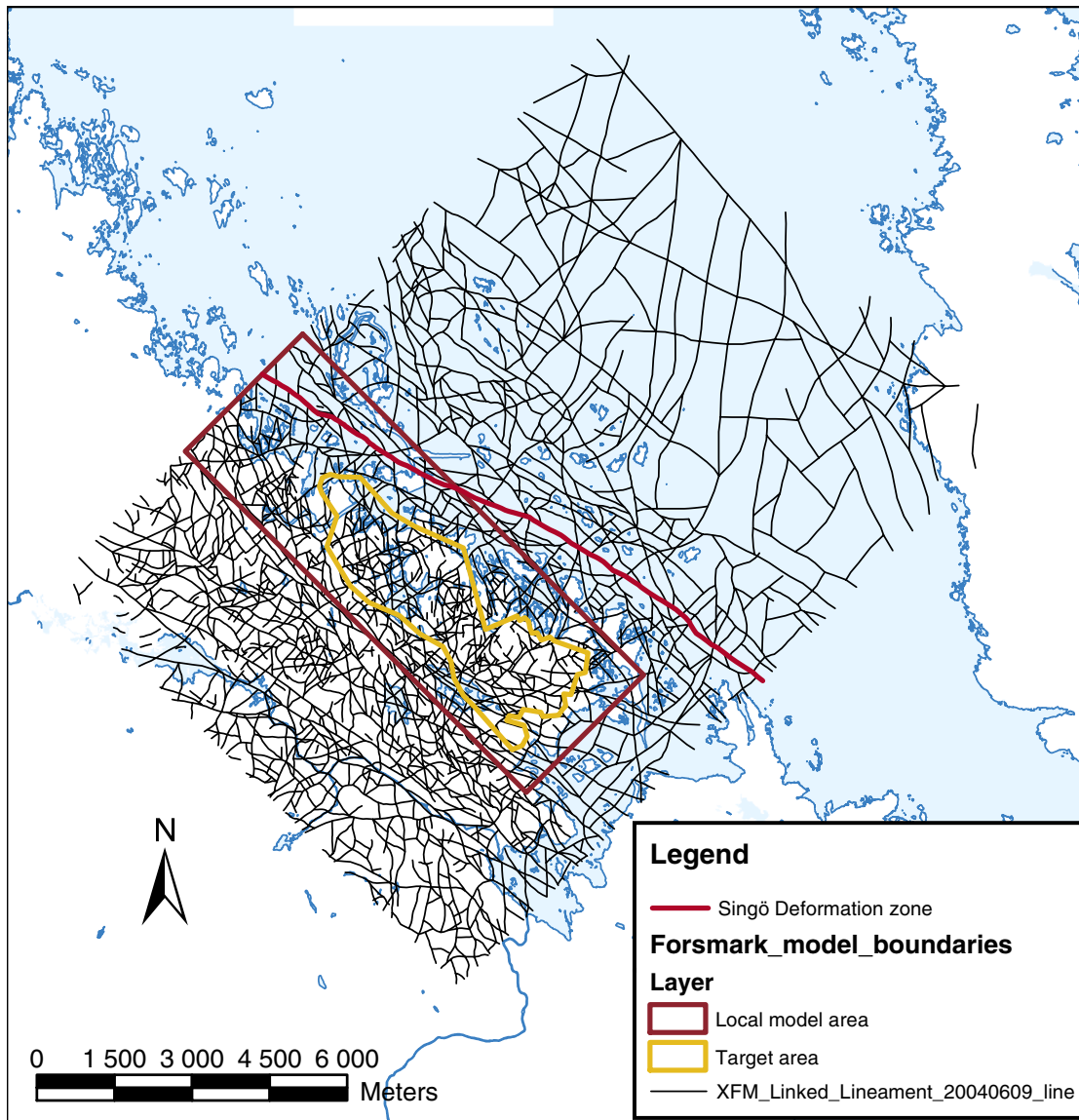


Figure 6-6. Lineament traces for the entire Forsmark region.

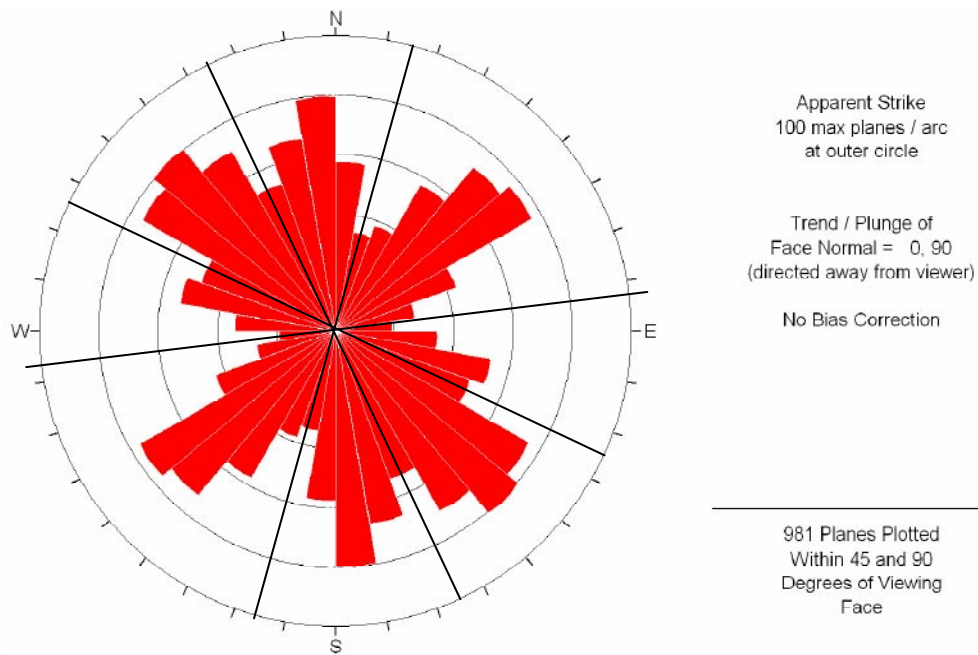


Figure 6-7. Rosettes for lineaments belonging to southwest (onshore) subset of lineaments. The black lines on the rosette indicate the set boundaries.

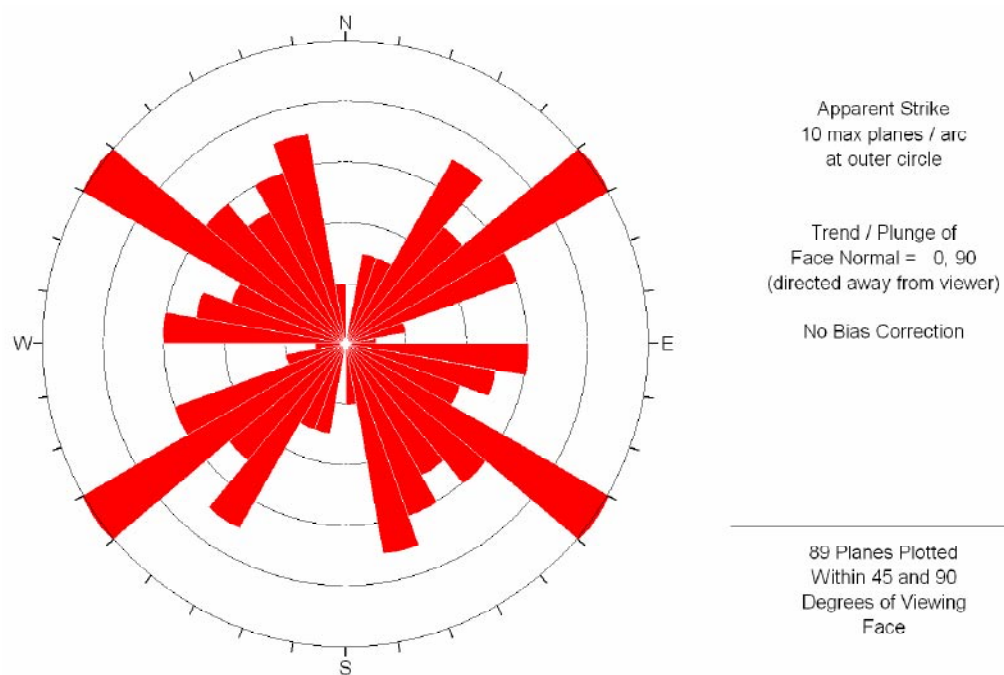


Figure 6-8. Rosettes for lineaments belonging to the southwest subset of lineaments for lineaments with weights greater than or equal to 4.0.

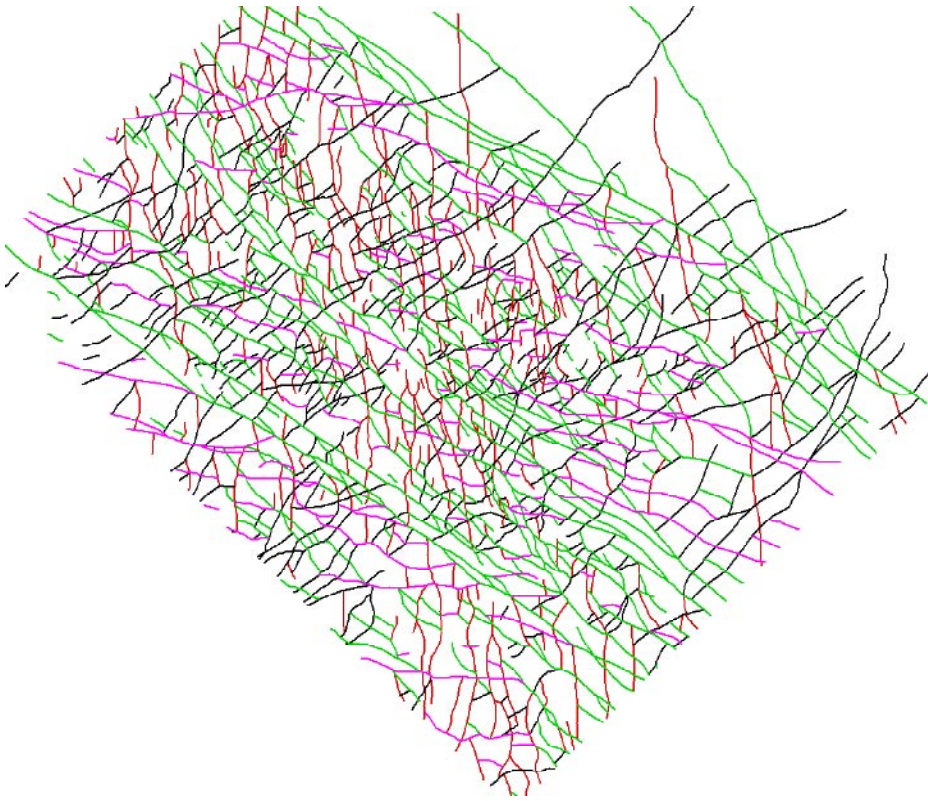


Figure 6-9. Lineaments color-coded according to the four sets shown in the previous lineament rosettes.

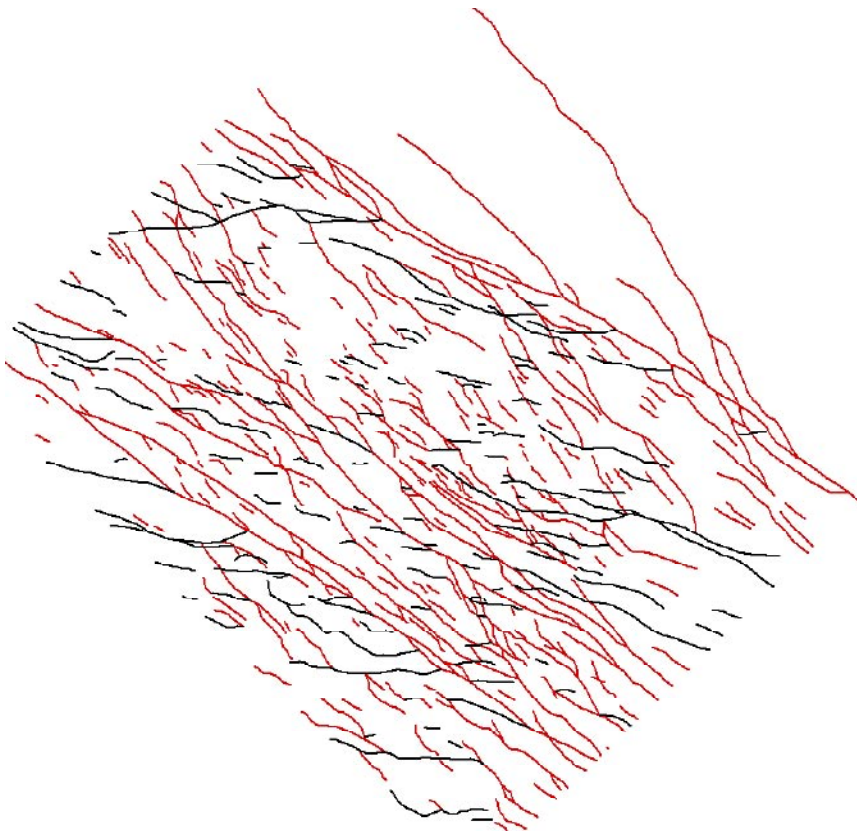


Figure 6-10. Lineament traces belonging to the northwest and east-west lineament sets. Note the difference in length between these two sets, and the tendency of the east-west set to terminate against the northwest set.

The orientations of the vertical sets seen in outcrops can be related to the major lineament trends. The division of the traces into sets according to the identified lineament sets is shown in Figure 6-11. The red-colored traces represent the horizontal set, which can have a wide variety of strikes, and hence do not necessarily show a consistent trend in traces.

The outcrop trace maps were subdivided into sets. The definition of the sets is given in Table 6-1. These definitions were used to classify all outcrop and borehole fractures into one of the four vertical sets or the horizontal set. In Figure 6-11, the NS set is colored black, the NE set is colored green, the NW set is colored purple, and the EW set is colored blue. The horizontal set is colored red.

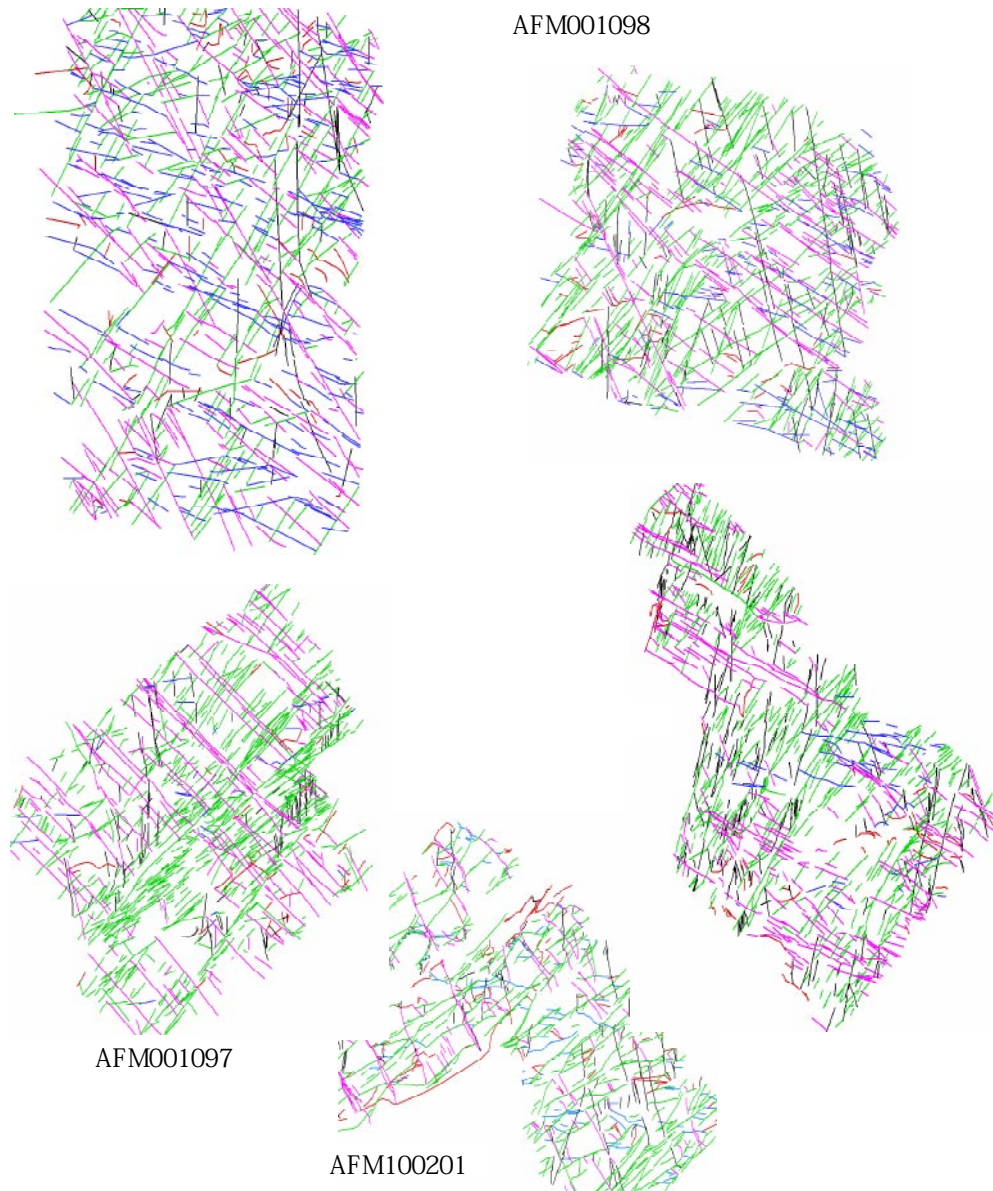


Figure 6-11. Illustration of sets based on assignment from lineament trends. Red-colored traces belong to the subhorizontal set, and have many strikes. North is up in the picture.

Table 6-1. Definitions of fracture strike and dip used to separate fractures in outcrop into sets.

Set Name	Strike Range	Dip Range
L1 (NS)	335–20	50–90
L2 (NE)	20–80	50–90
L3 (NW)	115–155	50–90
L4 (EW)	80–115	50–90
HZ	Any	0–50

Orientation analysis for the four lineament-related sets and the remaining subhorizontal set was carried out to estimate the best orientation parameters for each set. The results of statistical testing for orientation distribution for each set are presented in Table 6-2 and Table 6-3. The alternative orientation models are statistically evaluated using the Kolmogorov-Smirnov Goodness-of-Fit test. The null hypothesis for this test is that the observed fracture orientations represent a random, finite sample from the theoretical orientation model. The first number is the Kolmogorov-Smirnov test statistic, and the second parameter is the probability (expressed as a % significance) that the test statistic would be observed if the measured data represents a random finite sample drawn from the hypothetical theoretical distribution. Models were considered to be statistically significant if they had a significance of 90% or greater. Note that none of the significance values meet this threshold, although clearly some distributions are more probable than others. The distribution with the highest probability is shown in red in the table. The fact that none of the orientation models have proven statistically significant suggests that it may be more appropriate to bootstrap the orientations for fracture models, or at least to assess whether the lack of significance is important for the intended use. This assessment is beyond the scope of the current model.

The best models for the different orientation sets are given in Table 6-3 and are also illustrated in Figure 6-12. The dispersion for the Bingham distribution is specified with two parameters, k_1 and k_2 (Mardia, 1972). The terms referring to the “Major Axis” are used to indicate the trend and plunge of the pole to the great circle passing through the cluster of data. Since the three vectors (Pole, major axis of ellipse and minor axis of ellipse) are orthogonal, specification of the pole and the orientation of the major axis completely specifies the Bingham orientation distribution.

Table 6-2. Results of the statistical testing for the different orientation sets.

Set	Univariate Fisher	Bivariate Fisher	Bingham
NS (L1)	0.078/0.01%	0.067/3.9%	0.083/0.3%
NE (L2)	0.0531/2.53e–05%	0.091/9.34e–04%	0.045/10.7%
NW (L3)	0.038/8.5%	0.237/< 1.0e–13%	0.125/1.36e–05%
EW (L4)	0.051/2.9%	0.195/2.46e–13%	0.096/0.0516%
Horizontal	0.041/54.6%	0.051/47.5%	0.066/19.1%

Table 6-3. Orientation statistics for the four subvertical lineament related fracture sets and the subhorizontal set.

Set	Best model	Other acceptable models	Mean Pole Trend	Mean Pole Plunge	Dispersion
NS (L1)	Bivariate Fisher	none	92.4	5.9	k1=19.31, k2=19.69
NE (L2)	Bivariate Bingham	Bivariate Fisher at 2.2%	137.3	3.7	k1=-17.09, k2=-9.1
NW (L3)	Fisher	none	40.6	2.2	k=23.9
EW (L4)	Fisher	none	190.4	0.7	k=30.63
HZ	Fisherall	others	342.9	80.3	k=8.18

Set	Major Axis Trend	Major Axis Plunge	KS Statistics	Significance
NS (L1)	355.3	50.2	0.06	8.80%
NE (L2)	38.1	68.2	0.045	10.30%

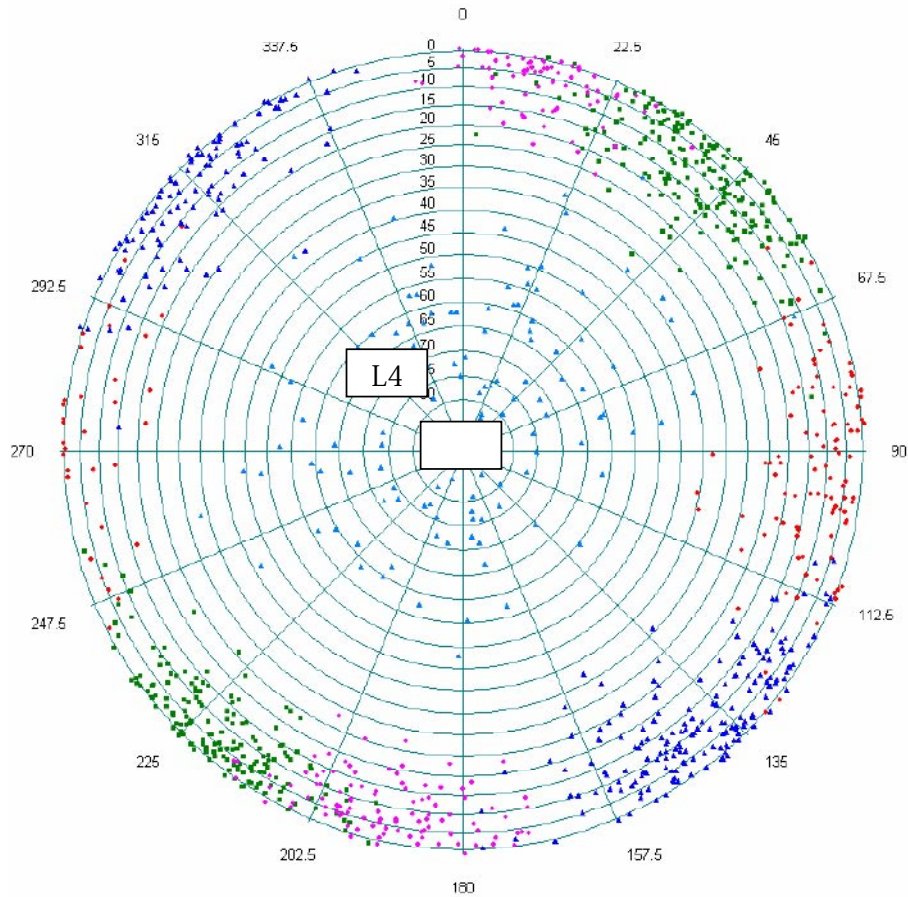


Figure 6-12. Stereonet of fracture sets based upon orientation parameters reported in Table 6-3.

Orientation parameter values for an assumed univariate Fisher are given for the NS and NE sets for practical reasons (Table 6-4), since future modeling use may require a univariate approximation to the bivariate distributions. However, use of any univariate approximation where the statistical tests have not shown the univariate Fisher model to be statistically valid needs to address the suitability and impact of using these univariate models, and the limitations they may impose on the usefulness of subsequent modeling results. It is strongly recommended that the bivariate distributions be used where the statistical tests indicate that a bivariate statistical model is valid, while a univariate statistical model is invalid.

The relative proportion of each fracture set is shown in terms of P_{21} and P_{32} , where P_{32} was calculated assuming the outcrop surface was horizontal (Table 6-5). Among the subvertical sets, the northeast and northwest sets are the most prominent. The subhorizontal set is also quite prominent for open fractures. The north-south and east-west sets are about half as intense as the other sets.

Comparison with the proportion of P_{32} for the cored boreholes (Table 6-6) shows a similar intensity pattern as the outcrops for open fractures, with the NE set being the greatest, next the horizontal, then the NW set, the NS set and lastly the EW set. The NE and NS subvertical sets are dominant for sealed fractures which is slightly different with what is observed on outcrops.

Table 6-4. Univariate fisher parameters for the NS and NE sub-vertical sets.

Set	Mean Pole Trend	Mean Pole Plunge	Dispersion, κ
NS (L1)	87.2	1.7	21.66
NE (L2)	135.2	2.7	21.54

Table 6-5. Relative P_{32} statistics for the four subvertical lineament related fracture sets and the subhorizontal set, open and closed fractures from outcrops, RFM029 only.

RFM029	Open		Closed	
	Proportion of P21	Proportion of P32	Proportion of P21	Proportion of P32
NS (L1)	7.41	6.78	13.18	12.90
NE (L2)	27.25	24.90	42.08	41.12
NW (L3)	35.19	32.42	25.28	24.91
EW (L4)	17.34	15.85	16.52	16.15
HZ	12.81	20.06	2.94	4.92

Table 6-6. P_{32} relative intensity statistics for the cored boreholes, fractures outside of identified deformation zones.

RFM029 Set	Proportion of P_{32}		
	Open	Partly open	Sealed
NS (L1)	10.53	14.25	17.21
NE (L2)	40.78	52.74	57.18
NW (L3)	14.38	15.55	9.92
EW (L4)	4.61	5.3	76.19
HZ	29.70	12.09	9.50

The relative proportion of P_{21} of open fractures was calculated for each set. The data of all five outcrops are used for the calculation. Table 6-7 shows that the relative intensity of open and sealed fractures remains relatively constant in the four subvertical fracture sets. For the horizontal set of open fractures the percentage is nearly double. The reason for this higher percentage is not known, although it may be due to some surficial stress relief. If so, then the ratio of open to sealed fractures in the subsurface for the horizontal set should not be based on the outcrop data, but the borehole data that extends below the zone of potential surficial stress relief. Overall, the percentage is close to 20% because it is dominated by vertical fracturing.

Examination of the open fractures from the percussion boreholes for the horizontal set only in portions of the borehole outside of identified deformation zones shows a similar percentage, though slightly higher (Figure 6-13). Given the variability among the intervals, the value calculated from the outcrops (42.22%) is well within the range of the subsurface data. This suggests that the ratio of P_{10} of open and partly open horizontal fractures outside of identified deformation zones to the total equivalent P_{10} intensity does not appear to be a surface effect. Why the horizontal fracturing should have a higher ratio than the vertical fracturing is not clear, but it does suggest that horizontal fractures may be, on average, more likely to be conduits for fluid flow than vertical fractures, all other factors being equal.

It should be noted that the relative proportion of each of these sets may vary by rock domain, and as the outcrop data is restricted to only three rock domains out of the many in the site, these proportions may not be valid for the remainder of the site.

Table 6-7. Percentage of P_{21} fracture intensity in open and closed fractures for the four subvertical sets and the subhorizontal set identified in outcrops AFM000053, AFM000054, AFM001097, AFM001098 and AFM100201.

Set	P_{21} % in Open Fractures	P_{21} % in Closed Fractures
All	19.90%	80.1
H	42.22%	57.78
L1	19.80%	80.2
L2	16.48%	83.52
L3	21.49%	78.51
L4	20.29%	79.71

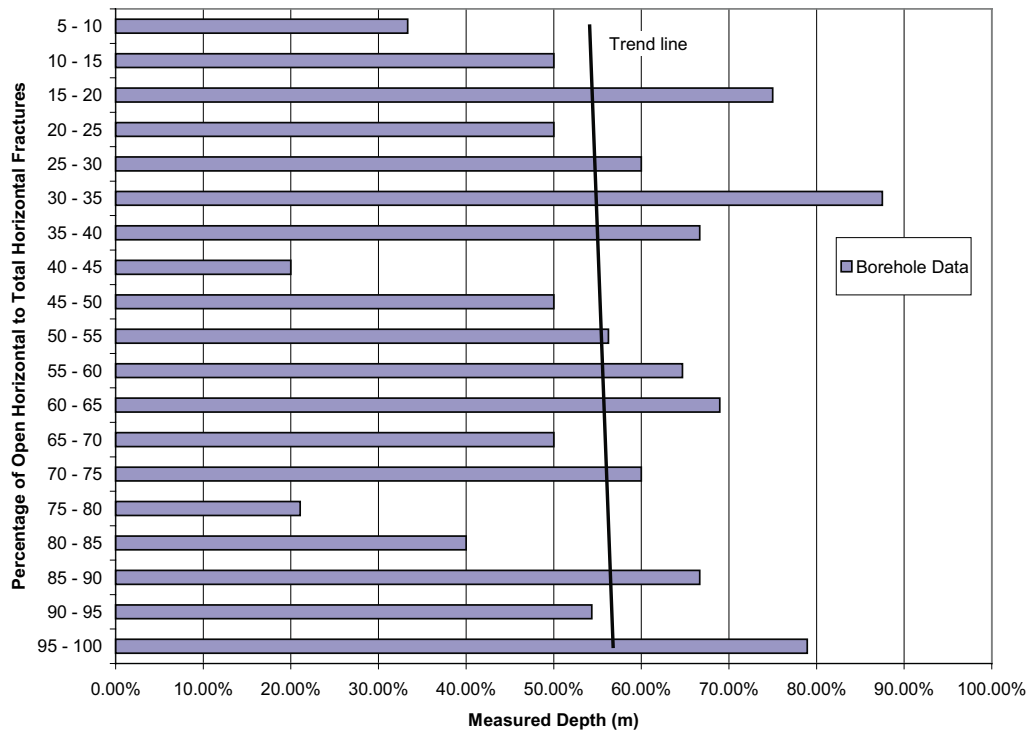


Figure 6-13. Percentage of open and partly open horizontal fractures in relation to total fractures (P_{10} open and partly open to P_{10} total); average or 5 m intervals for the top 100 m of the percussion borehole data. The percentage is generally around 55%.

6.2 Estimation of fracture sizes

The size distribution parameters were estimated by first computing the mass dimension, and then using the mass dimension for determining the appropriate area renormalization scaling. If the mass dimension was close to 2.0, then the scaling is approximately Euclidean and the area re-normalization is accomplished by simply dividing the number of fractures by the outcrop or lineament map area.

Figure 6-14 through Figure 6-18 show the mass dimension plots for each identified outcrop fracture set. The mass dimension parameters are shown in Table 6-8. The mass dimension analyses for each fracture data set show that intensity is often well approximated by Euclidean (non-fractal) scaling, as many of the mass dimensions are close to 2.0. Thus, a Poissonian scaling model is suggested by these plots, and for the area-renormalization of the trace length plots to determine fracture size.

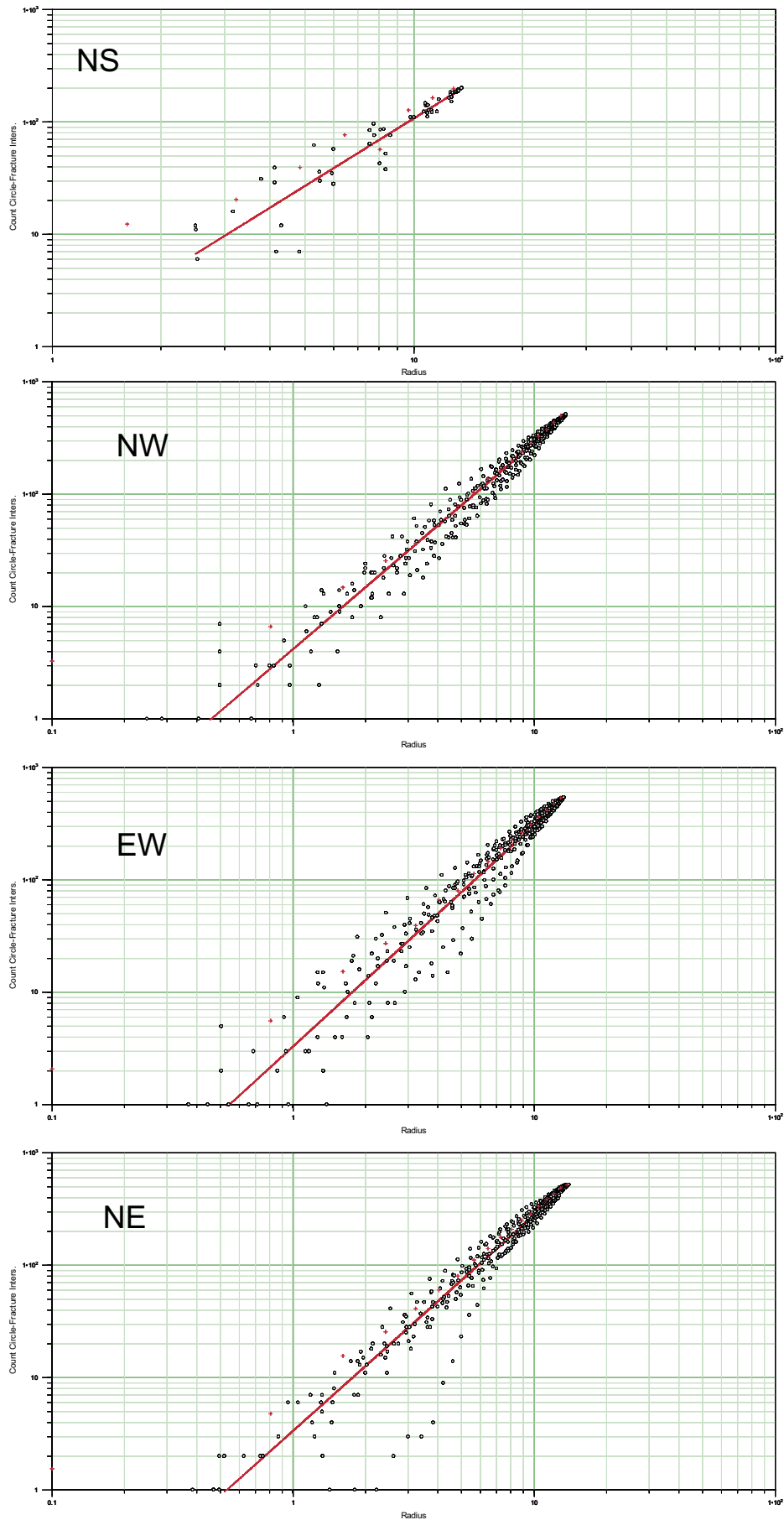


Figure 6-14. Mass dimension calculations for individual fracture sets identified in outcrop ASM000053.

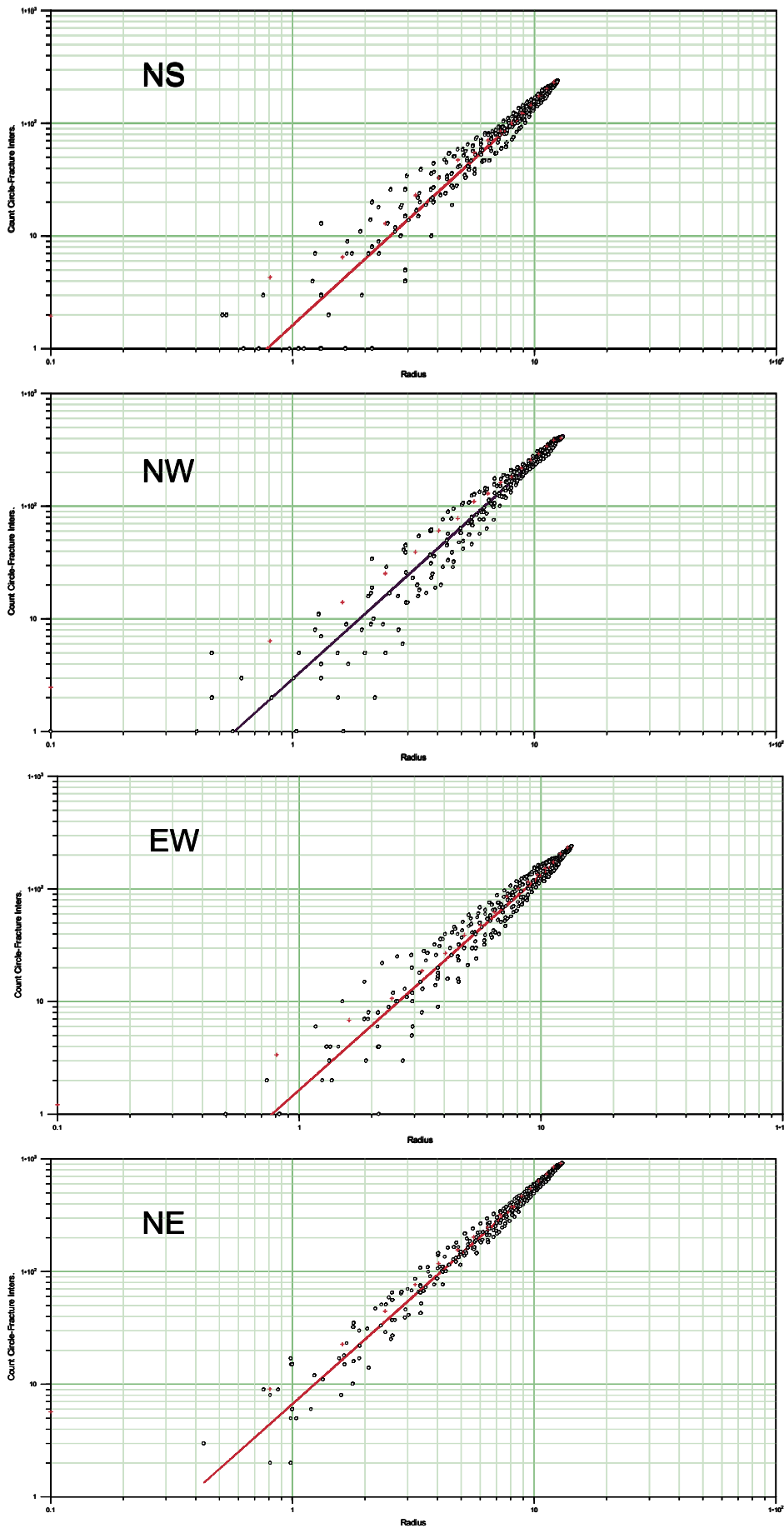


Figure 6-15. Mass dimension calculations for individual fracture sets identified in outcrop ASM000054. **Figure 6-16.** Mass dimension calculations for individual fracture sets identified in outcrop AFM001097.

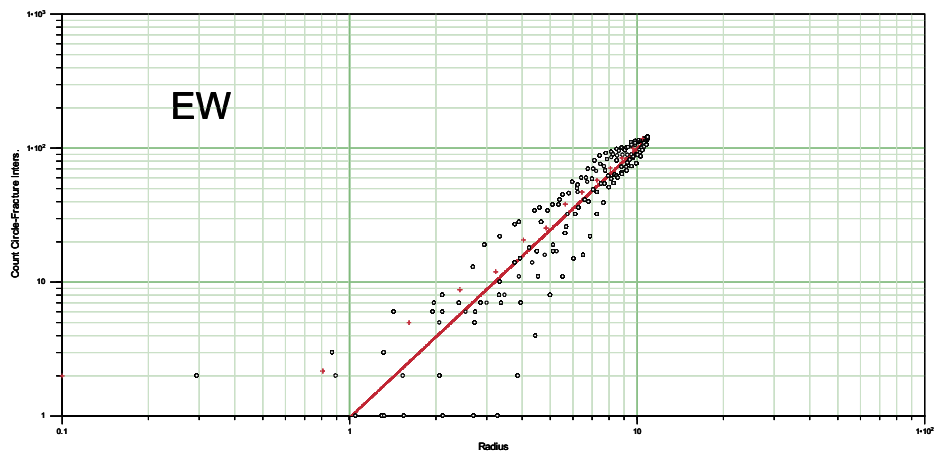
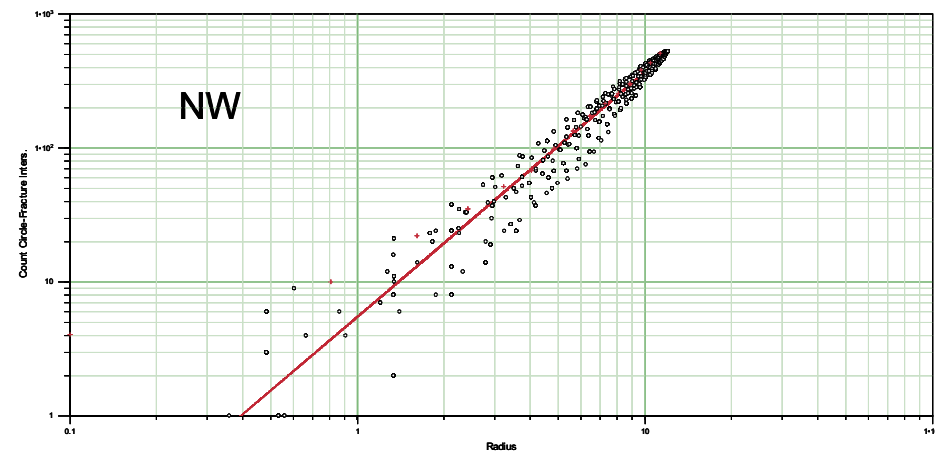
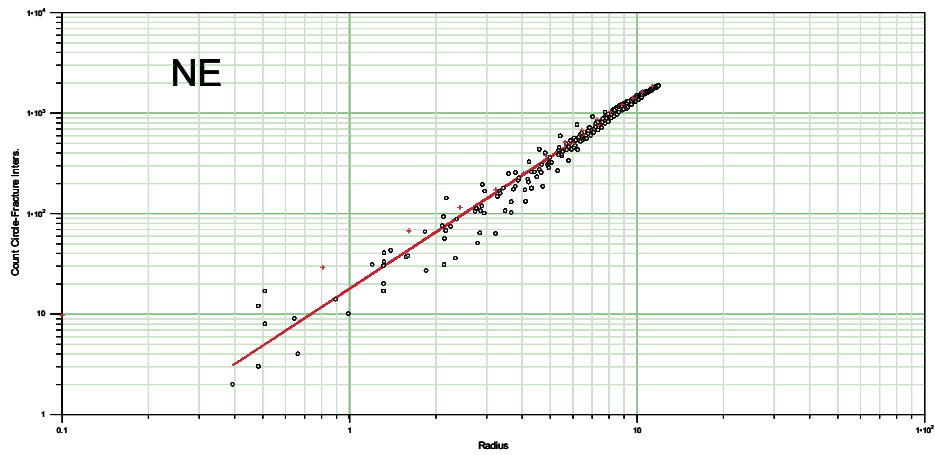
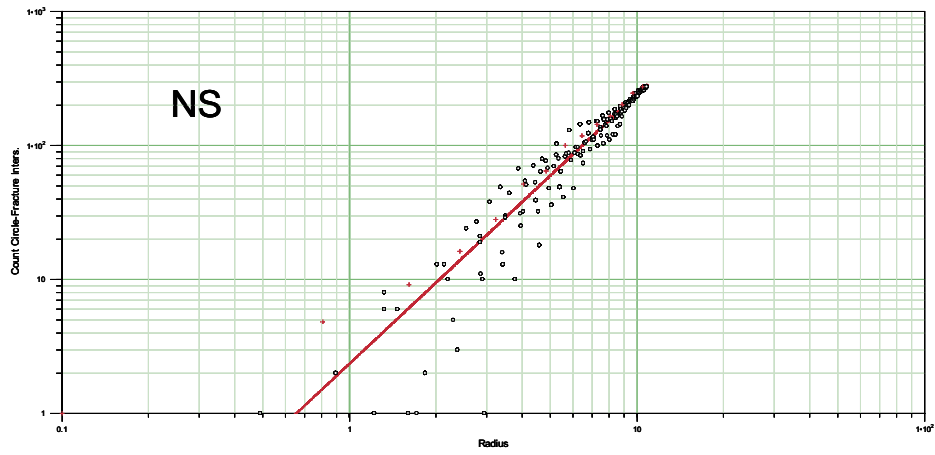


Figure 6-16. Mass dimension calculations for individual fracture sets identified in outcrop AFM001097.

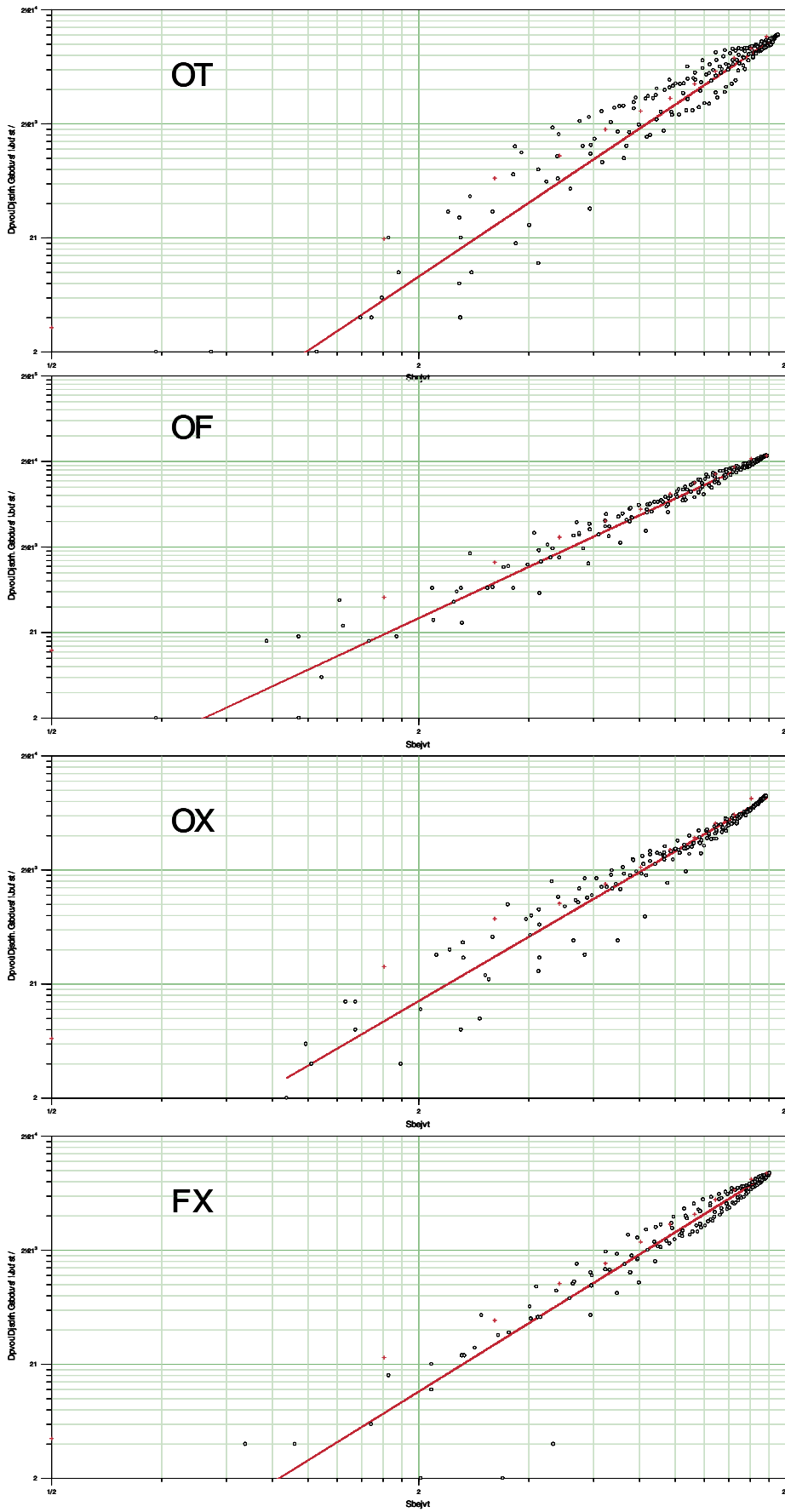


Figure 6-17. Mass dimension calculations for individual fracture sets identified in outcrop ASM001098.

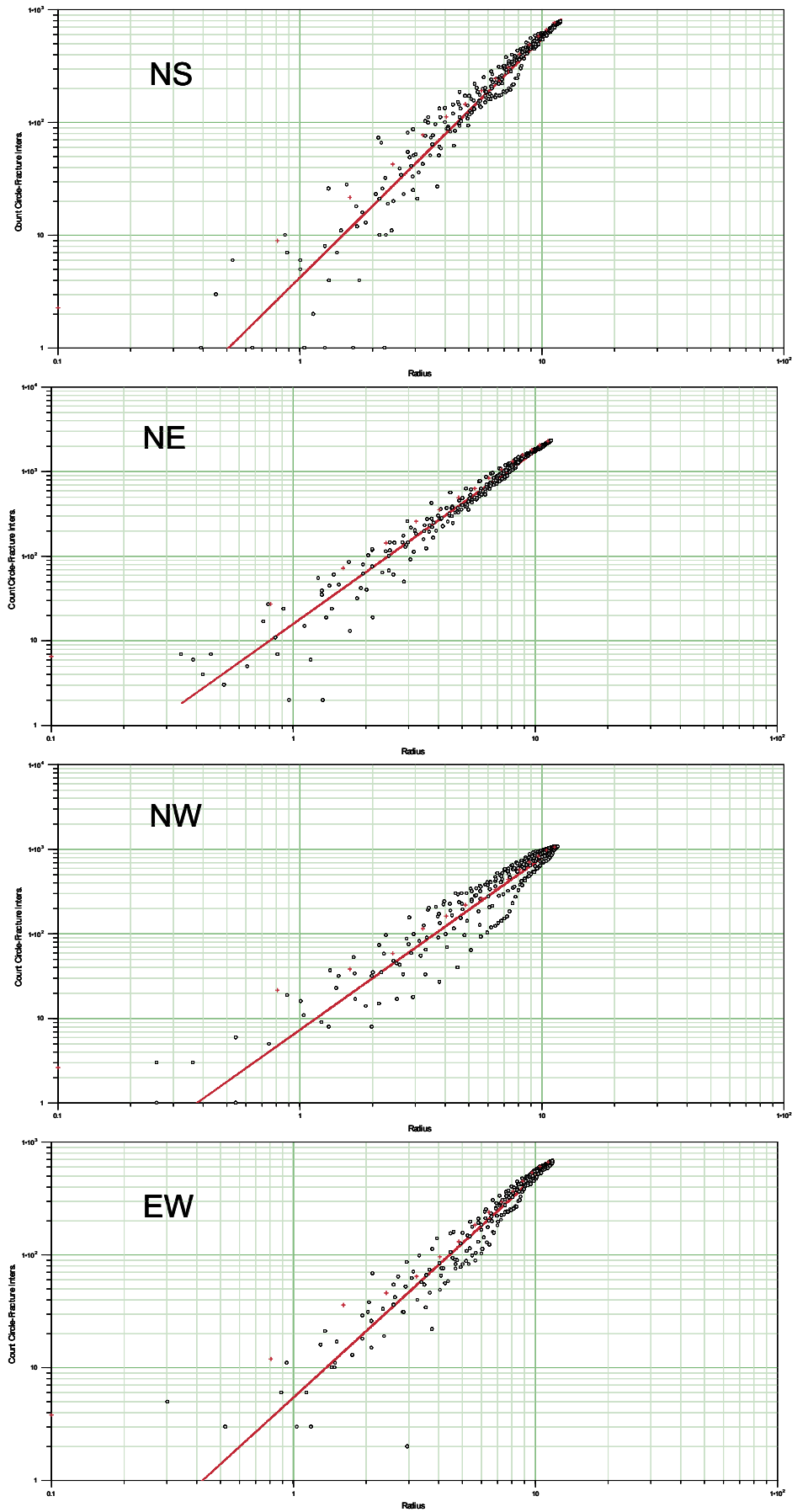


Figure 6-18. Mass dimension calculations for individual fracture sets identified in outcrop ASM100201.

Table 6-9 shows the areas used for each outcrop that were used in normalizing the trace length plots. The effective radius refers to the radius of a circle with area equal to the area of the outcrop.

Table 6-8. Mass dimension parameters for the outcrop data sets

Outcrop	Set Name	ρ	D_{mass}	Sum of Squared Errors	Standard Deviation of Errors
AFM000053	L1 (NS)	1.08	2.00	83,381	9.68
AFM000053	L2 (NE)	3.38	1.92	1.87E+06	24.98
AFM000053	L3 (NW)	4.21	1.83	1.70E+06	23.78
AFM000053	L4 (EW)	3.31	1.97	2.82E+06	30.94
AFM000054	L1 (NS)	1.63	1.97	279,175	9.80
AFM000054	L2 (NE)	6.70	1.91	2.19E+06	26.95
AFM000054	L3 (NW)	2.94	1.93	1.02E+06	18.72
AFM000054	L4 (EW)	1.65	1.91	458,540	12.57
AFM001097	L1 (NS)	2.37	2.01	648,772	15.02
AFM001097	L2 (NE)	18.00	1.88	1.16E+07	62.16
AFM001097	L3 (NW)	5.54	1.83	2.06E+06	26.29
AFM001097	L4 (EW)	0.98	2.01	310,234	10.27
AFM001098	L1 (NS)	4.60	2.16	3.59E+06	35.29
AFM001098	L2 (NE)	14.79	2.00	5.43E+06	42.82
AFM001098	L3 (NW)	7.12	1.88	1.50E+06	22.57
AFM001098	L4 (EW)	5.78	2.00	1.23E+06	20.60
AFM100201	L1 (NS)	4.24	2.12	3.43E+06	34.54
AFM100201	L2 (NE)	15.95	2.04	2.02E+07	82.56
AFM100201	L3 (NW)	7.39	2.04	3.56E+07	110.25
AFM100201	L4 (EW)	5.46	1.96	3.78E+06	36.08

Table 6-9. Areas and effective radii used for mass dimension calculations.

Outcrop	Area (m ²)	Effective Radius (m)
AFM000053	600	13.82
AFM000054	550	13.23
AFM001097	525	12.93
AFM001098	325	10.17
AFM100201	488	12.46
Lineament Map	161,019,975	7,159.21

The trace length scaling plots (Figure 6-19 through Figure 6-22) show the renormalized data and three lines fit visually to the data. These plots are defined in Section 5.3.2. All linked lineaments longer than 1,000 m are used for the size analysis. The lines labelled as “Upper” and “Lower” represent the upper and lower bounds on the data, and are quantifications of the uncertainty in the trace length scaling calculations. The median line is the visual best fit to the data (all outcrop and lineament data). The two bounding cases (identified as upper and lower) are lines that approximate the shallowest and steepest lines that could be fit through the data. These represent the span of possible size variation given the existing data. The slope of the line is labelled as k_t . To avoid confusion, the intercept is not shown.

The calculation of the size of the traces involves simulation. It is based on simultaneously matching both outcrop and borehole data. As explained in Section 5, the exponent describing the radius distribution of the fractures, k_r , is equal to $k_t + 1$. The minimum size radius value, x_{r0} , is not determinable from the area-normalized cumulative number plots.

The calculation of the value for x_{r0} was carried out by domain. In order to make these calculations, it is necessary to have a target P_{21} and P_{10} for each set. Domain 29 has the most abundant borehole and outcrop data, and so it was selected for calibration. As there is no indication at the current stage of site investigation that fractures in Domain 29 differ in size from fractures in other domains, nor that fractures designated as sealed differ from those designated as open, the minimum radius exponent for each set estimated from Domain 29 are assumed to be useful for other rock domains. This assumption should be checked as additional future data from other domains makes it possible to robustly estimate fracture sizes for domains other than 29.

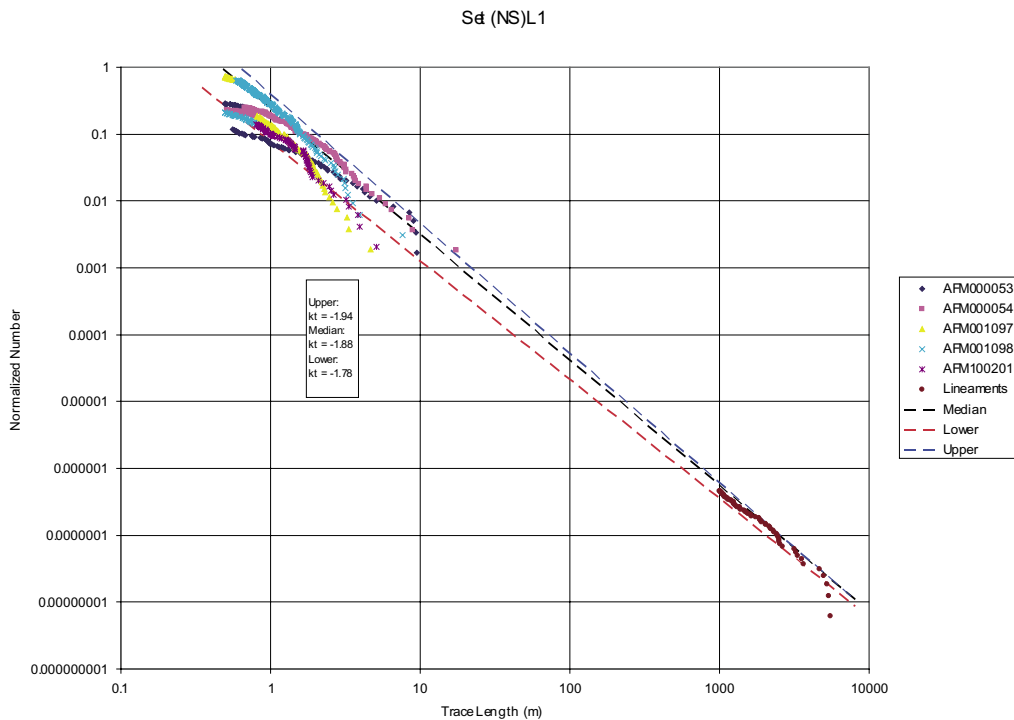


Figure 6-19. Trace length scaling plot for the NS set.

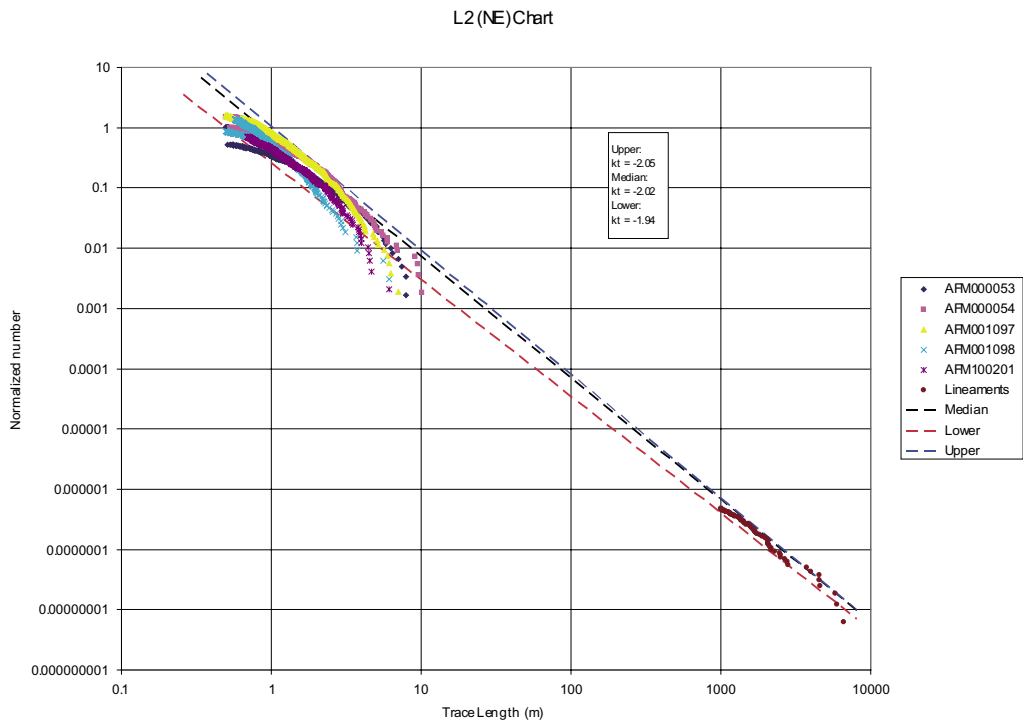


Figure 6-20. Trace length scaling plot for the NE set.

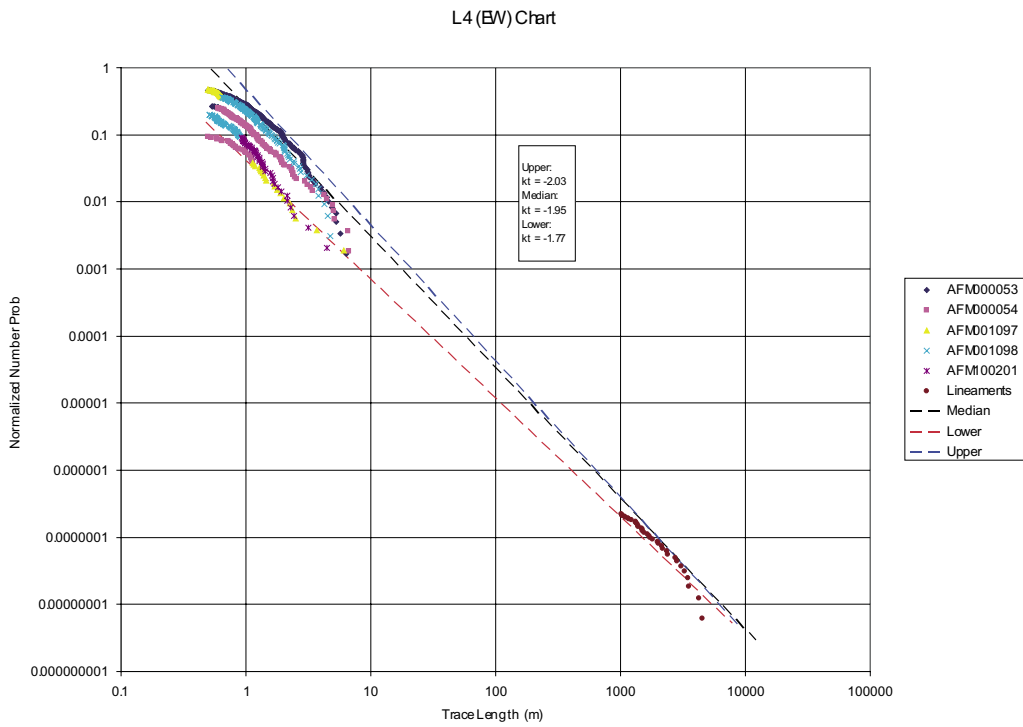


Figure 6-21. Trace length scaling plot for the EW set.

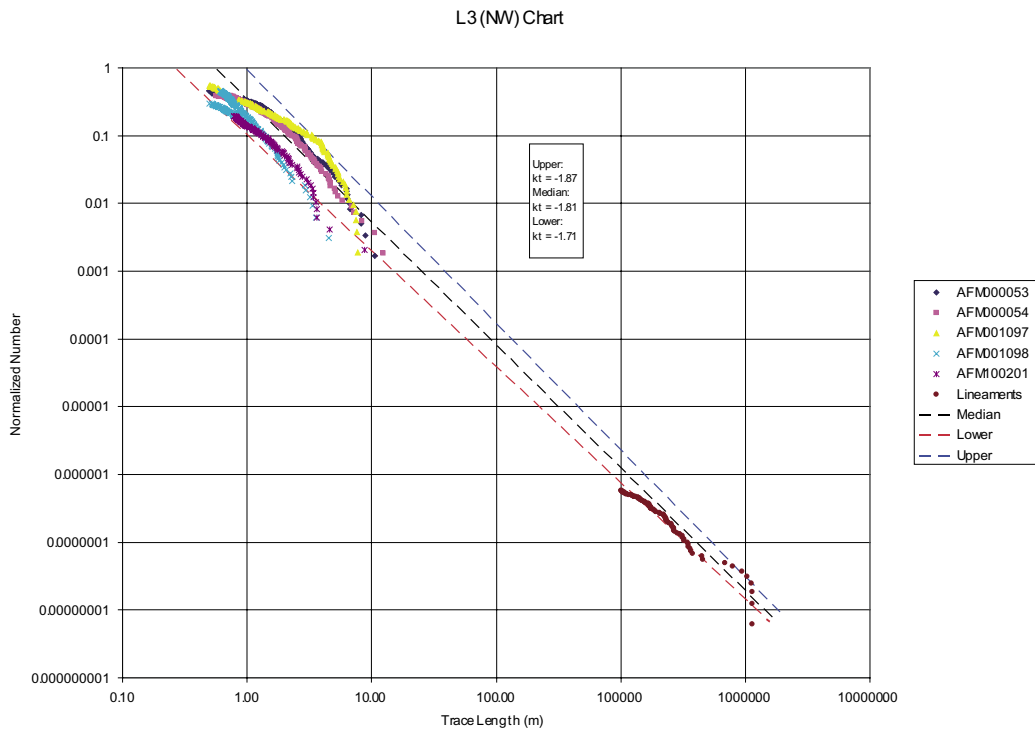


Figure 6-22. Trace length scaling plot for NW set.

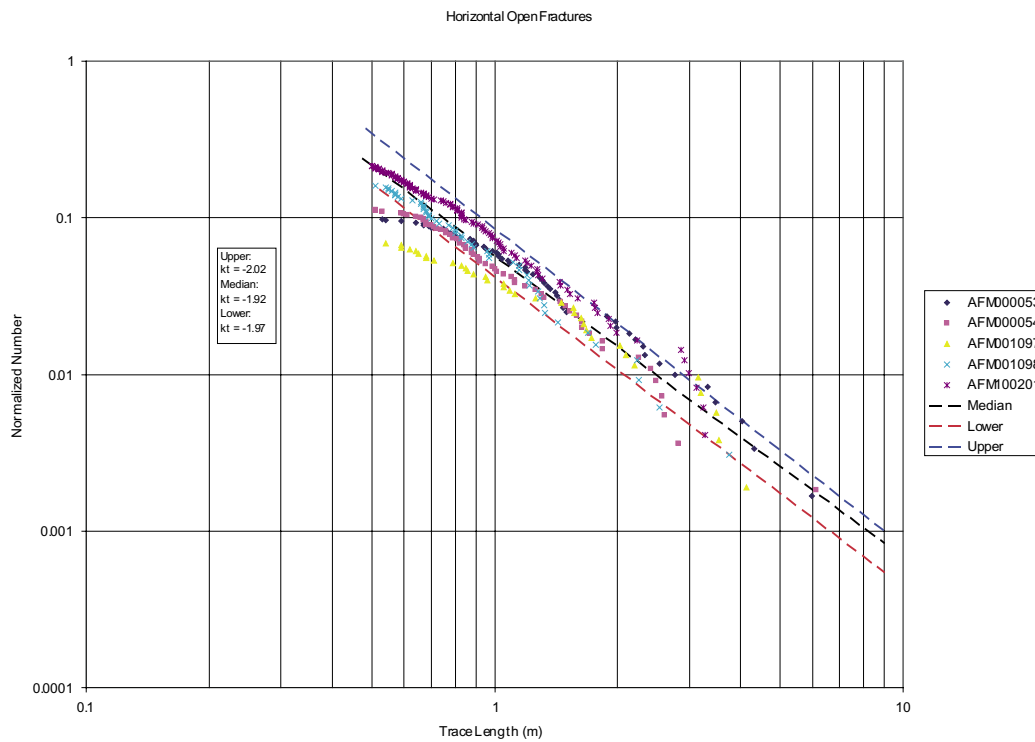


Figure 6-23. Trace length scaling plot for Horizontal set.

The target P_{21} and P_{10} values for each set are listed in Table 6-10, along with the basis for their calculation.

Monte Carlo simulations for combinations of P_{32} and x_{r0} for each set were run, using the value of k_r calculated from the trace length scaling plots (Figure 6-19 through Figure 6-22). The results of the matches are shown in Table 6-11.

The results for the calculations for the parent population are given in Table 6-12. The table gives the parameters for the parent fracture radius distribution exponent for the upper, median and lower bound lines. The value of x_{r0} corresponding to the upper and lower bound lines was not calculated as there were no equivalent values in the cored boreholes to use for simulation matching. If such values are needed, then corresponding minimum or maximum outcrop P_{21} and borehole P_{10} values would first need to be identified.

The size distribution of subhorizontal fractures is very difficult to assess as the only source of information is outcrops which present a bias towards subvertical fractures. Analyses of the mineral filling in the different fracture orientation sets showed that some of these fractures also have epidote mineralogy that suggests at least some of these subhorizontal fractures are old. In that sense their size distribution might be similar as the one identified for the subvertical sets and the subhorizontal fractures were fitted in a normalized plot.

Table 6-10. Values used for calculation of x_r through simulation.

Parameter	NS	NE	NW	EW	Horizontal
% Open out of total P_{21} by fracture set	19.80%	16.48%	21.49%	20.29%	19.90%
Total Open P_{21} (Domain 29)	0.33	1.17	0.67	0.4	0.18
Target P_{21}	0.07	0.19	0.14	0.08	0.03
% P_{10} in each set in cored boreholes in Domain 29	6.78%	24.90%	32.42%	15.85%	20.06%
Total Open and Partly Open P_{10} in cored boreholes, Domain 29	0.64 (from Table 6-23)				
Target P_{10}	0.043	0.159	0.207	0.101	0.128

Table 6-11. Results of simulations used to calculate x_{r0} .

Parameter	NS	NE	NW	EW	Horizontal
Target P_{21} (m^{-1})	0.07	0.19	0.14	0.08	0.03
Simulation Match P_{21} , traces truncated at 0.5 m. (m^{-1})	0.07	0.21	0.16	0.08	0.03
Target P_{10} (m^{-1})	0.043	0.159	0.207	0.101	0.128
Simulation Match P_{10} (m^{-1})	0.040	0.142	0.205	0.104	0.121
P_{32} (m^{-1})	0.10	0.276	0.35	0.18	0.085
x_{r0} (m)	0.28	0.25	0.14	0.15	0.25

Table 6-12. Fracture size parameters for fracture sets.

SET	Size model	Powerlaw (parent radius distribution)		
		Upper k_r	Median k_r/X_{r0}	Lower k_r
NS (L1)	Power law	2.94	2.88/0.28	2.78
NE (L2)	Power law	3.05	3.02/0.25	2.94
NW (L3)	Power law	2.87	2.81/0.14	2.71
EW (L4)	Power law	3.03	2.95/0.15	2.77
SubH	Power law	3.02	2.9/0.25	2.97

One of the interesting aspects of the results of the trace length fitting is how similar the size characteristics of the horizontal set appear to be to the subvertical, lineament-related sets. The horizontal trace set was fit entirely from outcrop data, and yet its dimension and constant term are within the variation of the vertical sets. This might imply that the horizontal set is also related to tectonic structures, but the lineaments of horizontal features are unlikely to be found in the lineament data sets.

Because the possibility exists from this plot that horizontal fractures may reach radii of hundreds or more meters in extent, which would have significant impact on flow and transport predictions, it is worthwhile to focus on conducting future studies to determine how large these subhorizontal fractures might indeed be.

6.3 Spatial model

The spatial model describes how the fracture pattern may change in terms of orientation, length and intensity throughout the region of interest. These changes may be best modelled by a statistical description for the entire region or for specific domains, or the pattern may relate to changes in the underlying mappable geology.

Deformation zones can needlessly complicate the analysis by obscuring how the fracture pattern changes, as these brittle and ductile zones have a spatial contiguity and higher intensity than fracturing in the surrounding rock. All the analyses described in this section are only for fractures outside brittle and ductile deformation zones.

The initial analyses focused on individual boreholes, with an emphasis on determining whether there were intervals along the wellbore where fracture intensity and orientation was homogeneous or heterogeneous.

If spatially homogeneous intervals were apparent, the next step was to assess if any of the measured geological parameters, such as rock type, alteration degree, rock domain, and so on, were associated with these intervals. While any association does not constitute a casual relation, it does indicate whether certain hypotheses are consistent or not consistent with the data.

As a final evaluation, all boreholes were compared in terms of fracture intensity. Fracturing that is spatially homogeneous must at least show evidence of similar intensity patterns among boreholes.

Taken together, the identification of intervals, the assessment of possible geological controls, and the comparison of intensity patterns among all boreholes provides the basis for postulating a spatial model and calculating its numerical parameters for fracturing outside the deformation zones.

Two different depth concepts are used in the analyses: measured depth (MD) and true depth vertical subsea (TVDS). The measured depth is the arc length from the reference point in each borehole. The TVDS refers to the true z-coordinate relative to sea level. The MD is used in all analyses where boreholes were studied per se, for example in the CFI plots that aim to identify intervals of more-or-less constant intensity in each borehole. Nevertheless TVDS is used for spatial correlation of high or low intensity intervals between boreholes.

6.3.1 Intensity intervals in individual boreholes

The delineation of intensity intervals was aided by calculating cumulative fracture intensity (CFI) plots for each well. A cumulative intensity representation is not biased by any choice of interval length, and also minimizes the impact of local variations in intensity. Small scale details of the fracture intensity are obscured by CFI plots, which makes it easier to identify large scale statistically homogeneous intensity domains. While conventional moving average plots may be very useful for identifying deformation zones and individual hydraulic conductors, the work on evaluating correlations between geology and intensity is considered better done through CFI plots. CFI plots are well-suited for identifying spatially contiguous domains of statistically homogeneous fracture intensity and evaluating possible geological factors that explain the intensity variations.

The rotary cored boreholes are of primary importance, as these boreholes typically extend to greater depths than the percussion boreholes. However, percussion boreholes typically include fracture information from within a few meters of the surface, which may be absent in the cored boreholes. Thus both are useful in determining whether spatially contiguous intensity patterns exist. Moreover, these analyses provide data on whether fracture intensity near the surface differs from that at depth. Such differences with depth might suggest that outcrop data may not represent fracturing within the proposed repository horizon, and that inferences and statistics calculated from outcrop data may require adjustment or a lower importance than borehole data. The results for the cored boreholes are shown in Figure 6-24 through Figure 6-29. The results for illustrative percussion borehole are shown in Figure 6-30 and Figure 6-31.

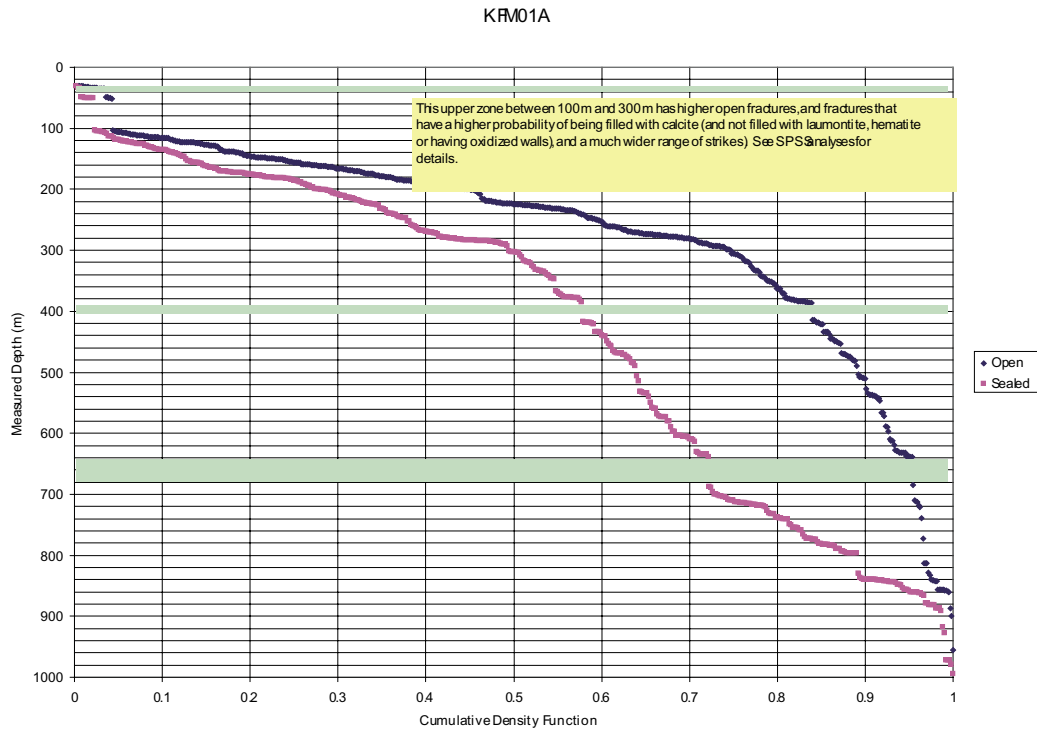


Figure 6-24. CFI plot for open and sealed fractures outside deformation zones for borehole KFM01A. Green shaded regions indicate identified ductile or brittle deformation zones (identified in one hole interpretation).

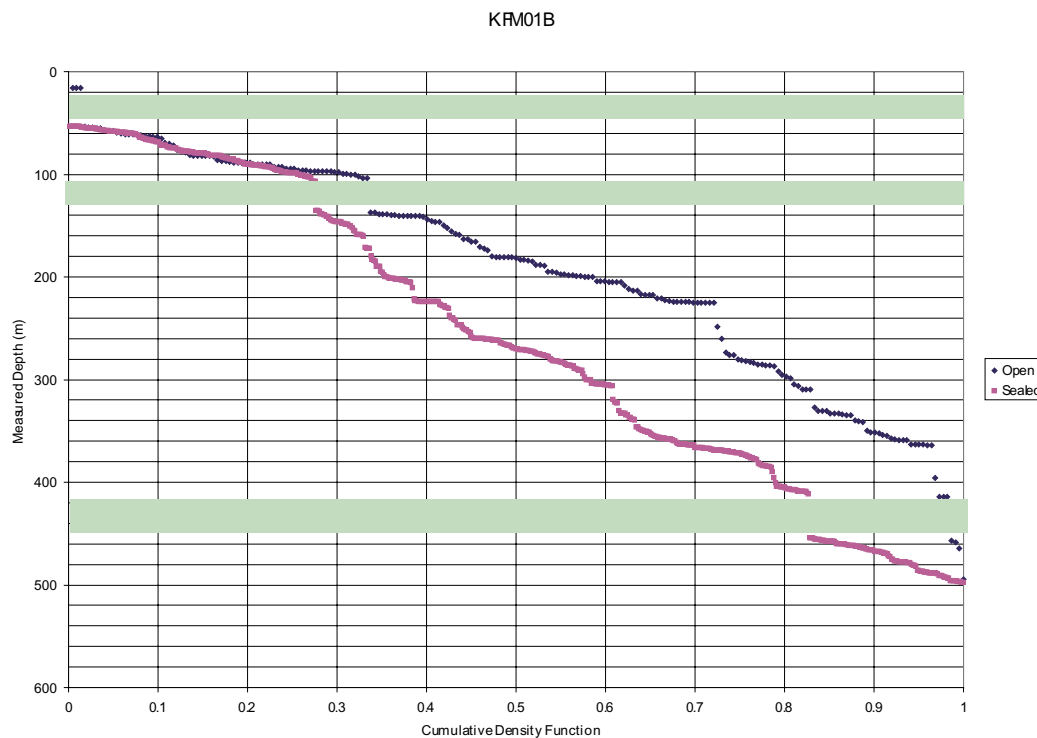


Figure 6-25. CFI plot for open and sealed fractures outside deformation zones for borehole KFM01B.

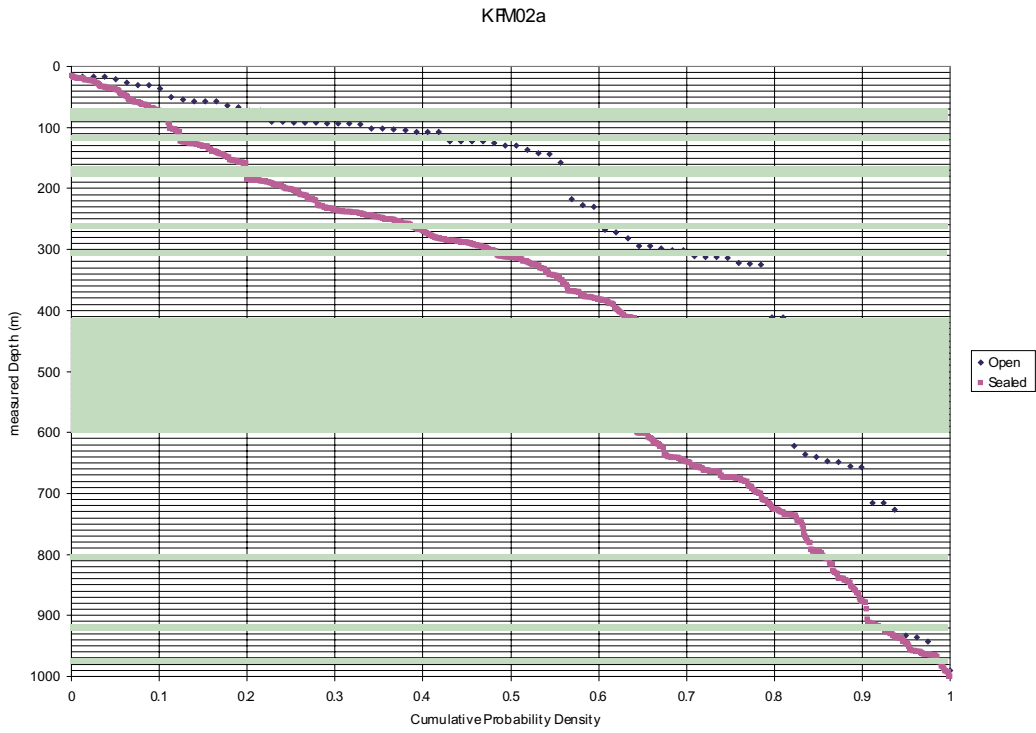


Figure 6-26. CFI plot for open and sealed fractures outside deformation zones for borehole KFM02A.

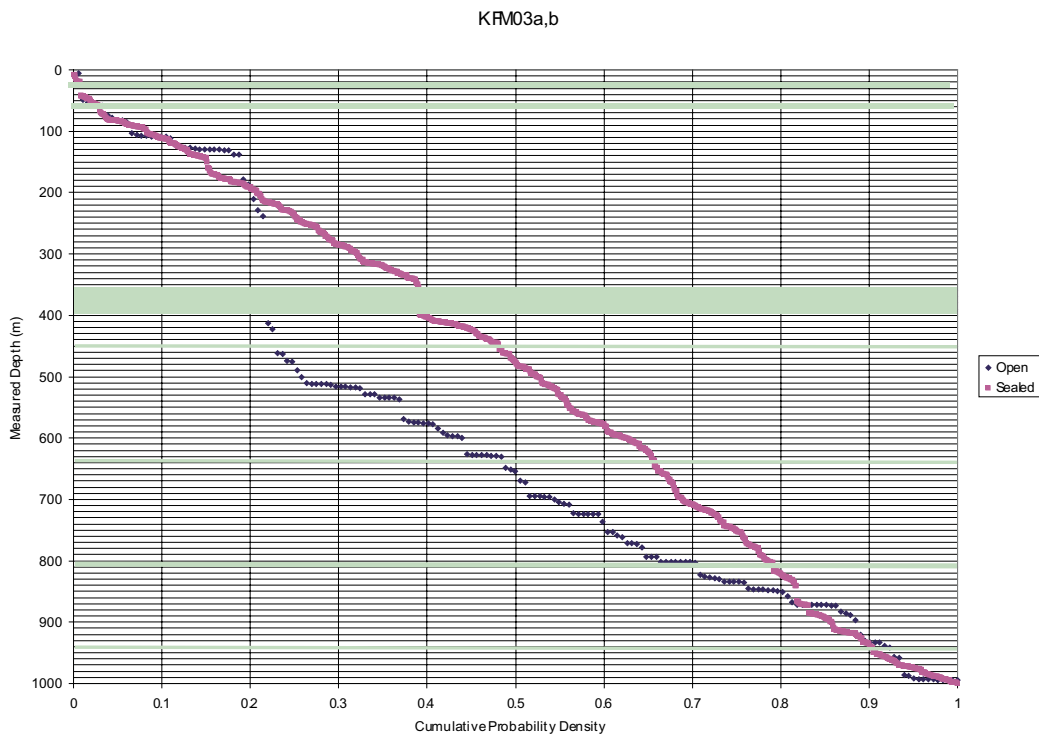


Figure 6-27. CFI plot for open and sealed fractures outside deformation zones for borehole KFM03A,B.

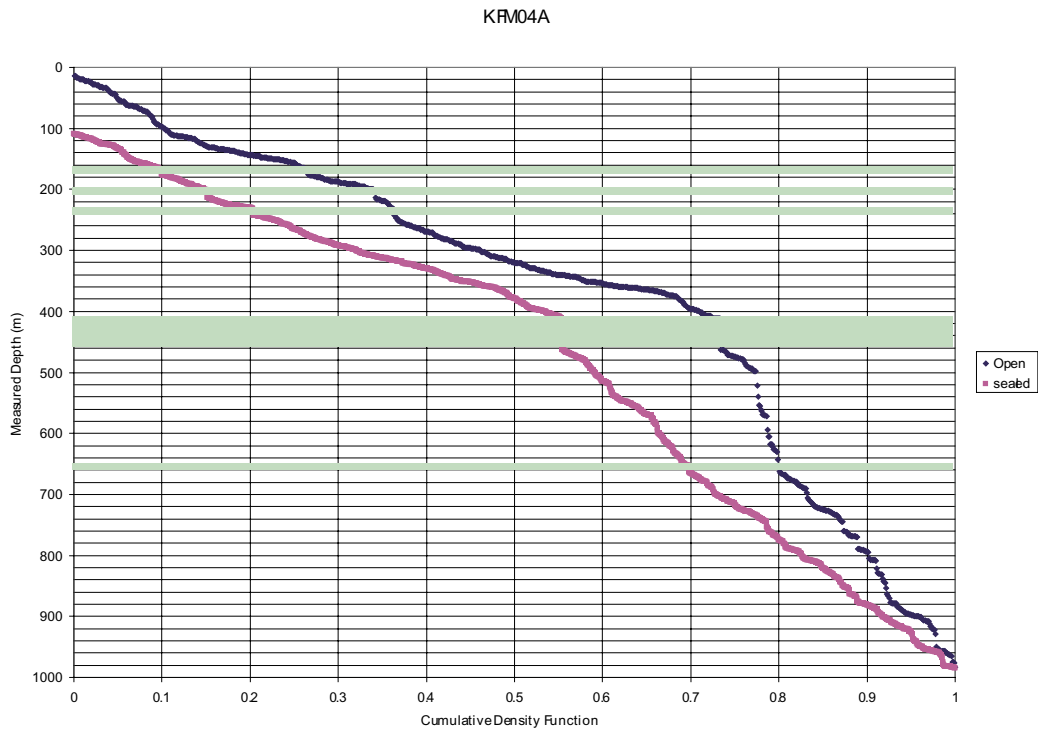


Figure 6-28. CFI plot for open and sealed fractures outside deformation zones for borehole KFM04A.

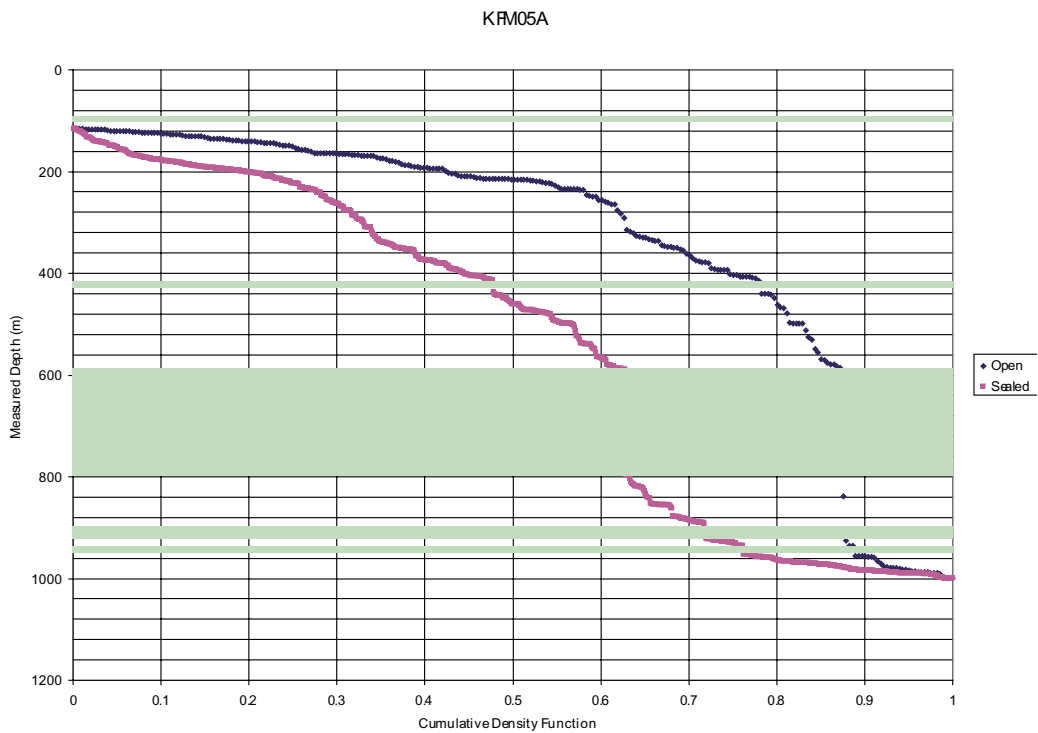


Figure 6-29. CFI plot for open and sealed fractures outside deformation zones for borehole KFM05A.

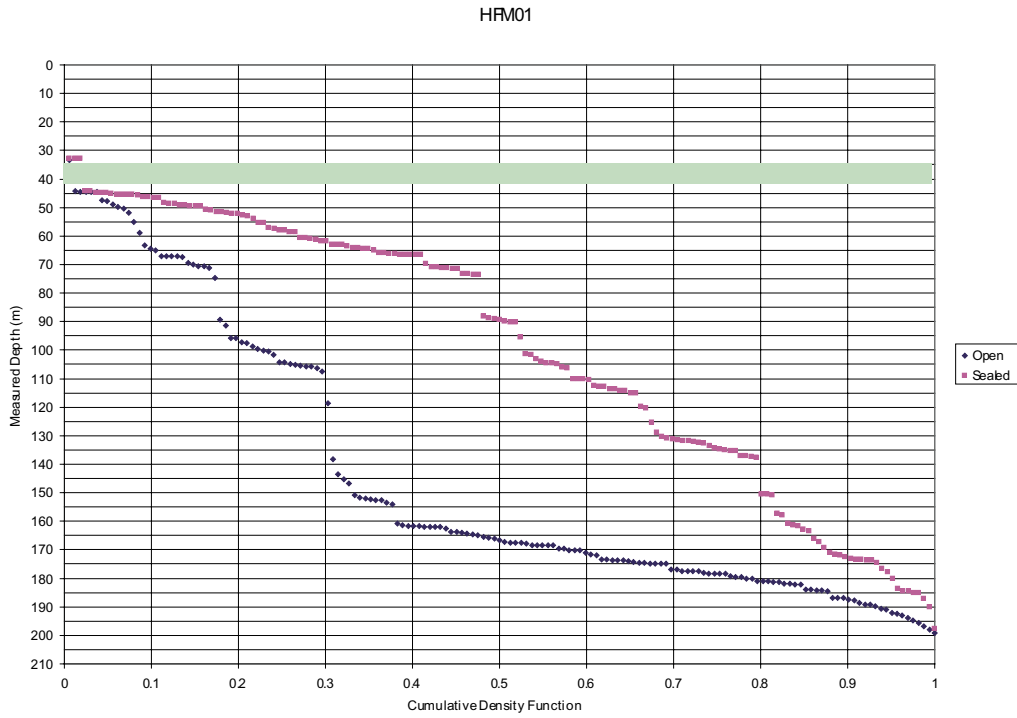


Figure 6-30. CFI plot for open and sealed fractures outside deformation zones for borehole HFM01.

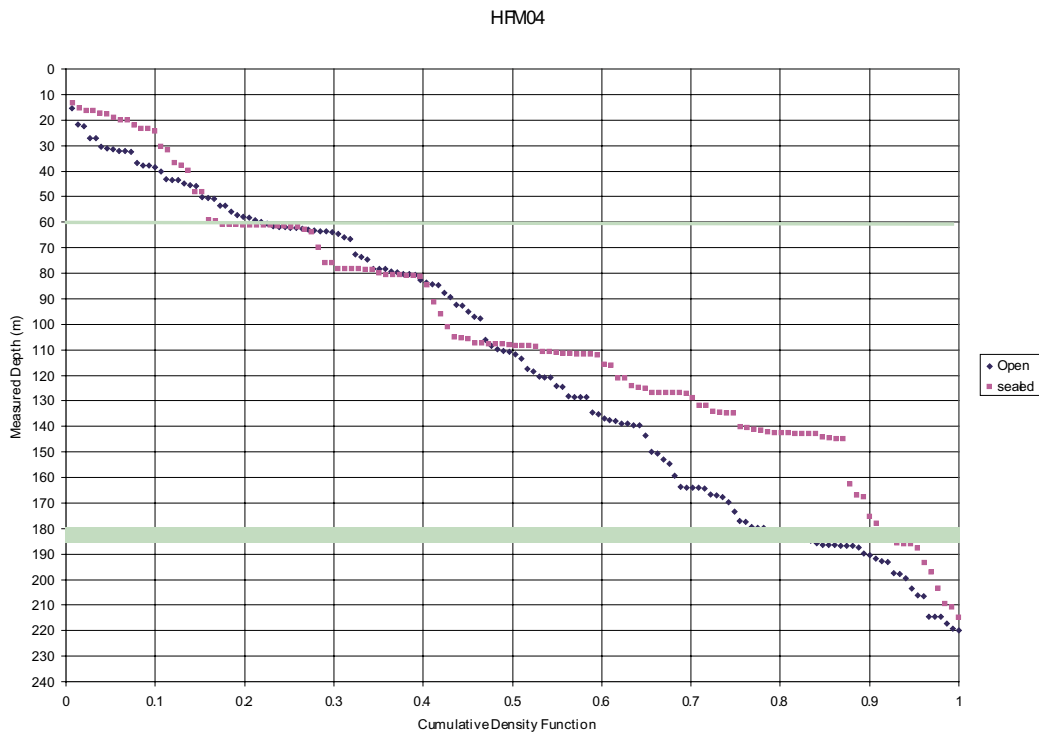


Figure 6-31. CFI plot for open and sealed fractures outside deformation zones for borehole HFM04.

These CFI plots show that there are one or two intervals of relatively constant fracture intensity that are spatially contiguous, and also a variety of intensity patterns with depth that are not consistent with surficial stress relief. For example, in KFM01A, the open fracture intensity between 30 and 50 m is much lower than the open fracture intensity between 100 and 200 m. In KFM04A, the open fracture intensity is constant between 10 m and 360 m. In HFM01, the open fracture intensity is highest in the lower 40 m of the borehole; in HFM04 there is little change in open fracture intensity from 10 m to over 200 m. In borehole KFM02A, the highest open fracture intensity extends from 10 m to over 250 m as a single zone.

All of these plots show no pattern consistent with surficial stress relief. The upper few meters do not show a higher open or sealed fracture intensity. While it is sometimes true that the upper intervals of the borehole have the highest fracture intensity, these intervals may extend a few meters or a few hundred meters in depth; moreover, there are an equal number of boreholes where the highest open fracture intensity is not the shallowest interval.

Figure 6-32 shows the cumulative number of open fractures vs measured depth for all percussion boreholes. There is little evidence to support the hypothesis that fracturing is more intense near the surface. Rather, there are three types of patterns: constant intensity with depth; slightly decreasing intensity with depth; and variations in intensity that show no obvious pattern with depth. This is also apparent when fracture intensity is averaged over 10 m intervals and plotted as a function of measured depth (Figure 6-33).

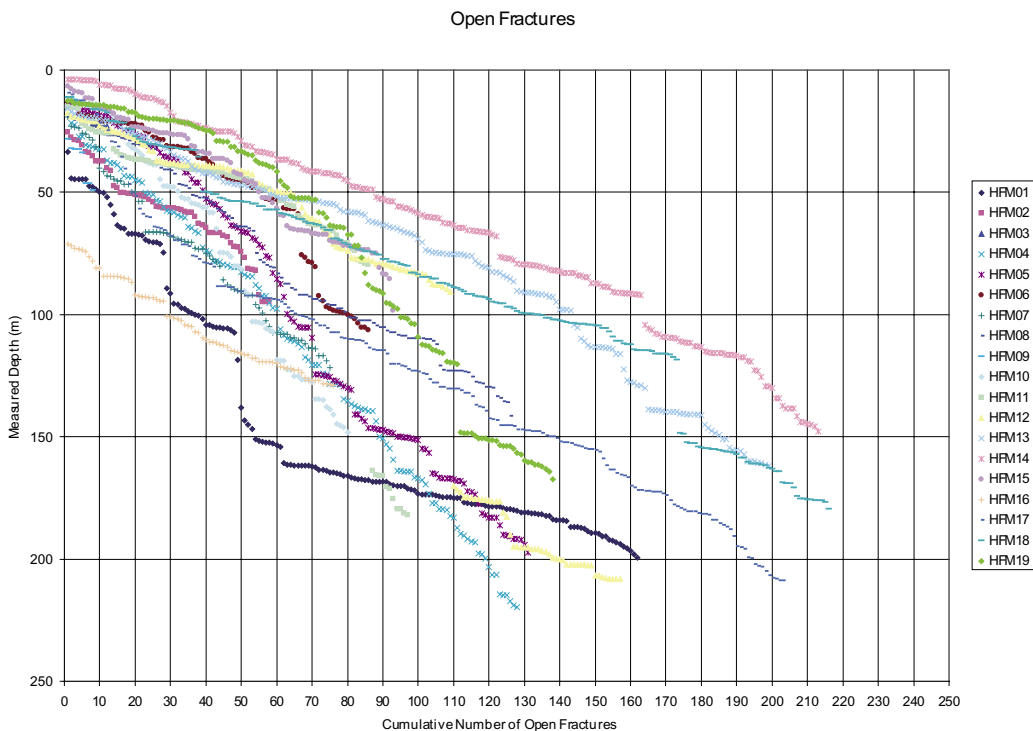


Figure 6-32. Cumulative number of open fractures vs measured depth for all percussion boreholes.

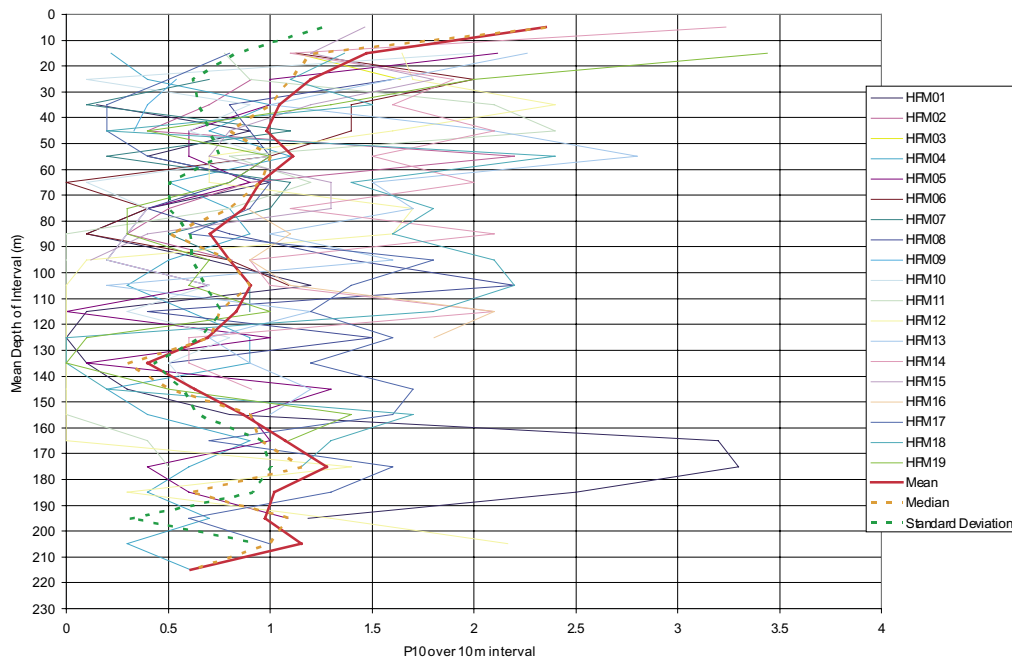


Figure 6-33. Open fracture intensity over 10 m intervals as a function of measured depth, all percussion boreholes.

6.3.2 Relation of fracture intensity and geological factors

The next series of investigations focused on determining whether any recorded geological factors were associated with higher or lower fracture intensities. This involved two series of analyses:

1. Statistical tests for the association of intensity with geological factors; and
2. Plots of orientation vs depth.

The reason for the plots of orientation vs depth was a part of the investigation of why fracture intensity might vary with depth. As it turns out, the presence of additional fracture sets, particularly the subvertical northwesterly striking set, is often associated with zones of higher open fracture intensity. The 2-way contingency table results and their associated statistics are shown for fracture openness and rock domain in Table 6-13 through Table 6-16. The other tables are shown in Appendix 2. The statistical tests evaluate the null hypothesis that intensity is not associated with a particular variable. Significance values below 0.05 are interpreted as a rejection of this null hypothesis at a statistically significant probability.

The results for fracture openness (Table 6-13 and Table 6-14) show that the high intensity fracture intervals (identified as 1.0 in the following tables) tend to have more open and partially open fractures, and fewer sealed fractures, than the normal or low intensity intervals (identified as .0 in the following tables).

Table 6-13. Contingency table of fracture openness vs fracture intensity.

Crostab

			OPENNESS			Total	
			Open	Partly	Sealed		
SHIZ	.0	Count	1	1,134	185	5,800	7,120
		Expected Count	.7	1,660.3	241.4	5,217.6	7,120.0
		% within SHIZ	.0%	15.9%	2.6%	81.5%	100.0%
		% within OPENNESS	100.0%	45.3%	50.8%	73.7%	66.3%
		% of Total	.0%	10.6%	1.7%	54.0%	66.3%
	1.0	Count	0	1,369	179	2,066	3,614
		Expected Count	.3	842.7	122.6	2648.4	3,614.0
		% within	.0%	37.9%	5.0%	57.2%	100.0%
		% within OPENNESS	.0%	54.7%	49.2%	26.3%	33.7%
		% of Total	.0%	12.8%	1.7%	19.2%	33.7%
Total		Count	1	2,503	364	7,866	10,734
		Expected Count	1.0	2,503.0	364.0	7,866.0	10,734.0
		% within SHIZ	.0%	23.3%	3.4%	73.3%	100.0%
		% within OPENNESS	100.0%	100.0%	100.0%	100.0%	100.0%
		% of Total	.0%	23.3%	3.4%	73.3%	100.0%

Table 6-14. Statistical test results for crosstabulation of fracture openness vs fracture intensity.

Chi-Square Tests

	Value	df	Asymp. Sig. (2-sided)
Pearson Chi-Square	728.239 ^a	3	.000
Likelihood Ratio	703.098	3	.000
N of Valid Cases	10,734		

^a 2 cells (25.0%) have expected count less than 5. The minimum expected count is .34.

Directional Measures

			Asymp.Std. Error ^a	Approx. T ^b	Approx. Sig.	
Nominal by Nominal	Lambda	Symmetric	.036	.008	4.702	.000
		SHIZ Dependent	.065	.013	4.702	.000
		OPENNESS Dependent	.000	.000	.c	.c
Goodman and Kruskal tau		SHIZ Dependent	.068	.005		.000 ^d
		OPENNESS Dependent	.059	.005		.000 ^d
Uncertainty Coefficient		Symmetric	.050	.004	13.222	.000 ^e
		SHIZ Dependent	.051	.004	13.222	.000 ^e
		OPENNESS Dependent	.048	.004	13.222	.000 ^e

^a Not assuming the null hypothesis.

^b Using the asymptotic standard error assuming the null hypothesis.

^c Cannot be computed because the asymptotic standard error equals zero.

^d Based on chi-square approximation.

^e Likelihood ratio chi-square probability.

Symmetric Measures

		Value	Approx. Sig.
Nominal by Nominal	Phi	.260	.000
	Cramer's V	.260	.000
	Contingency Coefficient	.252	.000
N of Valid Cases		10,734	

a. Not assuming the null hypothesis.

b. Using the asymptotic standard error assuming the null hypothesis.

Table 6-15. Contingency table of rock domain vs fracture intensity.

Crostab

		ROCK_DOM					Total
			RFM012	RFM017	RFM018	RFM029	
SHIZ	.0	Count	132	111	0	6,877	7,120
		Expected Count	1,194.6	73.6	358.2	5,493.6	7120.0
		% within SHIZ	1.9%	1.6%	0%	96.6%	100.0%
		% within ROCK_DOM	7.3%	100.0%	.0%	83.0%	66.3%
		% of Total	1.2%	1.0%	.0%	64.1%	66.3%
	1.0	Count	1,669	0	540	1,405	3,614
		Expected Count	606.4	37.4	181.8	2,788.4	3,614.0
		% within SHIZ	46.2%	.0%	14.9%	38.9%	100.0%
		% within ROCK_DOM	92.7%	.0%	100.0%	17.0%	33.7%
		% of Total	15.5%	.0%	5.0%	13.1%	33.7%
Total		Count	1,801	111	540	8,282	10,734
		Expected Count	1,801.0	111.0	540.0	8,282.0	10734.0
		% within SHIZ	16.8%	1.0%	5.0%	77.2%	100.0%
		% within ROCK_DOM	100.0%	100.0%	100.0%	100.0%	100.0%
		% of Total	16.8%	1.0%	5.0%	77.2%	100.0%

Table 6-16. Statistical test results for crosstabulation of rock domain vs fracture intensity.

Chi-Square Tests

	Value	df	Asymp. Sig. (2-sided)
Pearson Chi-Square	4,962.360 ^a	3	.000
Likelihood Ratio	5,228.092	3	.000
N of Valid Cases	10,734		

^a. 0 cells (.0%) have expected count less than 5. The minimum expected count is 37.37.

Directional Measures

			Asymp.Std. Error ^a	Approx. T ^b	Approx. Sig.	
Nominal by Nominal	Lambda	Symmetric	.386	.012	25.785	.000
		SHIZ Dependent	.575	.009	4.702	.000
		ROCK_DOM Dependent	.108	.021	4.767	.000
	Goodman and Kruskal tau	SHIZ Dependent	.462	.008		.000 ^c
		ROCK_DOM Dependent	.330	.008		.000 ^c
	Uncertainty Coefficient	Symmetric	.365	.007	44.960	.000 ^d
		SHIZ Dependent	.381	.008	44.960	.000 ^d
		ROCK_DOM Dependent	.349	.007	44.960	.000 ^d

^a Not assuming the null hypothesis.

^b Using the asymptotic standard error assuming the null hypothesis.

^c Based on chi-square approximation.

^d Likelihood ratio chi-square probability.

Symmetric Measures

		Value	Approx. Sig.
Nominal by Nominal	Phi	.680	.000
	Cramer's V	.680	.000
	Contingency Coefficient	.562	.000
N of Valid Cases		10,734	

^a Not assuming the null hypothesis.

^b Using the asymptotic standard error assuming the null hypothesis.

Table 1 and Table 2 in Appendix 2 show that high intensity intervals are found in certain lithologies, especially 101056 (Granodiorite, metamorphic) and 103076 (Felsic to intermediate volcanic rock, metamorphic), and less likely to be found in 101051 (Granite, granodiorite and tonalite, metamorphic), 101061 (Pegmatite, pegmatitic granite), 111058 (Granite, fine- to medium-grained), and 101054 (Tonalite to granodiorite, metamorphic). The high intensity intervals also occur in 101057 (Granite to granodiorite, metamorphic, medium-grained), but not with any higher probability than intervals of lower fracture intensity.

Considering these relations, it appears that the high intensity intervals preferentially occur in rock type groups A and B, and not in groups C and D /SKB, 2004/. Table 6-15 and Table 6-16 show interesting associations with rock domains. The high intensity intervals are positively associated with domains 12 and 18, and negatively associated with domains 17 and 29. Domains 12 and 18 are in relatively narrow, northwesterly-trending zones of high deformation (Figure 6-34). Domain 29 is a much larger region of lower deformation. Domain 17 is a tonalite/granodiorite body that is also in a region of lower deformation.

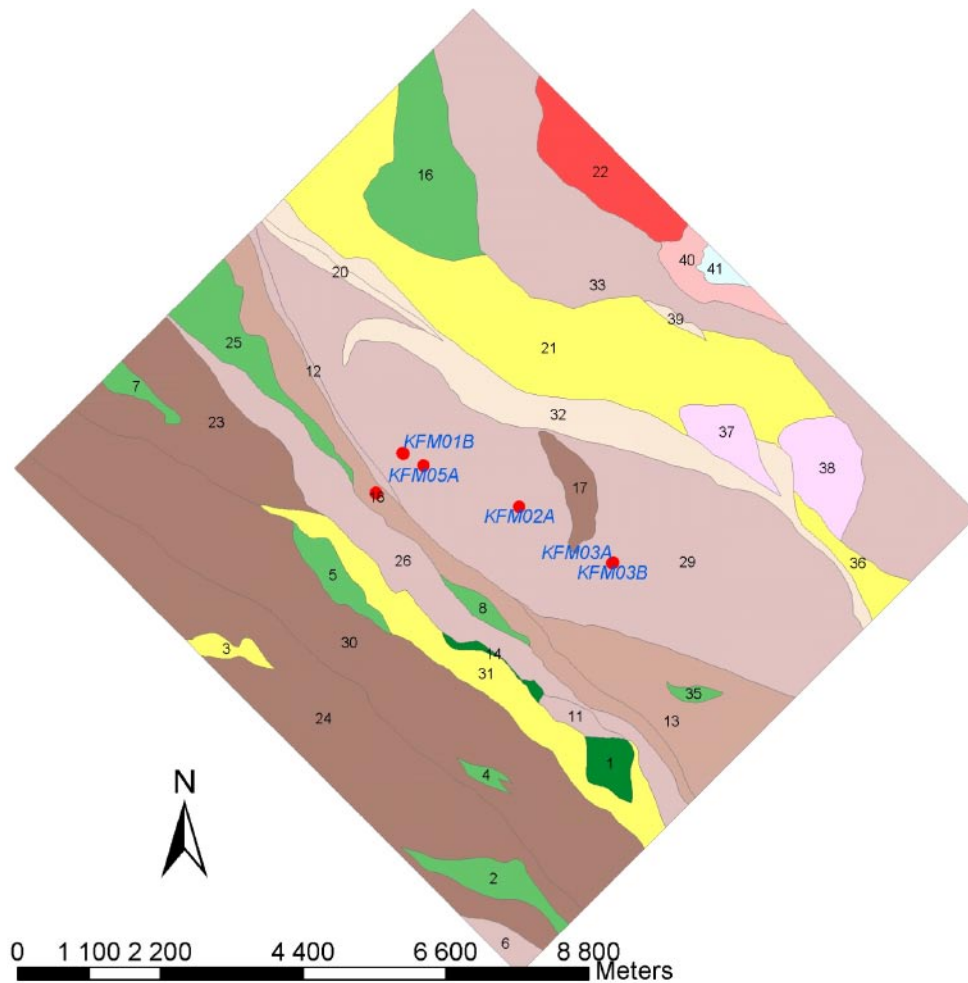


Figure 6-34. The rock domains at the surface in the model area.

The associations with primary and secondary (MIN1 and MIN2 variables) mineral fillings and high intensity intervals are shown in Table 3 through Table 6 in Appendix 2. The occurrence of minerals can be correlated to their sequence of mineralization (Table 6-17). The high intensity intervals fractures seem to be preferentially associated with primary calcite, epidote, pyrite and hematite fillings, and negatively associated with goethite, laumontite, oxidized walls and quartz.

In general, many of the fractures in the high intensity zones have a positive association with the first and second generation of mineral fillings, and negative associations with younger generations of mineralizations. The positive association with epidote is perhaps the clearest example, as epidote only occurs in the earliest mineralization. Positive associations with calcite and possibly prehnite are also examples. Quartz is ambiguous, as it occurs in generation 1 and Generation 4, as is chlorite and calcite. The negative association with clay minerals and laumontite (Generations 3, 4 and 5) are in keeping with this interpretation of the fractures in the high intensity intervals having a preferential association with the early generations of mineralization.

Table 6-17. Sequence of mineralizations at Forsmark (personal communication from E.-L. Tullborg).

Minerals	Gen 1	Gen 2	Gen 3	Gen 4	Gen 5
Quartz					
Epidote					
Titanite					
Kfsp		Adularia		Adularia	
Albite					
Prehnite					
Laumontite					
Calcite					
Pyrite					
Hematite					
Chlorite		Mg-Chlorite	Fe-Chlorite		Fe-Chlorite
Clay-mineral					
Analcime					
Barite					

However, consideration of the presence or absence only of a mineral infilling provides a different result. Table 6-18 shows the Kendall Tau correlation coefficients between the presence of a mineral in the fracture and the presence of the fracture in a zone of high intensity. The presence of epidote, for example, is given a value of 1 if epidote is present anywhere in the fracture, regardless of whether it is MIN1, MIN2, etc. This table shows that the strongest correlation is a negative one with oxidized walls, a strong positive correlation with pyrite, and weaker negative correlation with quartz, and weaker positive correlations with clay minerals and epidote. The positive correlation with pyrite and clay minerals, and the negative correlation with quartz suggests that fractures in the high intensity zones may be later stage (Stage 5, see Table 6-17), although the positive association with epidote does not support this hypothesis. In any event, it does not seem that fractures that are found in the high intensity zones have a mineral filling assemblage that ties them clearly to any single specific mineralization phase.

There is no strong association with roughness (Table 7 and Table 8 in Appendix 2).

Alteration is a mixed result, showing no clear pattern (Table 9 through Table 12 in Appendix 2). There are associations between some alteration classes and intensity, but the pattern is not consistent. For example, fractures in high intensity intervals have a positive association with ISRM class 3, a negative association with class 4, and a positive association with class 5. If there is an association with alteration, it is not strong.

Table 6-18. Kendall Tau correlation coefficients for mineral presence vs presence in a high intensity zone. Data are sorted from highest magnitude correlation (negative or positive) to lowest.

High Intensity Zone	Correlation Coefficient	Sig. (2-tailed)	N
OxidizedWalls	-0.189	0.000	10,734
Pyrite	0.131	0.000	10,734
Quartz	-0.097	0.000	10,734
ClayMinerals	0.073	0.000	10,734
Chlorite	0.061	0.000	10,734
Epidote	0.053	0.000	10,734
Hematite	0.045	0.000	10,734
RedFeldspar	-0.037	0.000	10,734
X9	-0.033	0.001	10,734
Biotite	-0.032	0.001	10,734
Calcite	0.024	0.014	10,734
Laumontite	0.019	0.053	10,734
Zeolites	-0.015	0.125	10,734
PotashFeldspar	-0.014	0.162	10,734
X1	-0.010	0.314	10,734
Goethite	0.009	0.372	10,734
WhiteFeldspar	-0.004	0.653	10,734
Prehnite	-0.001	0.932	10,734

The last two tables (Table 13 and Table 14 in Appendix 2) show the association of high intensity intervals with increased intensity of vertical fracturing as opposed to horizontal fracturing. The positive association is strongest with the northwest subvertical set. Graphs showing the presence of different fracture strike azimuths at depth (Figure 6-35 and Figure 6-36) and stereoplots of fracture orientations (Figure 6-37 through Figure 6-53) show that the presence of additional subvertical sets often distinguishes the high intensity intervals from the lower intensity intervals. The depth sections are identified from the CFI curves analysed in Section 6.3.1. The plots of TVDSS vs fracture strike have also been done for every borehole. These are presented in Appendix 3.

The high intensity interval in borehole KFM01A, roughly 0 to 300 m in measured depth, has much better developed subvertical northeasterly and northwesterly striking sets, than the lower intensity portion below this upper interval (Figure 6-37 and Figure 6-38). The high intensity interval in KFM01B, on the other hand, shows very little change in orientation (Figure 6-39 and Figure 6-41). Boreholes KFM04A and KFM05A also show high intensity intervals in their upper portions. The upper portion of KFM04A has a much broader range of fracture strikes (Figure 6-35) than the lower part, and a more intense amount of northwesterly-striking subvertical fracturing (Figure 6-47 and Figure 6-48). KFM05A, on the other hand, has more intense subhorizontal fracturing in the upper 100 m than in the interval of lower intensity between 200 to 600 m, yet this intermediate interval shows well-developed subvertical fracturing not commonly present in the high intensity interval above or the high intensity interval below (Figure 6-49 through Figure 6-51). HFM01 is interesting as the fracture data extends from near surface, rather than beginning 100 m or so below the surface. In this case, the intensity is lower in the upper interval (Figure 6-30) and higher in the lower interval for the open fractures. The stereoplots (Figure 6-52 and Figure 6-53) show that the high intensity interval is dominated by northwesterly striking subvertical fractures, while the lower intensity interval has mainly subhorizontal fractures.

While not conclusive, these plots suggest that:

- 1) Orientations of fractures are not constant with depth for the same borehole.
- 2) The intervals of higher or lower fracture intensity in a borehole almost always correspond to sections with distinct fracture orientation differences, usually the presence or absence of one or more fracture sets, rather than completely different orientations.
- 3) Most often, high intensity intervals are characterized by the additional presence of subvertical fracture sets.

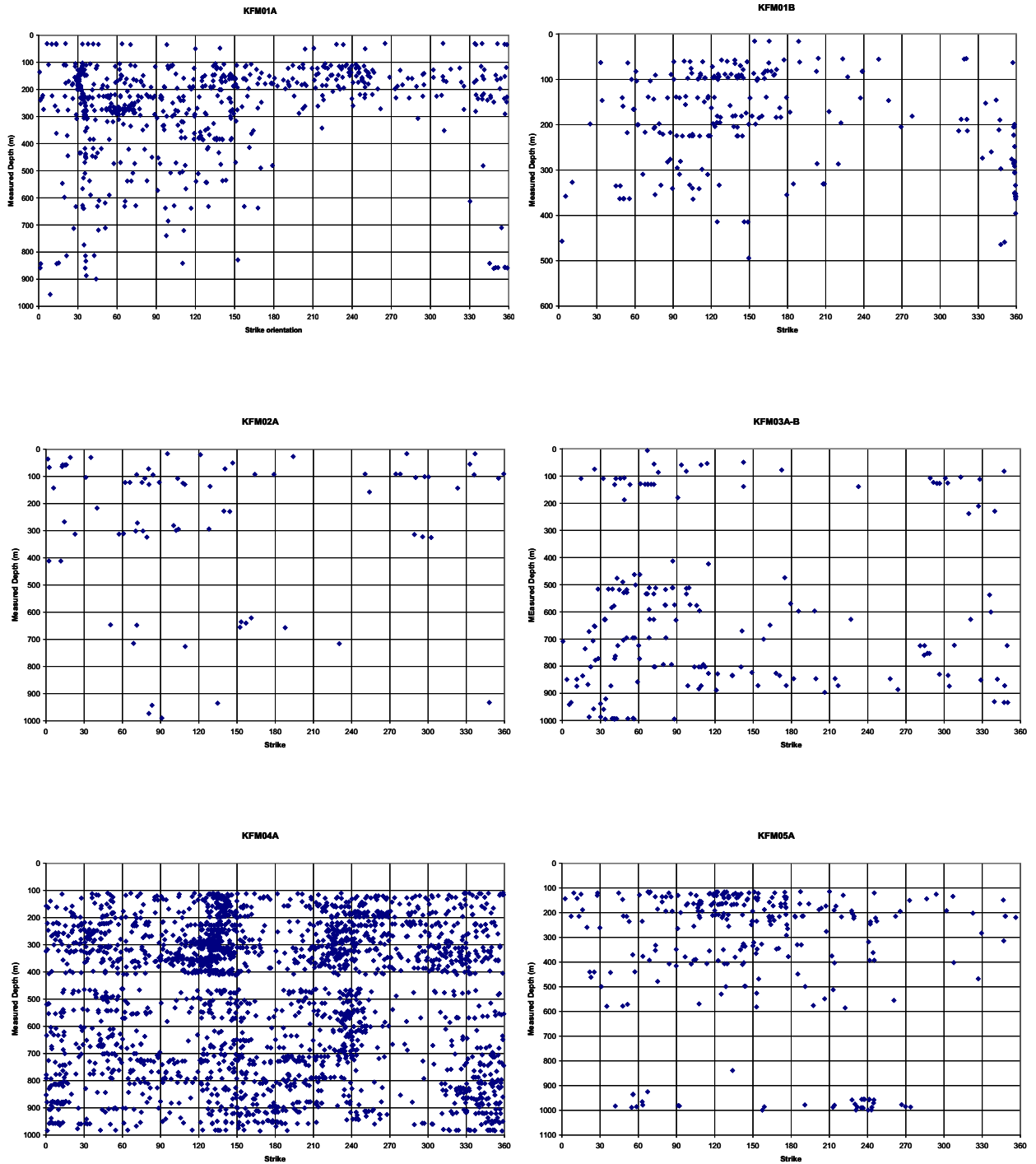


Figure 6-35. Variation of fracture strike with depth, cored boreholes KFM01A, KFM01B, KFM03A,B, KFM04A, and KFM05A, open fractures only.

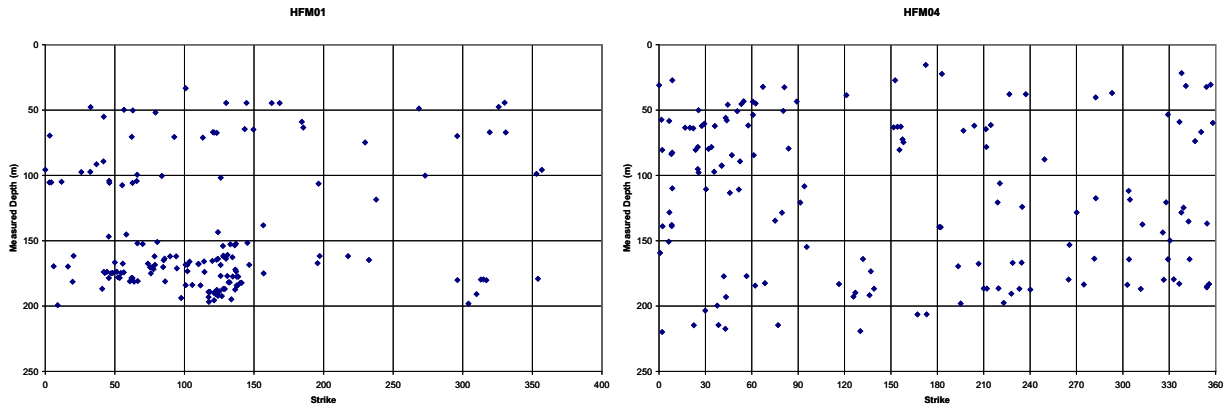


Figure 6-36. Variation of fracture strike with depth, percussion boreholes HSM01 and HSM04, open fractures only.

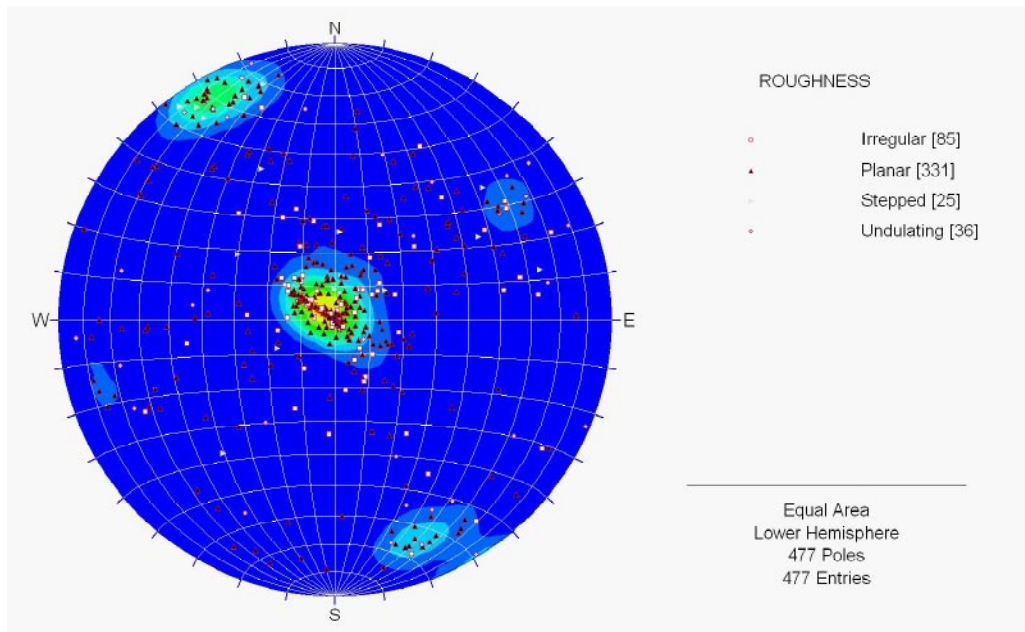


Figure 6-37. Stereoplot of poles to open fractures outside of deformation zones in the measured depth range 0 to 300 m, borehole KFM01A.

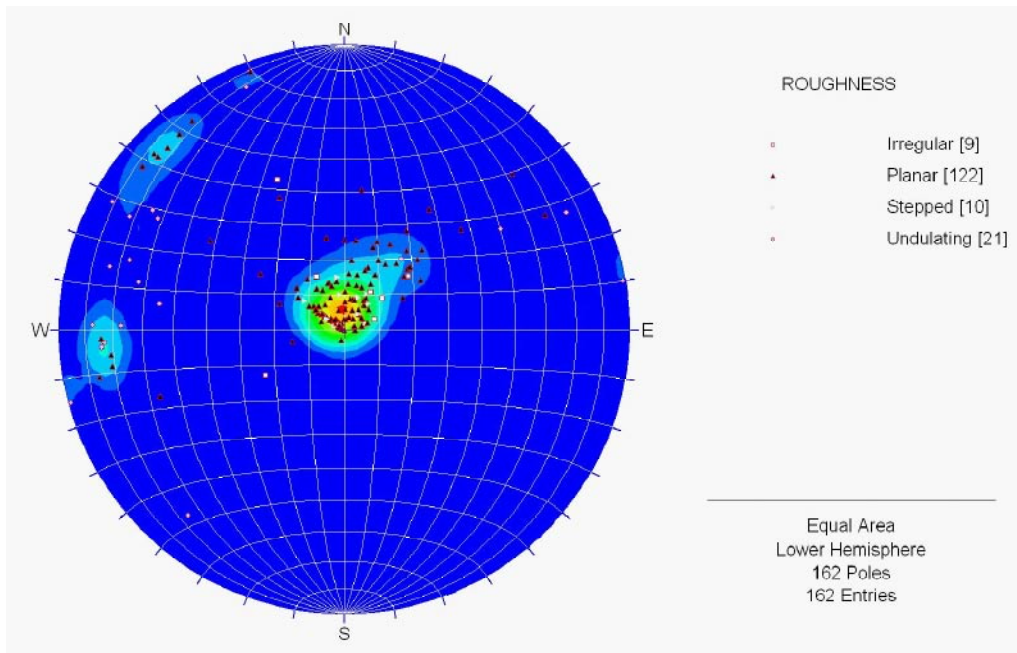


Figure 6-38. Stereoplot of poles to open fractures outside of deformation zones in the measured depth range 300 m to bottom, borehole KFM01A.

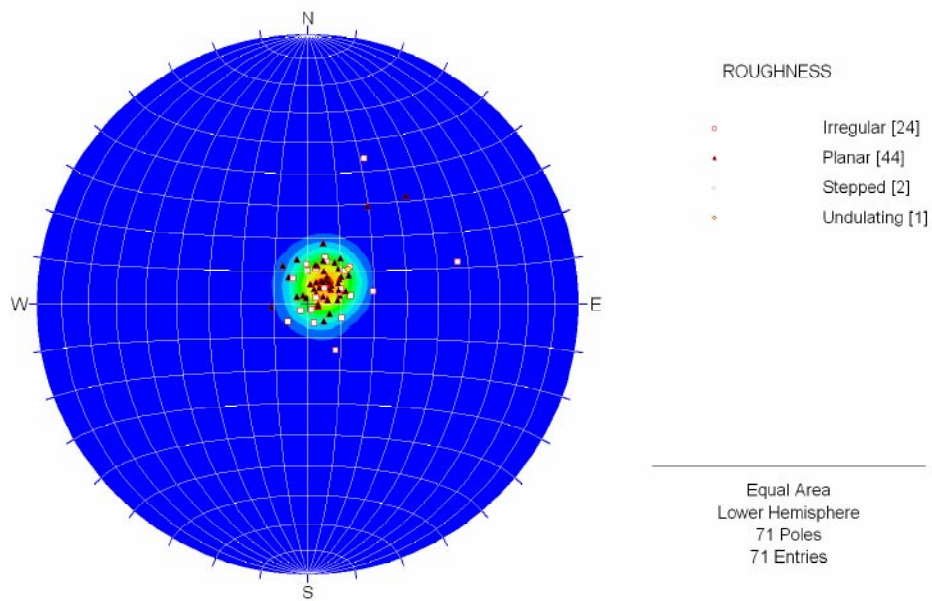


Figure 6-39. Stereoplot of poles to open fractures outside of deformation zones in the measured depth range 40 to 110 m, borehole KFM01B.

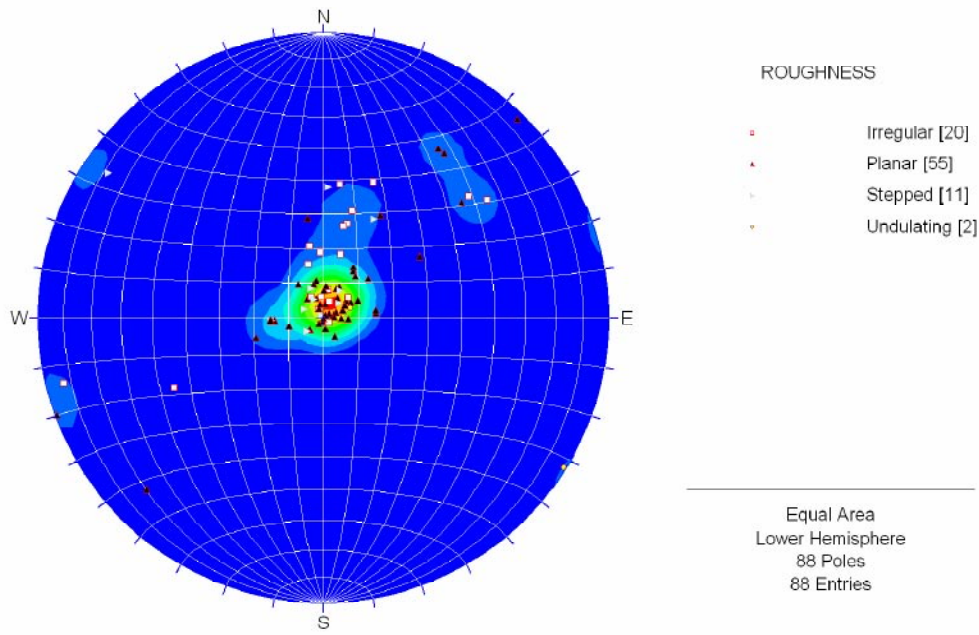


Figure 6-40. Stereoplot of poles to open fractures outside of deformation zones in the measured depth range 130 to 260 m, borehole KFM01B.

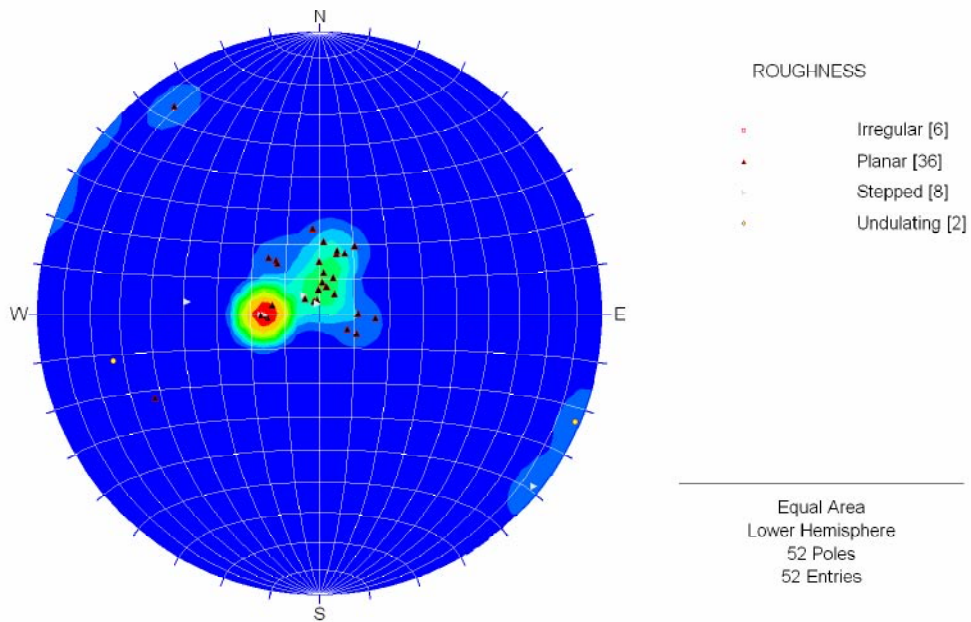


Figure 6-41. Stereoplot of poles to open fractures outside of deformation zones in the measured depth range 260 to 390 m, borehole KFM01B.

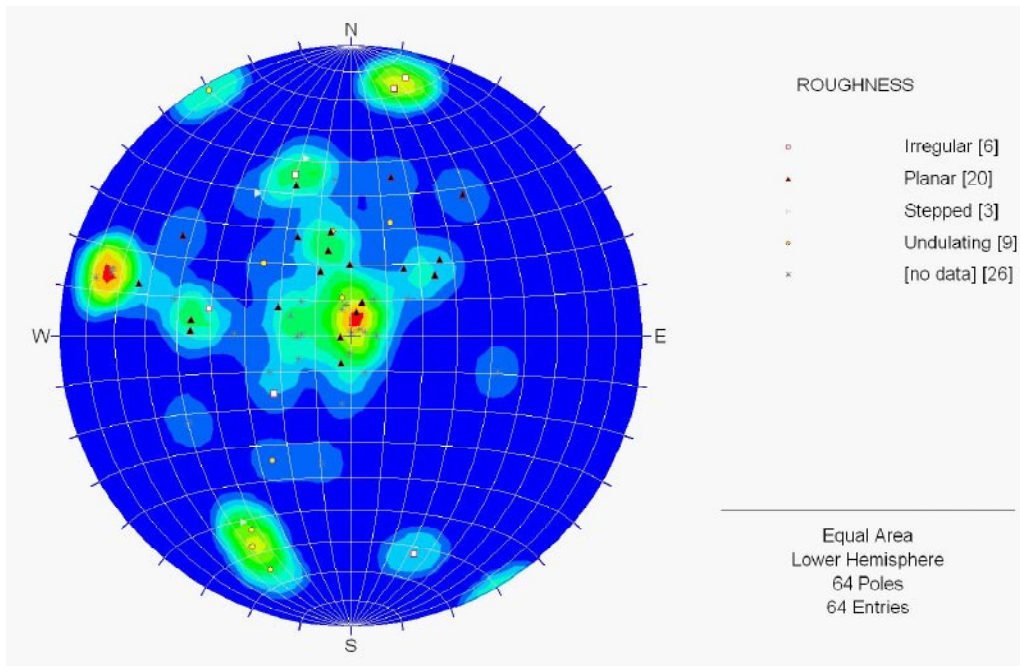


Figure 6-42. Stereoplot of poles to open fractures outside of deformation zones in the measured depth range 0 to 400 m, borehole KFM02A.

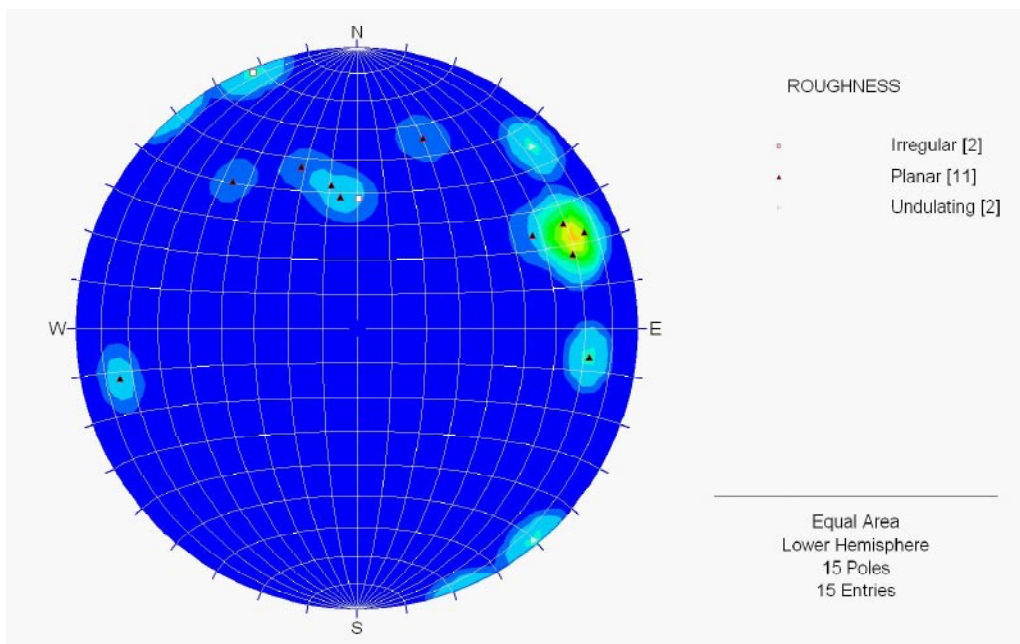


Figure 6-43. Stereoplot of poles to open fractures outside of deformation zones in the measured depth range 600 m to bottom, borehole KFM02A.

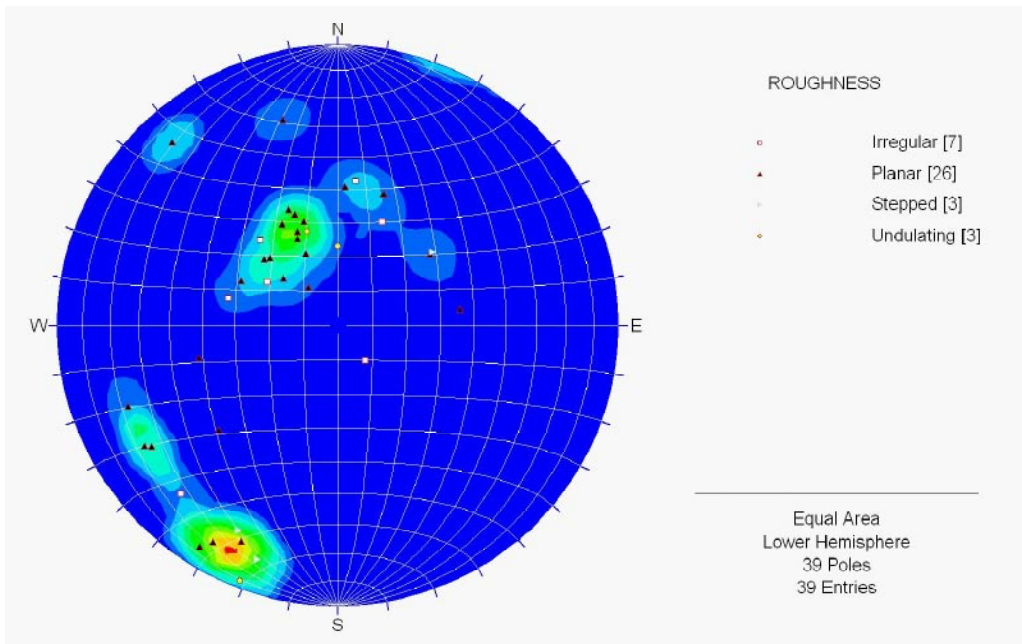


Figure 6-44. Stereoplot of poles to open fractures outside of deformation zones in the measured depth range 0 to 300 m, borehole KFM03A,B.

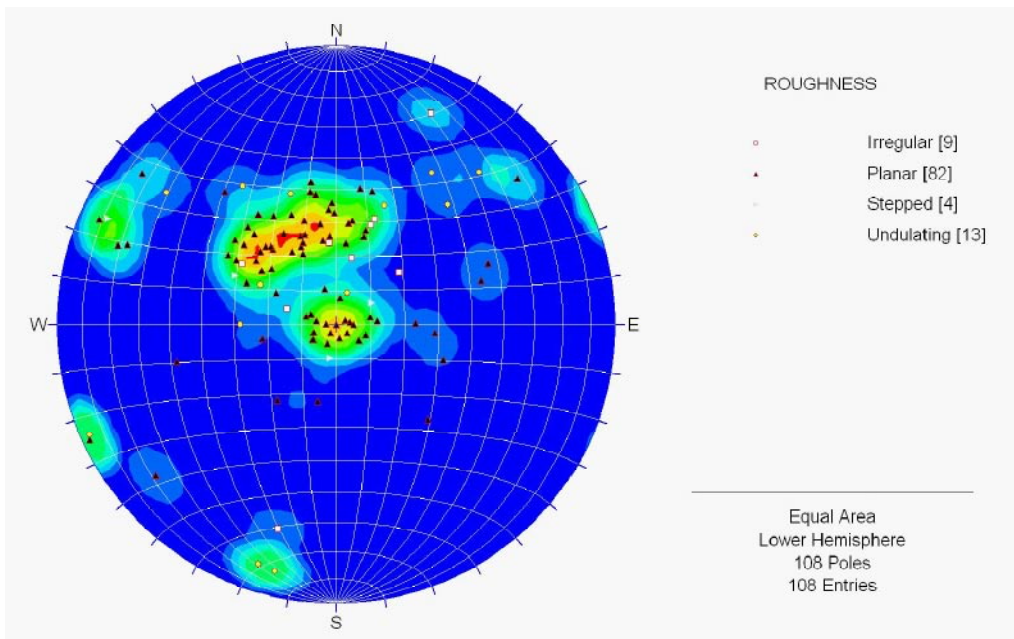


Figure 6-45. Stereoplot of poles to open fractures outside of deformation zones in the measured depth range 510 m to 873 m, borehole KFM03A,B.

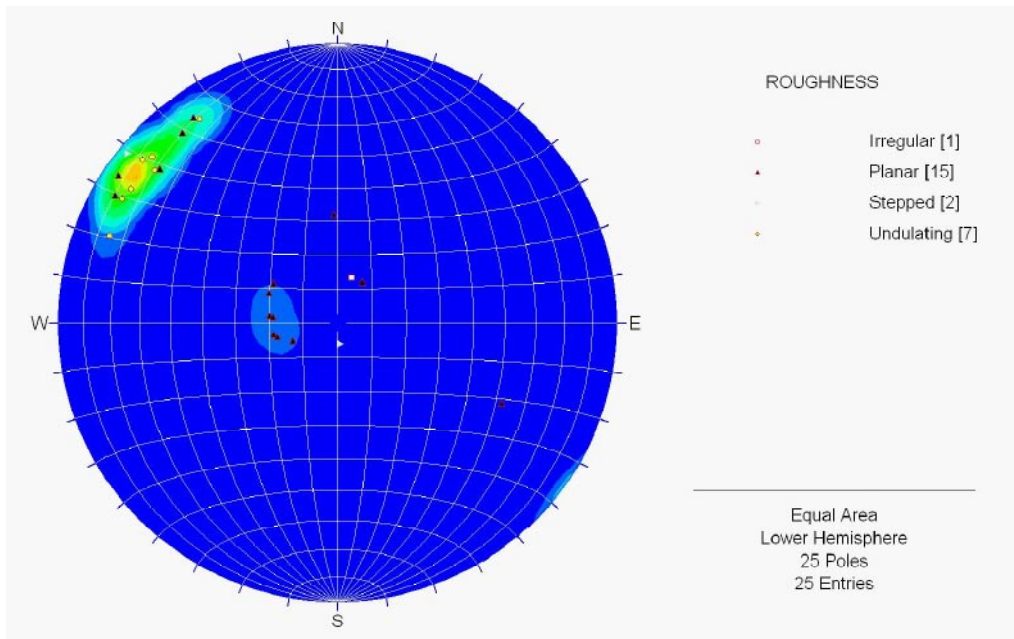


Figure 6-46. Stereoplot of poles to open fractures outside of deformation zones in the measured depth range 875 m to bottom, borehole KFM3A,B.

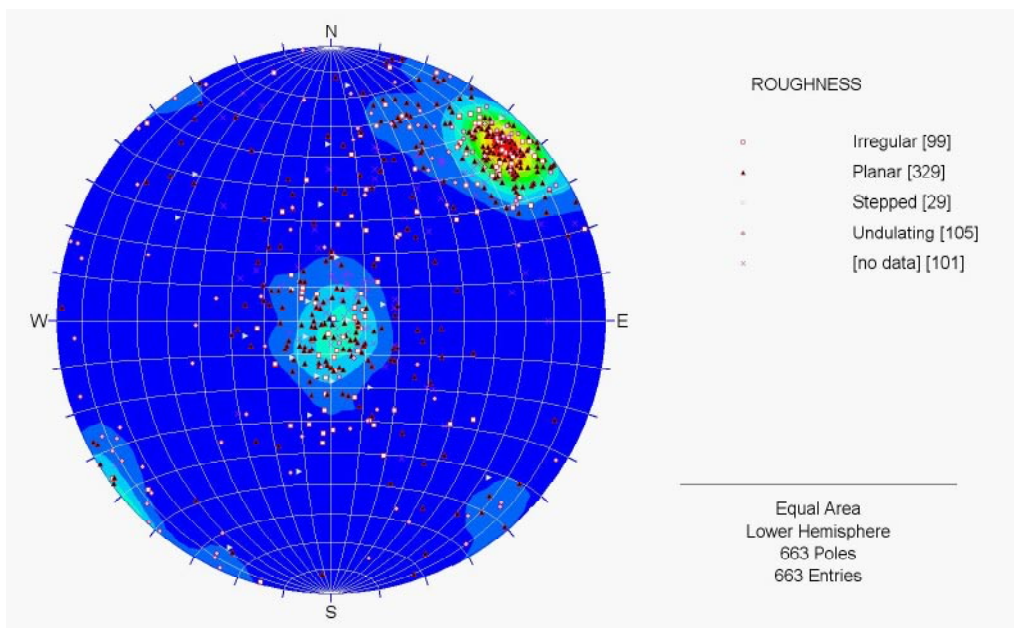


Figure 6-47. Stereoplot of poles to open fractures outside of deformation zones in the measured depth range 0 to 400 m, borehole KFM04A.

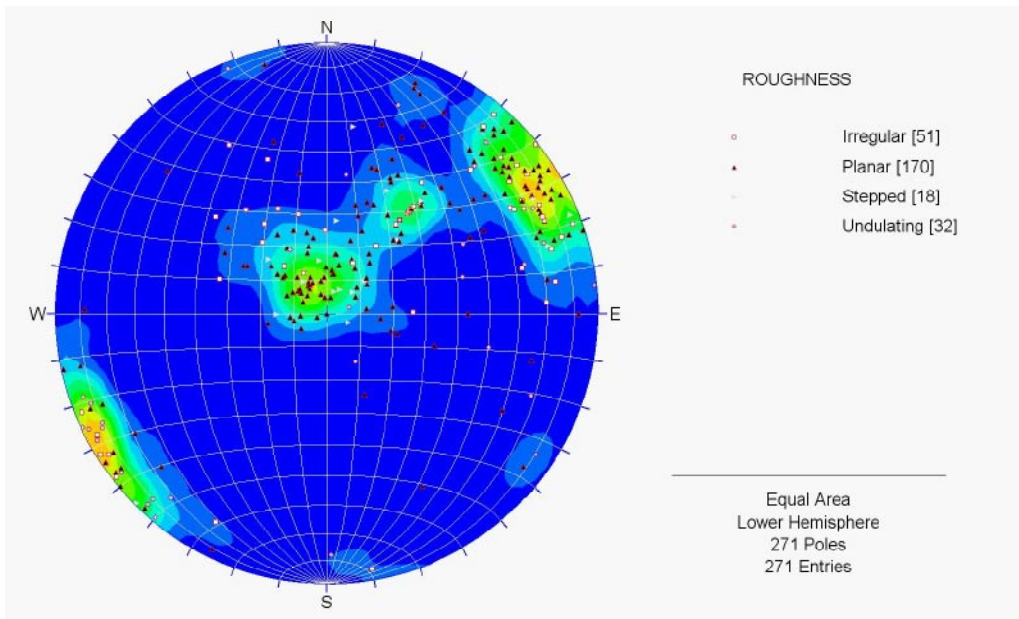


Figure 6-48. Stereoplot of poles to open fractures outside of deformation zones in the measured depth range 400 m to bottom, borehole KFM04A.

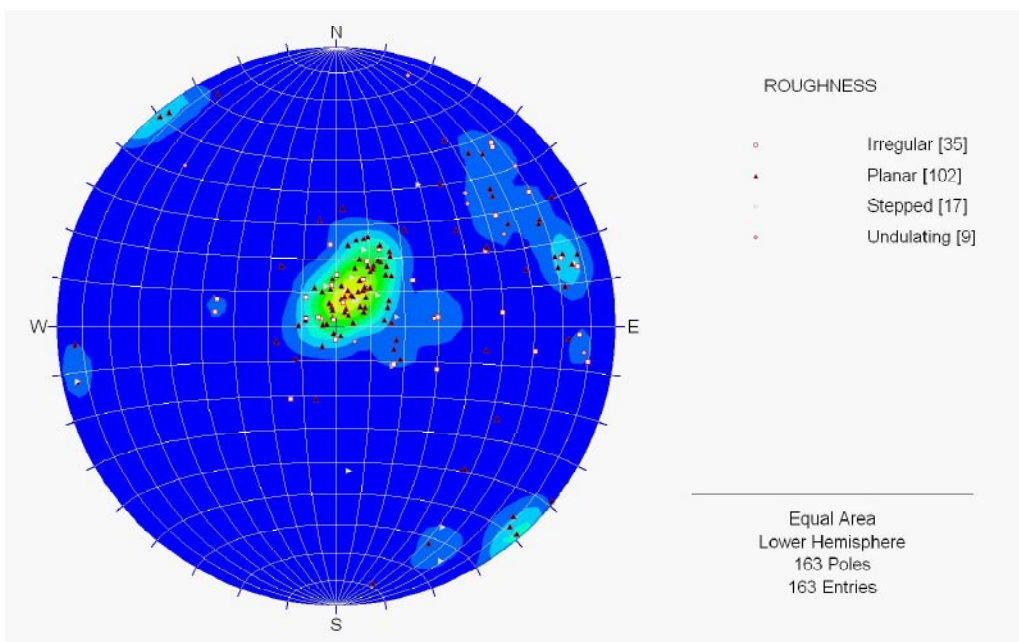


Figure 6-49. Stereoplot of poles to open fractures outside of deformation zones in the measured depth range 100 to 200 m, borehole KFM05A.

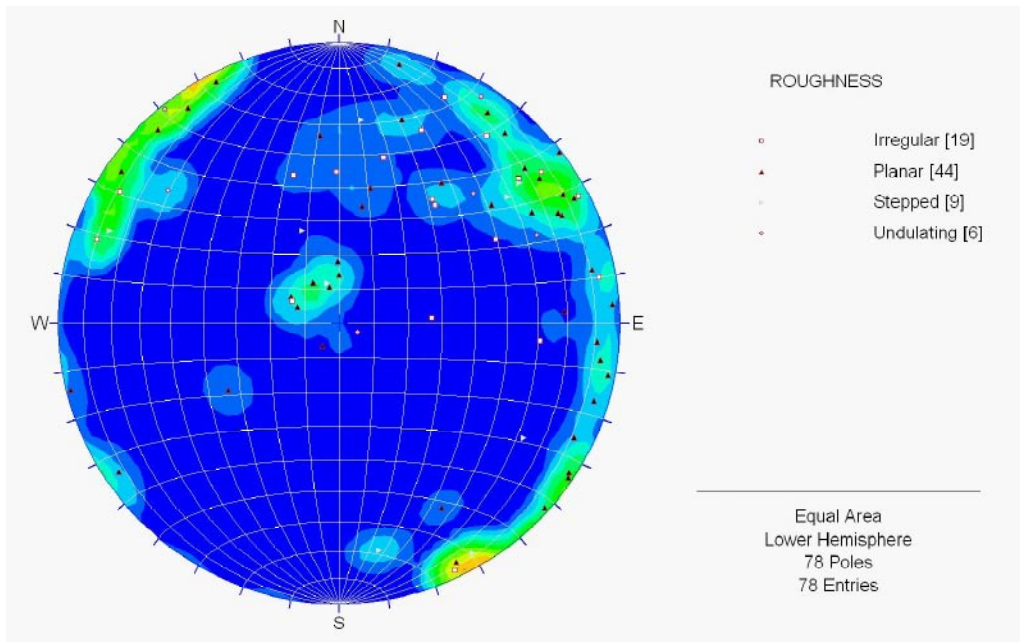


Figure 6-50. Stereoplot of poles to open fractures outside of deformation zones in the measured depth range 200 to 600 m, borehole KFM05A.

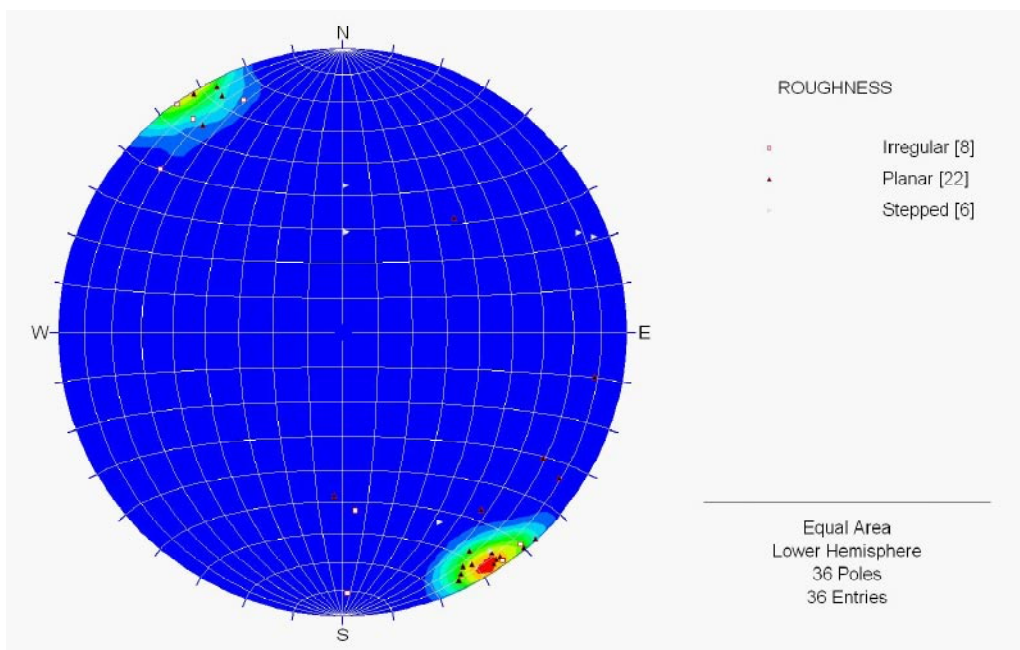


Figure 6-51. Stereoplot of poles to open fractures outside of deformation zones in the measured depth range 800 m to bottom, borehole KFM05A.

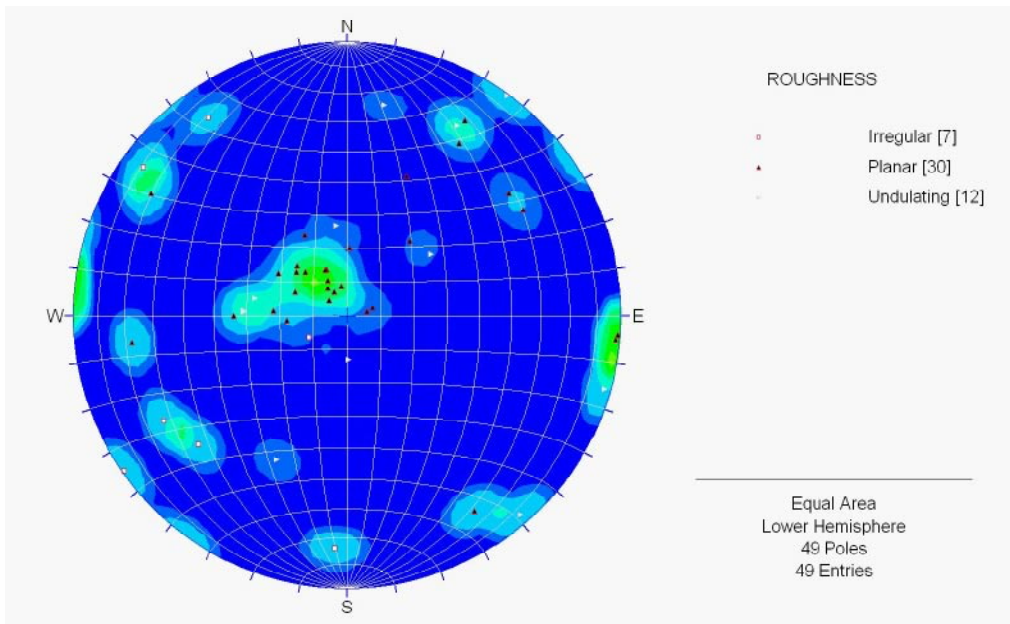


Figure 6-52. Stereoplot of poles to open fractures outside of deformation zones in the measured depth range 0 to 125 m, borehole HFM01.

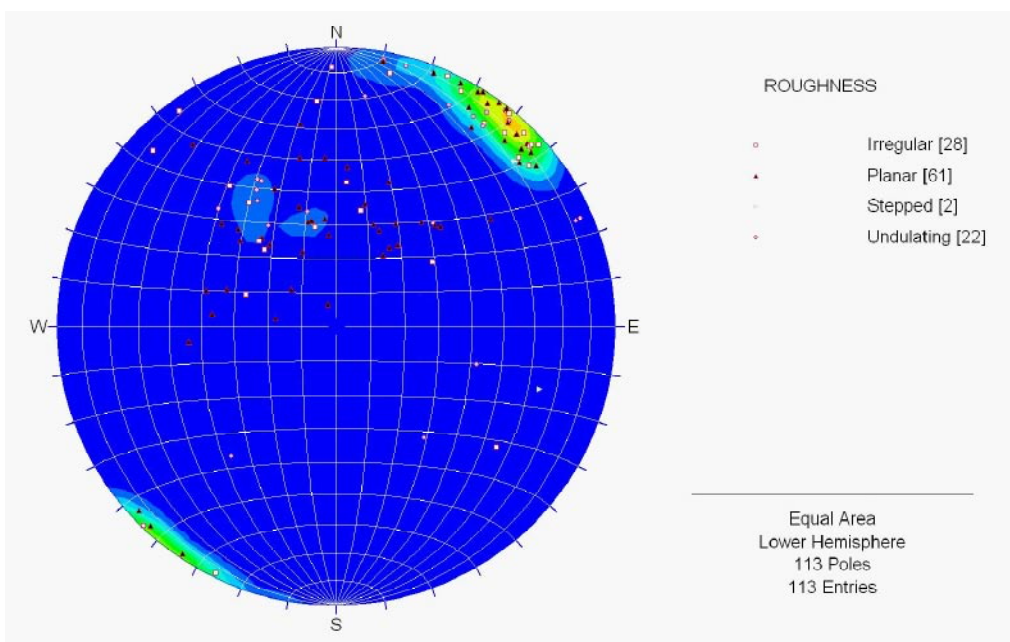


Figure 6-53. Stereoplot of poles to open fractures outside of deformation zones in the measured depth range 125 m to bottom, borehole HFM01.

6.3.3 Lateral correlation of fracture intensity

In an attempt to examine the larger scale variations in fracture intensity, the open fracture intensity in the percussion boreholes, outside of identified deformation zones, was calculated over 10 m intervals (Figure 6-55). For the purpose of the spatial analysis the TVDSS was used in order to correct for the different inclinations of the boreholes. The percussion borehole data was used because there are approximately 19 boreholes with data that cover a much wider spatial area than the cored boreholes (Figure 6-54), and the data is roughly equivalent in quality, so that any effects of mixing data from cored and percussion boreholes, which might have different intensities due to the nature of the drilling, are not present.

Non-parametric correlation coefficients were calculated for these intervals where there was vertical overlap (Table 6-19). Displays for boreholes with high positive and negative correlation coefficients are shown in Figure 6-56 through Figure 6-59.

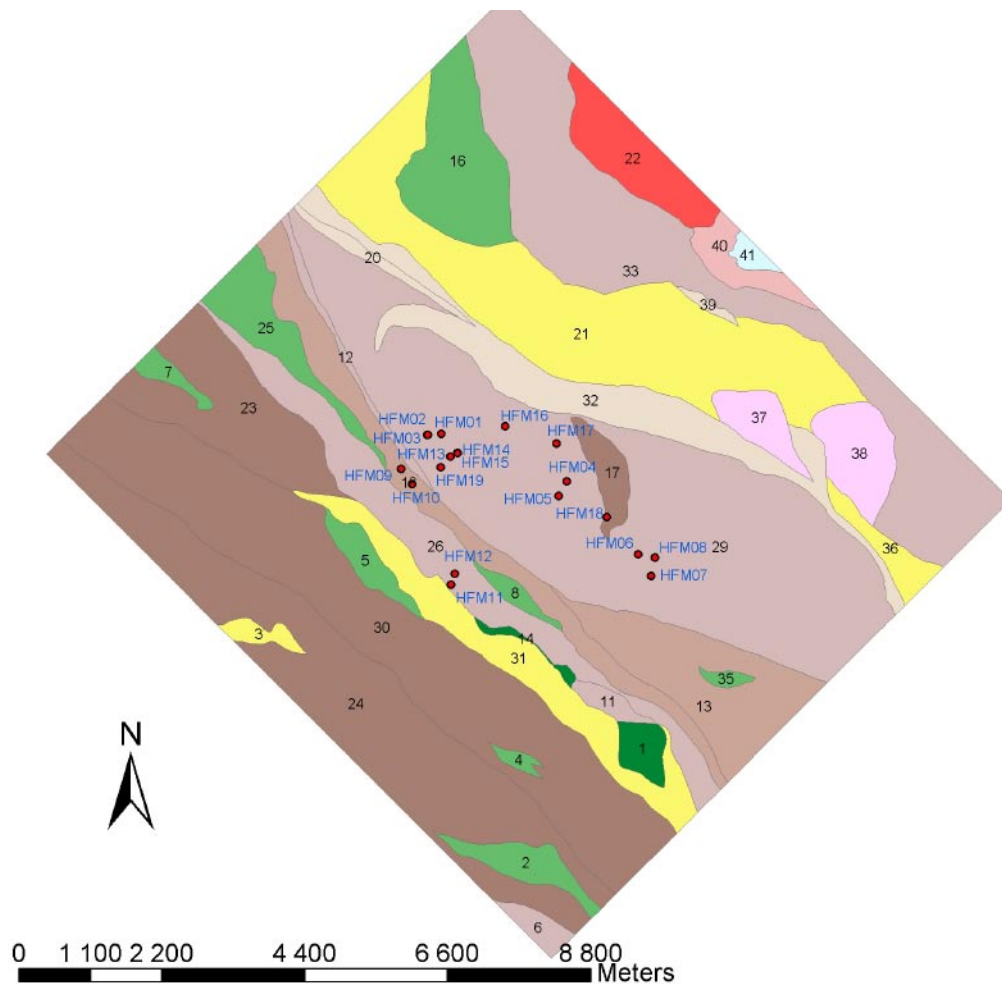


Figure 6-54. Localisation of the percussion boreholes in relation to the different rock domains.

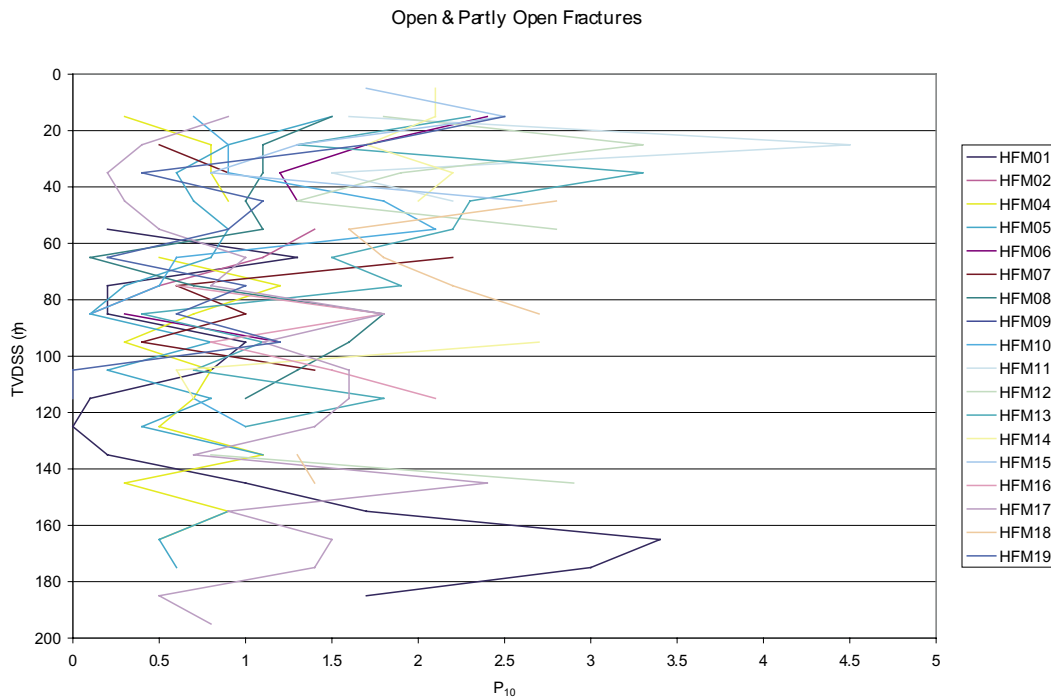


Figure 6-55. Plot of P_{10} fracture intensity averaged over 10 m intervals for open fractures outside of identified deformation zones for all percussion borehole data.

Table 6-19. Correlation coefficients for P_{10} of open fractures in borehole data. Positive correlations greater than 0.5 are shown in blue, and in red if they are negative.

	KFM01A	KFM01B	KFM02A	KFM03A	KFM03B	KFM04A	KFM05A	HFM01	HFM02	HFM04	HFM05	HFM06	HFM07	HFM08	HFM10	HFM11	HFM12
KFM01A	1.00																
KFM01B	0.03	1.00															
KFM02A	0.10	0.10	1.00														
KFM03A	-0.11	-0.09	0.17	1.00													
KFM03B	n/a	1.00	1.00	n/a	1.00												
KFM04A	0.62	-0.09	0.18	-0.01	0.54	1.00											
KFM05A	0.40	0.52	0.19	0.21	n/a	0.25	1.00										
HFM01	0.34	-0.66	-0.85	-0.61	-1.00	-0.02	-0.21	1.00									
HFM02	n/a	-0.40	1.00	n/a	-1.00	-0.71	n/a	0.37	1.00								
HFM04	-0.04	0.11	0.23	-0.07	1.00	-0.01	0.43	-0.32	-0.39	1.00							
HFM05	0.29	-0.11	-0.07	-0.40	-0.94	-0.17	-0.02	0.03	0.99	-0.24	1.00						
HFM06	1.00	-1.00	0.09	n/a	n/a	-0.15	n/a	1.00	n/a	-0.38	0.98	1.00					
HFM07	0.20	-0.79	-0.04	n/a	-1.00	0.01	n/a	0.56	0.80	-0.21	-0.06	-0.72	1.00				
HFM08	0.06	0.96	0.01	-1.00	0.65	0.38	-1.00	-0.32	-0.55	-0.30	-0.05	-0.34	-0.59	1.00			
HFM10	0.60	0.13	0.54	1.00	-0.07	-0.12	-1.00	-0.17	0.85	0.11	0.31	0.31	-0.16	-0.10	1.00		
HFM11	n/a	n/a	0.26	n/a	n/a	-0.57	n/a	n/a	n/a	0.47	0.24	-0.01	-1.00	-0.34	0.02	1.00	
HFM12	1.00	-0.47	0.10	-1.00	n/a	-0.37	-1.00	0.54	n/a	-0.50	-0.12	0.15	-1.00	-0.12	-0.02	0.86	1.00
HFM13	0.09	-0.36	-0.58	0.26	0.50	-0.47	0.32	-0.16	0.77	0.18	0.49	0.47	-0.09	-0.30	0.44	-0.20	-0.63
HFM14	-0.95	n/a	-0.63	1.00	-1.00	-0.86	1.00	0.64	n/a	-0.47	0.44	-0.38	-0.82	0.43	0.33	-0.98	-0.77
HFM15	n/a	n/a	0.68	n/a	1.00	0.91	n/a	n/a	n/a	-0.37	0.52	0.46	-1.00	0.34	0.44	-0.23	-0.55
HFM16	0.67	0.80	n/a	1.00	n/a	0.75	1.00	-0.42	-1.00	-0.17	-0.01	-1.00	0.77	0.25	0.00	n/a	n/a
HFM17	0.11	-0.19	0.05	0.22	-0.28	0.61	-0.04	0.07	-0.82	-0.44	-0.47	-0.48	0.29	0.31	-0.60	-0.55	0.29
HFM18	-0.81	0.38	0.85	-0.94	0.40	-0.75	-0.89	-0.06	-0.99	0.23	-0.24	-0.86	-0.30	-0.07	0.08	1.00	-0.20
HFM19	-0.77	0.76	0.31	n/a	0.81	-0.35	n/a	-0.23	-0.08	-0.12	0.65	0.87	-0.78	0.32	0.11	0.19	-0.17

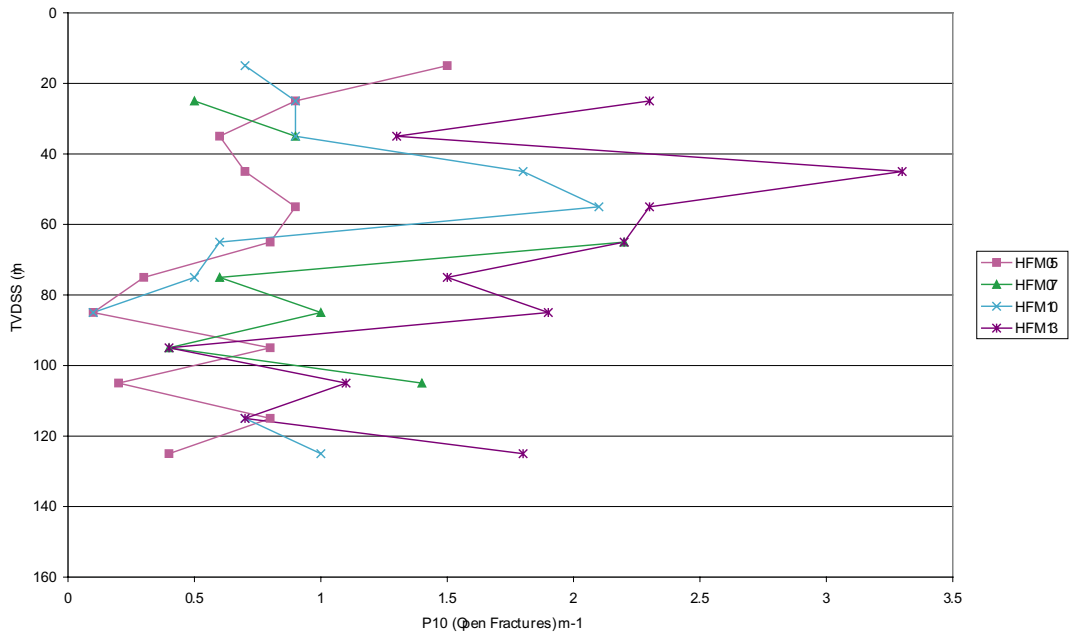


Figure 6-56. Plot of open fracture intensity with depth for four percussion boreholes with high positive correlations coefficients (05, 07, 10 and 13).

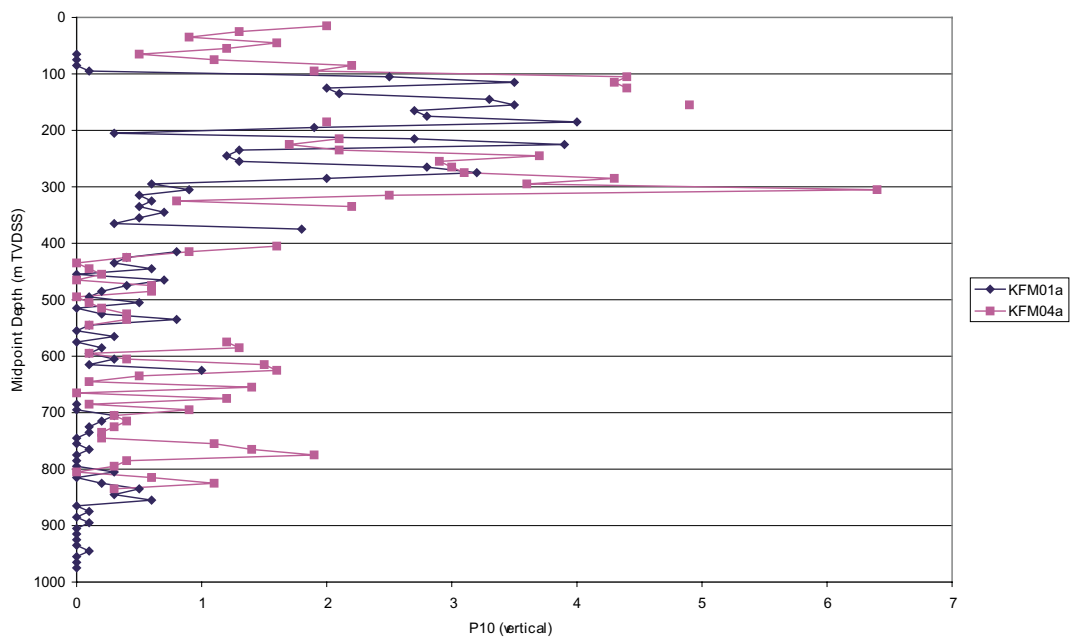


Figure 6-57. Plot of open fracture intensity with depth for two cored boreholes with high positive correlations coefficients (KFM01A and KFM04A).

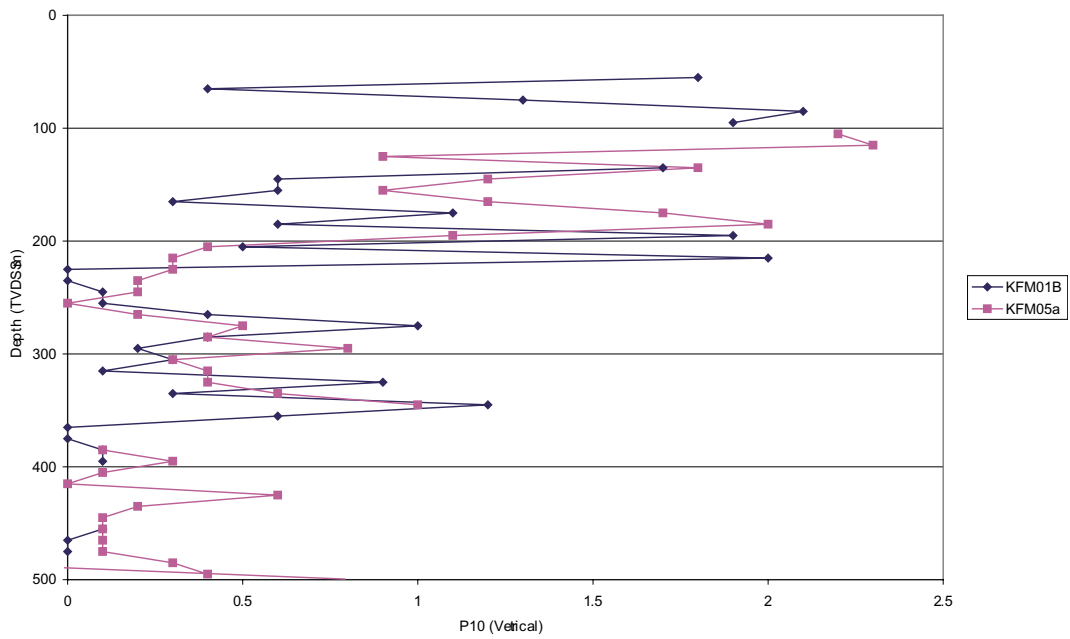


Figure 6-58. Plot of open fracture intensity with depth for two cored boreholes with high positive correlations coefficients (KFM01B and KFM05A).

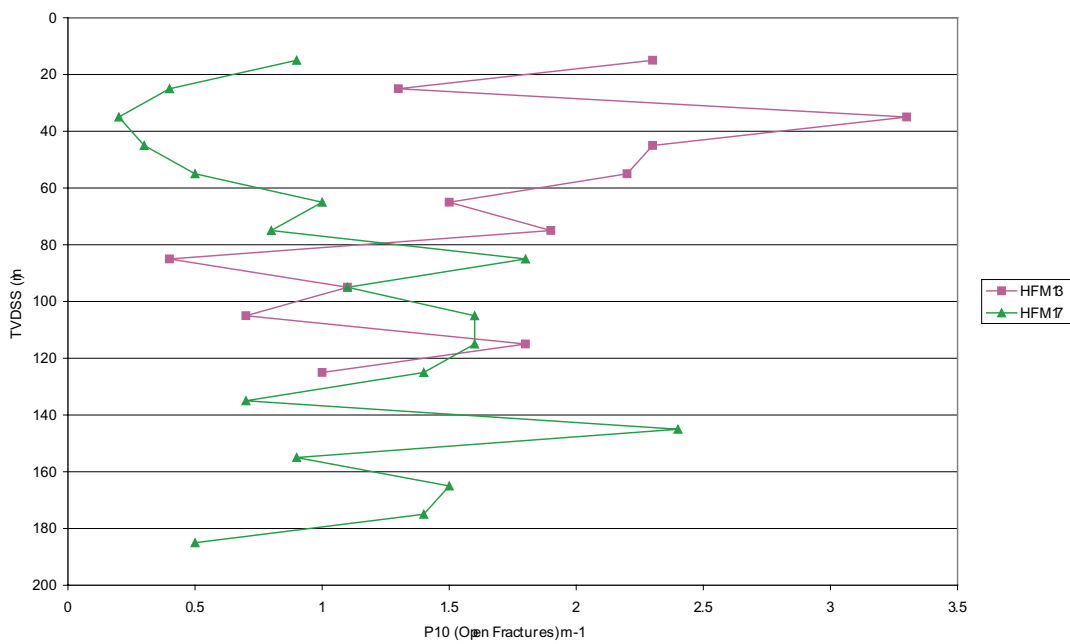


Figure 6-59. Plot of open fracture intensity with depth for two percussion boreholes with high negative correlations coefficients (13 and 17).

These plots show that some boreholes have visually similar intensity patterns. Sometimes these boreholes are close to one another (HFM05 and HFM19 or HFM11 and HFM12, for example), while other times they are quite far apart (HFM05 and HFM07). These longer-distance correlations tend to be due to high intensity intervals that might be unidentified deformation zones, but this has not been investigated. Boreholes HFM14 and HFM19, on the other hand, are spatially close to one another, but show strong negative correlation. Likewise, many well pairs close to one another show little, if any correlation.

This suggests that the lateral correlation of fracture intensity intervals outside of deformation zones has at best a short range of spatial correlation. As a result, a Poisson model for lateral variation in fracture intensity seems to most closely approximate the measured data.

A similar analysis was conducted on sealed fractures in percussion boreholes. Figure 6-60 illustrates the P_{10} of sealed fractures in all percussion boreholes versus the TVDSS. Non-parametric correlation coefficients calculated for intervals where there was vertical overlap are given in Table 6-20. Few boreholes are positively correlated (Figure 6-61), some of them not closed to each other like HFM05 and HFM14. On the other hand Figure 6-62 show boreholes that are very close to each other: two of them are positively correlated but the other pair (HFM06 and HFM07) do not show that much similarity. However HFM07 is as close to HFM06 and HFM08 but is dissimilar.

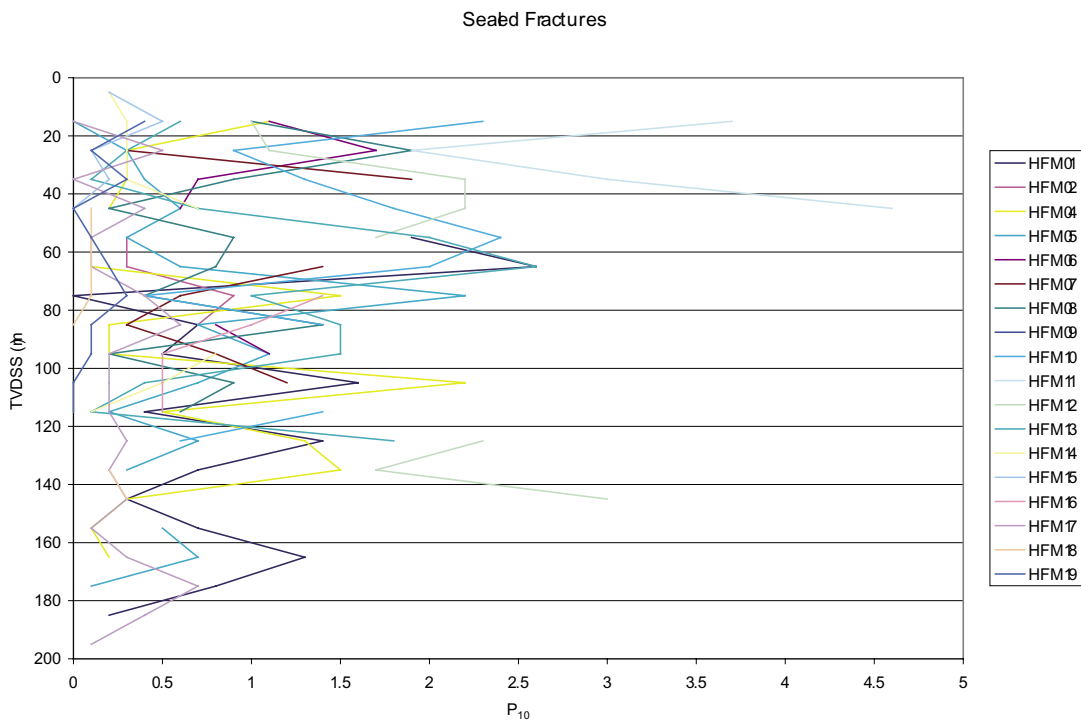


Figure 6-60. P_{10} vs TVDSS for sealed fractures, percussion boreholes only. The value of P_{10} was calculated over 10 m intervals.

Table 6-20. Correlation coefficients for P₁₀ of sealed fractures in borehole data. Positive correlations greater than 0.5 are shown in blue, and in red if they are negative

	KFM01A	KFM01B	KFM02A	KFM03A	KFM03B	KFM04A	KFM05A	HFM01	HFM02	HFM04	HFM05	HFM06	HFM07	HFM08	HFM10	HFM11	HFM12
KFM01A	1.00																
KFM01B	-0.47	1.00															
KFM02A	0.12	-0.29	1.00														
KFM03A	0.11	-0.47	0.02	1.00													
KFM03B	n/a	1.00	-1.00	n/a	1.00												
KFM04A	0.40	-0.51	0.15	0.17	n/a	1.00											
KFM05A	-0.07	-0.26	-0.06	-0.25	n/a	-0.32	1.00										
HFM01	0.01	0.18	-0.38	0.39	-1.00	-0.33	-0.10	1.00									
HFM02	n/a	0.30	n/a	n/a	1.00	0.33	n/a	-0.97	1.00								
HFM04	0.08	0.28	0.34	0.37	1.00	0.27	-0.59	0.00	0.80	1.00							
HFM05	-0.61	0.48	-0.58	-0.23	0.99	0.11	0.11	-0.36	0.85	0.21	1.00						
HFM06	1.00	-1.00	0.81	n/a	n/a	-0.02	n/a	-1.00	n/a	0.18	-0.24	1.00					
HFM07	0.43	-0.77	-0.92	n/a	-1.00	-0.12	n/a	0.83	-0.83	0.03	-0.27	-0.58	1.00				
HFM08	-0.02	0.23	0.67	1.00	-0.32	-0.16	-1.00	0.37	-0.20	-0.06	-0.44	0.61	-0.35	1.00			
HFM10	-0.22	-0.15	0.13	1.00	-1.00	-0.43	1.00	0.68	-0.96	-0.47	-0.63	-0.40	0.47	-0.09	1.00		
HFM11	n/a	n/a	-0.40	n/a	n/a	-0.61	n/a	n/a	n/a	-0.36	-0.20	-0.80	1.00	-0.95	0.86	1.00	
HFM12	-0.93	-0.44	-0.62	-0.99	n/a	0.46	0.82	-0.61	n/a	-0.28	0.86	-0.84	1.00	-0.71	-0.33	0.04	1.00
HFM13	-0.52	-0.44	0.16	-0.96	-0.49	0.12	-0.22	0.62	-0.93	-0.19	0.19	-0.16	-0.07	-0.13	0.23	-0.36	0.26
HFM14	-0.93	n/a	-0.62	1.00	1.00	0.44	-1.00	0.16	n/a	-0.09	0.85	-0.34	-0.20	-0.57	0.28	0.76	0.58
HFM15	n/a	n/a	0.63	n/a	-1.00	n/a	n/a	n/a	n/a	0.96	-0.93	0.12	1.00	0.15	0.61	0.00	-0.58
HFM16	-0.66	1.00	n/a	n/a	n/a	-0.77	n/a	-0.56	1.00	0.11	0.78	-1.00	-0.66	0.10	-0.83	n/a	n/a
HFM17	0.22	-0.15	0.14	0.46	0.62	0.17	0.06	-0.41	0.82	-0.05	0.16	0.18	-0.95	0.28	-0.54	-0.25	0.13
HFM18	0.02	-0.75	0.72	-0.79	0.00	-0.40	0.77	-0.21	-0.33	0.07	-0.35	0.87	0.28	0.16	0.43	-1.00	-0.55
HFM19	-0.75	0.51	0.33	n/a	0.66	-0.49	n/a	0.04	0.52	0.13	0.13	0.03	0.36	0.08	-0.02	-0.11	-0.55

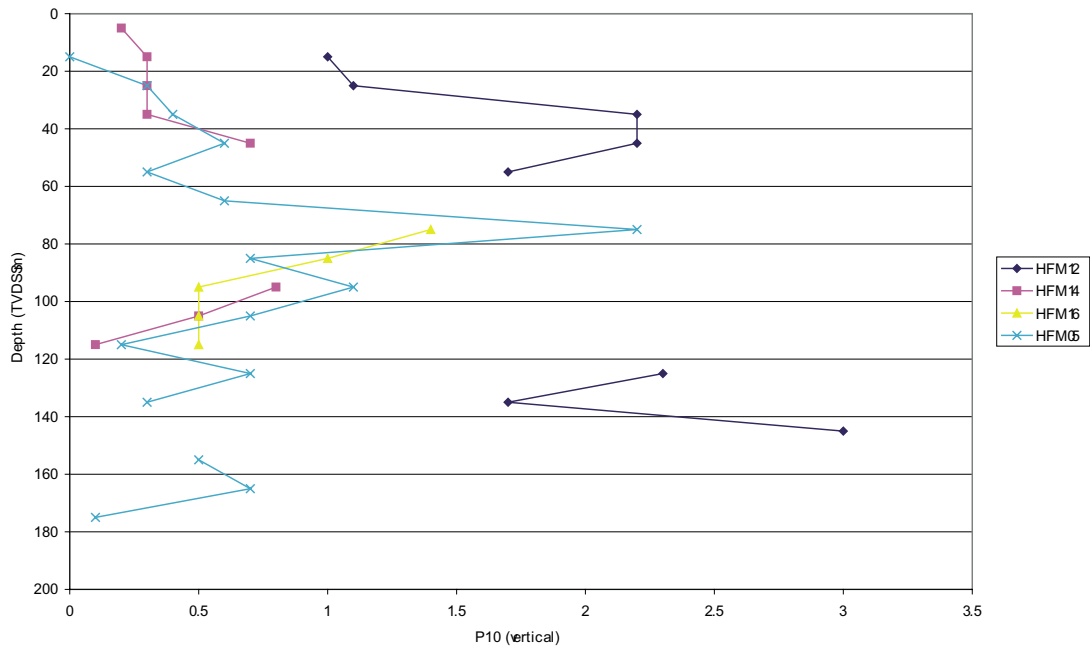


Figure 6-61. Plot of sealed fracture intensity with depth for four boreholes with positive correlation coefficients (05, 12, 14 and 16).

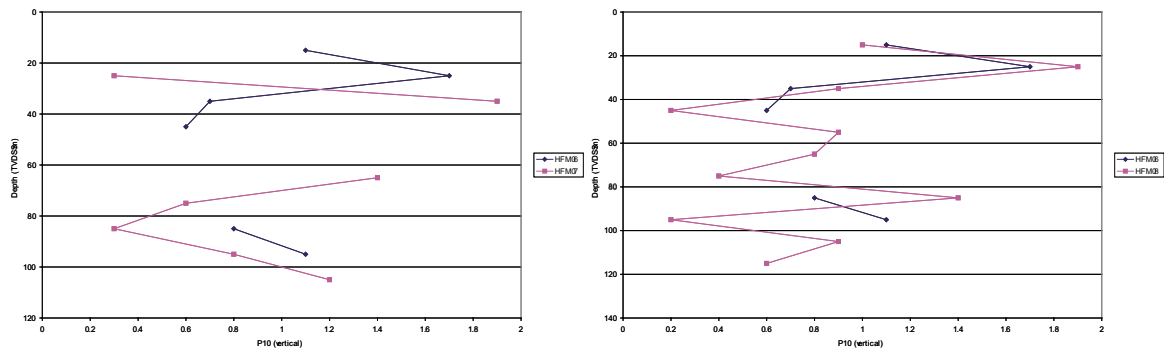


Figure 6-62. Plots of sealed fracture intensity with depth for boreholes that are pairwise close to each other.

Based on this analysis a Poissonian model seems to be suitable even for sealed fractures.

6.4 Intensity

The spatial analysis in the previous section suggests that the fracture intensity is a function of rock domain, and within that rock domain, there may be intervals both laterally and vertically of higher and lower fracture intensity. An important issue is how best to prescribe intensity variations in order to best conform to the measured data, and to reduce uncertainty in the model.

This task is carried out by calculating, through the non-parametric Kruskal-Wallis test, whether the P_{10} variation within rock domains is greater than or less than the variation between rock domains. If the variation within rock domains is less than the variation between, then it is appropriate to statistically stratify the data using rock domains. If the result is that the variation is greater within rock domains than between them, then either all of the data should be lumped without regard to rock domains, or other means of stratifying the fracture intensities need to be considered.

Table 6-21. Kruskal-Wallis test of P_{10} fracture intensity as a function of rock domain.

analysed with: Analyse-it + General 1.71

Test	Kruskal-Wallis ANOVA		
Comparison	Mean P10 by Domain: 12, 17, 26, 29		
Performed by	Paul La Pointe	Date	17 August 2004

n | 19

Mean P10 by Domain	n	Rank sum	Mean rank
17	1	18.0	18.00
18	2	4.0	2.00
26	2	25.0	12.50
29	14	143.0	10.21

Kruskal-Wallis statistic | 6.48
p | 0.0905 (chisqr approximation)

The Kruskal-Wallis ANOVA test was carried out on the percussion boreholes, as these are the only fracture data that include a sufficiently large number of rock domains (Table 6-21). The test shows significance at an $\alpha=0.10$ level, suggesting that the variance within rock domains is less than the variance between them. Therefore, it appears appropriate to characterize fracture intensity based on rock domains, and calculating ranges, means and standard deviations of intensities for each rock domain.

The P_{10} is calculated within each rock domain on the fracture frequency intervals identified in each individual borehole and discussed in Section 6.3.1. The mean value, standard deviation and span are calculated from all P_{10} interval values within a rock domain.

The values reported in these tables are calculated as follows:

- 1) All fractures and borehole intervals identified as being part of deformation zones are excluded from the analyses.
- 2) P_{10} values are calculated for open, partly open, sealed and total for each interval lying between deformation zones that are within a single rock domain. If more than one rock domain occurs between identified deformation zones, the P_{10} value is calculated separately for each rock domain interval.
- 3) The mean value of P_{10} is calculated by taking the arithmetic mean of all of the individual P_{10} values for a specific rock domain. The standard deviation, minimum and maximum values are also calculated from the interval values of P_{10} . Note that in this calculation, neither the mean nor the standard deviation are weighted by interval length. Previous calculations at Simpevarp suggested that the impact of not weighting by interval length is minimal compared to the much greater uncertainty related to the variation of P_{10} within a domain.

Table 6-22 summarizes the open fracture intensity from portions of the percussion boreholes that are outside of identified deformation zones. The standard deviations are relatively consistent, varying from 0.47 fracs/m to 0.71 fracs/m. The mean fracture intensity varies over a factor of about 3. The range varies between some intervals that had no open fractures, to others that have about 3 times the mean intensity.

The data shown below are for boreholes ranging from vertical to inclined, but even within the subset of near vertical boreholes, the same pattern is evident.

It may be that the cored boreholes give a better indication of the true amount of fracturing in the subsurface, due to the higher reliability of the data. To examine the relation between the intensity of open fractures in cored boreholes vs the intensity in percussion boreholes, the mean open fracture intensity was calculated for the interval identified in the CFI plots (Section 6.3.1), and separated into the appropriate rock domains as identified in the borehole logs.

Table 6-22. Open fracture intensity (P_{10}) for fractures outside of deformation zones based on the percussion borehole data. n represent the amount of fracture intensity intervals between deformation zones.

Domain	n	Mean	Standard Deviation	Min	Max
17	14	1.84	0.57	1.08	2.96
18	15	0.54	0.47	0.10	1.00
26	23	1.23	0.68	0.00	2.40
29	180	1.08	0.71	0.00	3.77

Table 6-23 and Table 6-24 show the results for P_{10} from the cored boreholes only. There is only one interval for domains RFM017 and RFM018, so statistics regarding the standard deviation, min and max are not applicable. The data for domains RFM012 and RFM029 are the most robust, as they consist of several intervals of data.

The values calculated in cored boreholes for open fractures do not compare very well with the percussion borehole data for open fractures (Table 6-22), although they seem to correspond better to a conceptual model where higher fracture intensity occurs in the narrow northwest-trending deformation zones like domains 12 and 18.

Table 6-23. Mean values and standard deviation of P_{10} intensities for open, partly open and sealed fractures outside of deformation zones, cored boreholes only. n represent the amount of intervals between deformation zones.

Domain	n	Mean – Open	Mean – Partly Open	Mean – Sealed	Std Dev – Open	Std. Dev – Partly Open	Std. Dev. Sealed
RFM012	4	1.33	0.45	3.89	1.00	0.48	2.58
RFM017	1	0.03	0.04	1.48	n/a	n/a	n/a
RFM018	1	1.59	0.22	1.61	n/a	n/a	n/a
RFM029	34	0.59	0.05	1.47	1.21	0.05	0.92

Table 6-24. Min and max values of P_{10} intensities for open and sealed fractures outside of deformation zones, cored boreholes only. n represents the amount of intervals between deformation zones.

Domain	Min – Open	Min – Partly Open	Min – Sealed	Max – Open	Max – Partly Open	Max – Sealed
RFM012	0.47	0.03	1.18	2.78	1.01	6.96
RFM017	n/a	n/a	n/a	n/a	n/a	n/a
RFM018	n/a	n/a	n/a	n/a	n/a	n/a
RFM029	0.00	0.00	0.00	6.06	0.20	4.55

Figure 6-63 shows the lack of relation between open and sealed fracture intensities over the same intervals in the cored boreholes outside of identified deformation zones.

The line shown on the figure represents perfect positive correlation. In general, the sealed intensity is greater than the open intensity, but not always. This suggests that open intensities cannot be used to calculate sealed intensities, and vice versa.

In order to estimate the values of P_{32} from borehole data, the coefficient C1 (defined in Section 5.5.3) has been calculated based on the P_{32} and P_{10} obtained from simulations of the DFN model.

Twenty-five Monte Carlo simulations of the DFN model were generated using the stochastic parameters for orientation sets and parent radius distribution given in Table 6-3 and Table 6-12. As mentioned, the proportions of each set conform to the global proportions deduced from the outcrops, and in particular, the proportions for the open fractures.

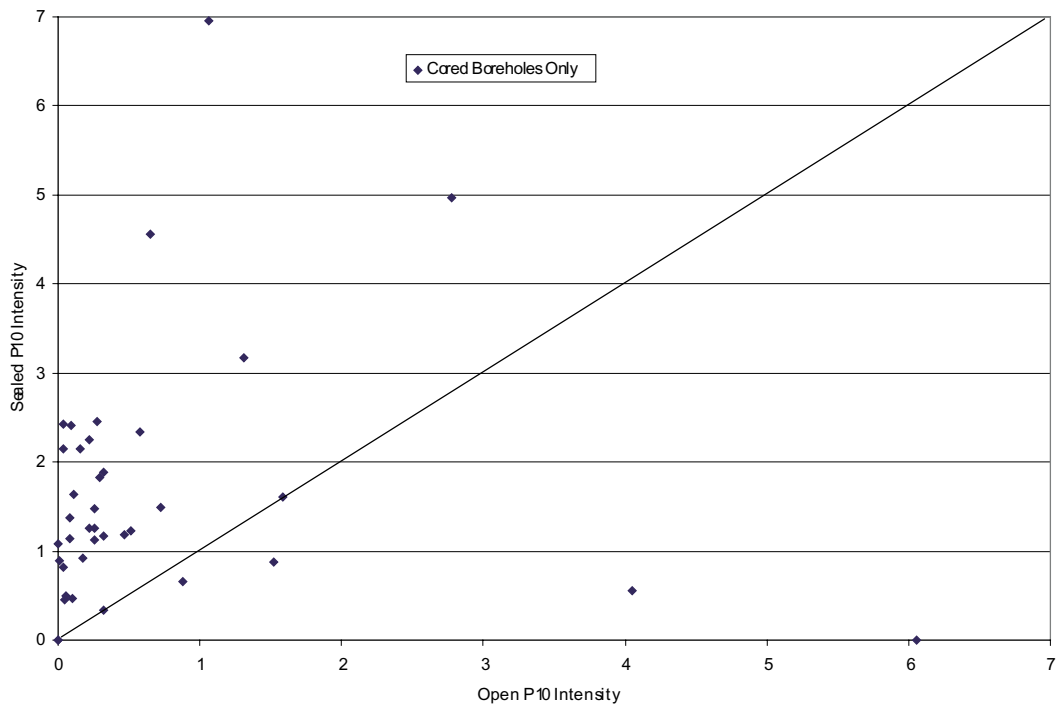


Figure 6-63. Relation between open and sealed P_{10} fracture intensities over the same depth intervals for the cored borehole data outside of identified deformation zones.

The best model is used for generating fracture orientation and the median values are used for simulating fracture size. The value of simulated P_{32} is calculated for each orientation set based on the relative proportion of open fractures. The sampling was done borehole by borehole, and a coefficient C1 was calculated for each individual hole. The P_{32} for the preliminary simulation is chosen to be large enough that the standard deviation of the amount of fractures intersected by the sampled boreholes is on the same order or less than the mean value. Then the P_{32} was calculated for each P_{10} interval in each borehole, and the resulting value for each rock domain and by fracture type is presented in Table 6-25 and Table 6-26.

To compute the P_{32} for each fracture orientation set, the overall P_{32} for each domain (Table 6-25) is multiplied by the P_{32} proportion for each set (Table 6-6). In other words, to compute the P_{32} for open and partly open fractures belonging to the NW set in Domain 29, the total open P_{32} is $1.13 + 0.09 = 1.22$ based upon the cored borehole data. Table 6-6 shows that the percentage of open fracture intensity for the NW set in Domain 29 is 14.38% of the total open fracture intensity, and 15.55% for the partly open fractures. Thus the total P_{32} for the open and partly open fractures is $1.13 \times 14.38\% + 0.09 \times 15.55\% = 0.17 \text{ m}^{-1}$.

Table 6-25. Mean values and standard deviation of P_{32} for Open, Partly open and Sealed fractures in different sampled rock domains (cored boreholes only).

	Mean – Open	Mean – Partly open	Mean – Sealed	Std Dev – Open	Std Dev – Partly open	Std Dev – Sealed
RFM012	2.06	0.71	6.05	1.56	0.74	4.01
RFM017	0.06	0.08	2.98	–	–	–
RFM018	2.47	0.34	2.5	–	–	–
RFM029	1.13	0.09	2.73	2.41	0.11	1.6

Table 6-26. Min and max values of P_{32} for Open, Partly open and Sealed fractures in different sampled rock domains (cored boreholes only).

	Min – open	Min – Partly open	Min – Sealed	Max – open	Max – Partly open	Max – Sealed
RFM012	0.72	0.04	1.84	4.32	1.57	10.82
RFM017	–	–	–	–	–	–
RFM018	–	–	–	–	–	–
RFM029	0.000	0.000	0.000	12.12	0.39	6.7

Table 6-27 summarizes the fracture model intensity parameters. The intensity values are provided for each rock domain for which there was fracture data in cored boreholes. Except for Domain 29, the data coverage was not large, and so the intensity values reported for Domains 12, 17 and 18 will most likely change as new data becomes available. As mentioned in Chapter 4, fractures have been assumed to be circular, planar discs. No analyses were undertaken to determine if other shapes might be more appropriate.

Table 6-27. Intensity parameters as a function of rock domain, fracture type and fracture set.

Intensity (P_{32} -m ² /m ³)	Name	Open	Partly Open	Sealed	Total
Domain 29	NS	0.12	0.01	0.47	0.60
	NE	0.46	0.05	1.56	2.07
	NW	0.16	0.01	0.27	0.45
	EW	0.05	0.00	0.17	0.23
	HZ	0.34	0.01	0.26	0.61
	All	1.13	0.09	2.73	3.95
Domain 18	NS	0.26	0.05	0.43	0.74
	NE	1.01	0.18	1.43	2.62
	NW	0.36	0.05	0.25	0.66
	EW	0.11	0.02	0.15	0.29
	HZ	0.73	0.04	0.24	1.01
	All	2.47	0.34	2.50	5.31
Domain 17	NS	0.01	0.01	0.51	0.53
	NE	0.02	0.04	1.70	1.77
	NW	0.01	0.01	0.30	0.32
	EW	0.00	0.00	0.18	0.19
	HZ	0.02	0.01	0.28	0.31
	All	0.06	0.08	2.98	3.12
Domain 12	NS	0.22	0.10	1.04	1.36
	NE	0.84	0.37	3.46	4.67
	NW	0.30	0.11	0.60	1.01
	EW	0.09	0.04	0.37	0.51
	HZ	0.61	0.09	0.57	1.27
	All	2.06	0.71	6.05	8.82

It is important to note that the P_{32} values shown in these tables derive strictly from boreholes, not from outcrop. The reason for this is that outcrop data cannot be used directly for estimating P_{32} because traces below 0.5 m were not measured. Thus the P_{21} derived from outcrop trace data is censored. The conversion factors (C_2) for each set calculated from the simulations to estimate x_{r0} depend upon the 0.5 m value, making it impossible to estimate the uncensored P_{32} from the trace data alone.

To determine the correct P_{32} value for the open and partly open NW fractures in Domain 29 for a minimum fracture size of 5 m, the value of 0.176 is put into Equation 5-16, using the values from Table 6-12. This table shows that $k_r=2.81$ and $x_{r0}=0.14$. Putting $x_2=\infty$ and $x_1=5.0$, the equation yields:

$$\frac{5^{2-2.81} - \infty^{2-2.81}}{0.14^{2-2.81}} * 0.176 = 0.0097 \tag{Equation 6-1}$$

Therefore, the correct P_{32} to use for specifying the NW set for Domain 29 for open and partly open fractures, with a minimum radius value of 5.0 m is 0.0097 m^{-1} . Figure 6-64 provides a graphical look-up for the correction factors for each set for a wide range of possible minimum radius values.

Figure 6-65 and Figure 6-66 show the final DFN model using the parameters for size, orientation and intensity derived in this report. The four subvertical sets and the one subhorizontal set are clearly shown in their relative intensities and orientation dispersion. The cumulative number plot for trace lengths is for the open horizontal fractures for Domain 29. The trace lengths derived from the simulation are superimposed on the horizontal traces for the three outcrops belonging to Domain 29. The consistency between the simulation and the measured data from which the simulation trace lengths were derived is quite good, not only in terms of slope and absolute numbers, but also in the maximum trace length found.

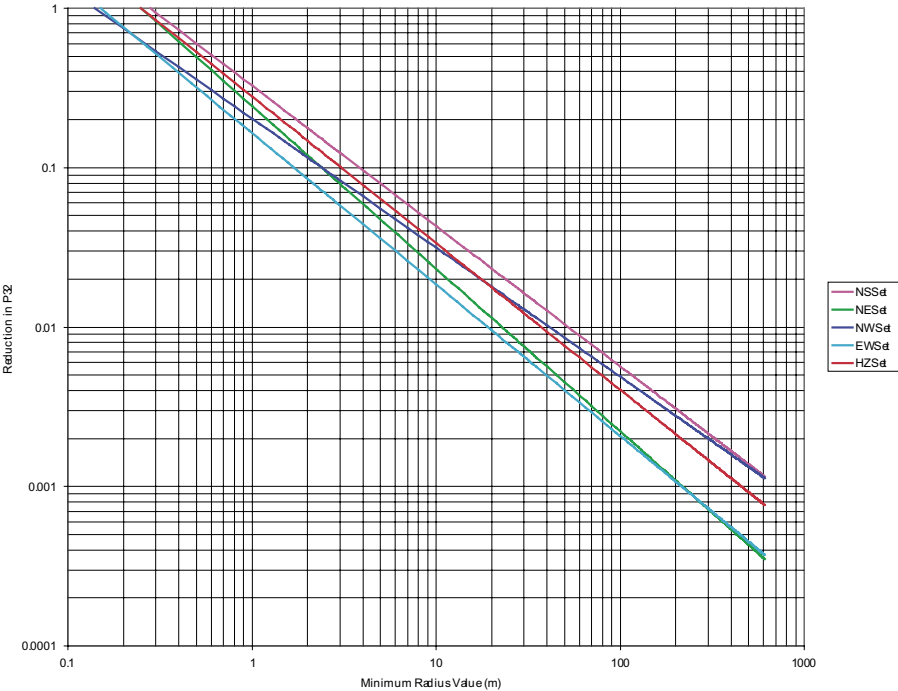


Figure 6-64. Correction to P_{32} value for various minimum radii by set.

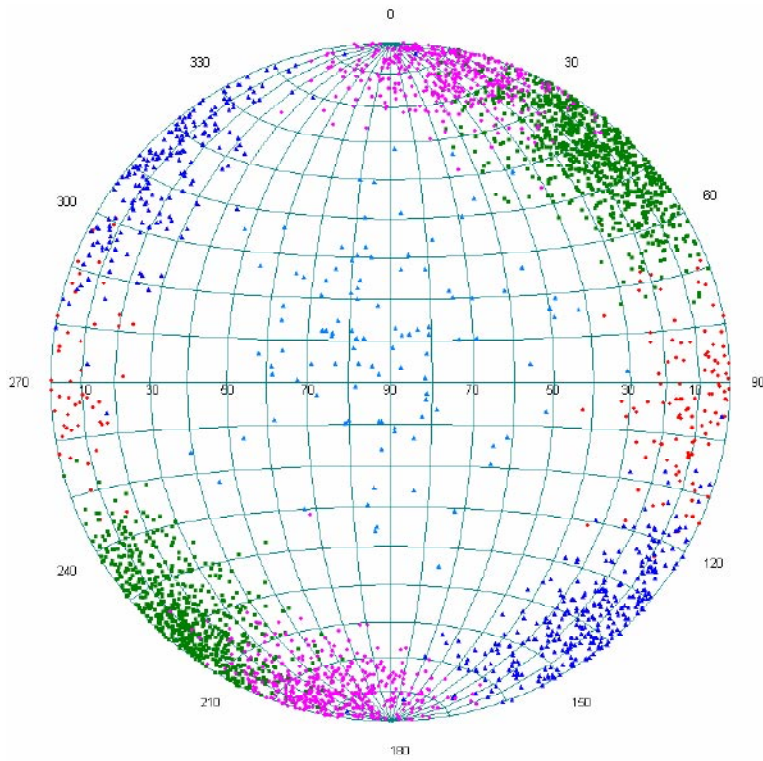


Figure 6-65. Stereonet of fracture poles for the fracture model.

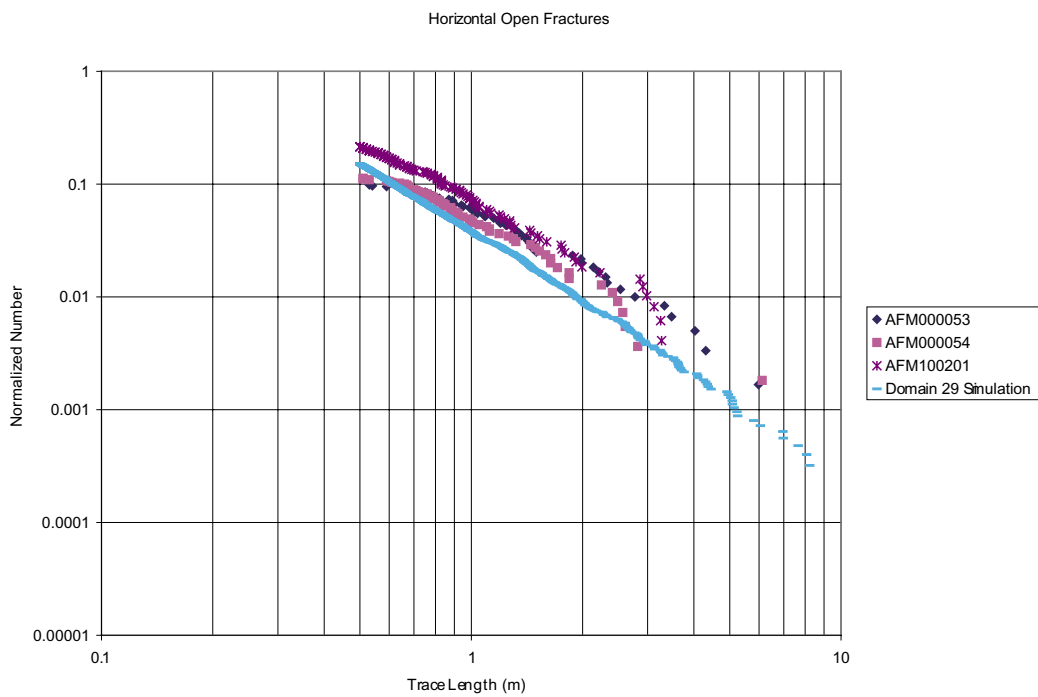


Figure 6-66. Area-normalized cumulative number trace length plot for simulated horizontal open set.

6.5 Model validation

Validation consists of a series of formal, documented steps that addresses whether a particular model is adequate for its intended purposes. One of the intended purposes is to predict fracture intensity at unsampled or undrilled locations. Validation includes confidence building exercises during model development, such as prediction of existing laboratory or field tests, as well as one or more post-model activities such as formal peer review, pre-model prediction of a post model experiment, comparison with other models, and comparison with published, peer-reviewed lab studies. The validation described in this report is quite limited in scope, as it focuses on using the DFN model to predict the fracturing in a single borehole, thus not validating the model for all rock domains, and only for fracture intensity and to a qualitative extent, fracture orientation. More thorough validation is warranted in future model versions as additional validation test data becomes available.

6.5.1 Procedure

The purpose of model validation is to build confidence in the stochastic parameters determined for the DFN model. The validation of the DFN model has been carried out in RFM029. Most of the shallow high intensity intervals are identified above or in the possible zone of influence of ZFMNE00A2. This model suggests that the moderately dipping deformation zone ZFMNE00A2 is a major structure that controls the fracture frequency in the rock mass. The value of fracture intensity below DZ2 in KFM01A probably best reflects the intensity of the rock away from deformation zones. The intensity for the DFN model is based on the specific P_{10} values for the mean fracture frequency for the intervals presented in Table 6-28. These values are based on the fractures recorded for KFM01A.

Table 6-28. P_{10} calculated for the sub-domains in RFM029 (outside of deformation zones).

Zone	Length	P_{10} – Open and Partly Open	P_{10} – Sealed	Depth Range
Above DZ 1	5.43	4.05	0.55	30.5–35.9
DZ1–DZ2	338.24	1.61	0.88	47.8–386.1
DZ2–DZ3	226.10	0.35	0.33	412.9–639.0
Below DZ3	309.50	0.10	0.47	684.3–993.8

25 realizations of the fracture model for open and partly open fractures were simulated. Each realization was sampled by a borehole in the same orientation as KFM01A. The mean value of P_{10} was 0.67 m^{-1} , about twice the value measured in KFM01A below DZ2, but considerably less than the values measured above DZ2. The value for sealed fractures was 1.51 m^{-1} , about three times greater than the values measured in KFM01A below DZ2.

While the results of the simulation are only a factor of 2 or 3 different, this difference could have an impact on the behaviour of models at the well scale. What this simple validation exercise shows is that, however good the current model may be for matching rock domain average values, it probably does not accurately predict intensities on a more local borehole scale at the level required. A borehole interval of 300 m is sufficiently large to be significant in a hydrological model, and whether over- or under-prediction of fracture intensity by a factor of three is acceptable is not determined in this report, but could possibly be significant.

More importantly, this very preliminary validation exercise points out the need to better understand why intensity values change significantly in the same rock domain and in the same borehole. This report has shown that in some zones, the changes in intensity coincide with the presence or absence of certain fracture sets, while in other cases, they do not. The size of these zones of relatively constant intensity often is several hundred meters, which is clearly large enough to be of consequence in hydrological and mechanical modelling. The lack of predictive accuracy in the validation shows that further investigations are needed to determine why there are large zones of varying intensity within a particular rock domain and borehole, and to develop a means to predict local intensity variations within a rock domain.

7 Alternative model approach based on orientation and size from the deformation zone model

The DFN model presented was based on lineaments with the assumption that all lineaments in the model volume represent fractures. Nevertheless the nature of a large amount of lineaments remains unspecified after the completion of the deformation zone model.

First three sections investigate the 2D deformation zone model and discusses possible differences to the base case DFN model.

The last section in this chapter describes an analysis made on detailed fracture data from one of the outcrops with a lower truncation length than 0.5 m (AFM100201).

7.1 Data sources

A horizontal cross section through the deformation zone model for Forsmark 1.2 gives the lengths and orientation of the deformation zones identified at surface level.

The files were imported into ArcView where the length of the traces of each structure is calculated. The orientation of the traces is given as the mean orientation for all segments of the deformation zone (1 segment in case of deformation zones not related to linked lineaments, several in case of a zone based on lineaments).

Data on outcrops and boreholes are identical to those presented in Section 2.

7.2 Orientation of deformation zone traces

Figure 7-1 illustrates the 2D deformation zone model used for the analysis.

Most of the steeply dipping deformation zones are related to linked lineaments but none of the gently dipping zone are.

The statistical analyses based on the 2D deformation zone model are quite poor as the amount of structures are low: The model consists of 14 gently dipping and 33 steeply dipping structures.

A rose diagram of the orientation of the structures is presented in Figure 7-2. The plot of orientation weighted with length is illustrated in Figure 7-3. Two main orientation sets, NW and NE, are clearly dominant. The NS and EW sets are barely significant. This image is enhanced when looking at the weighted rose diagram. The NW set is clearly the dominant one followed by the NE set. The NS set is not present at all.

The repartition of the orientation sets is very distinct between the steep and gently dipping structures (Figure 7-4). Steep dipping structures are mostly NW. Some NE and 1 NS structures are also identified. The gently dipping structures are exclusively oriented NE to EW.

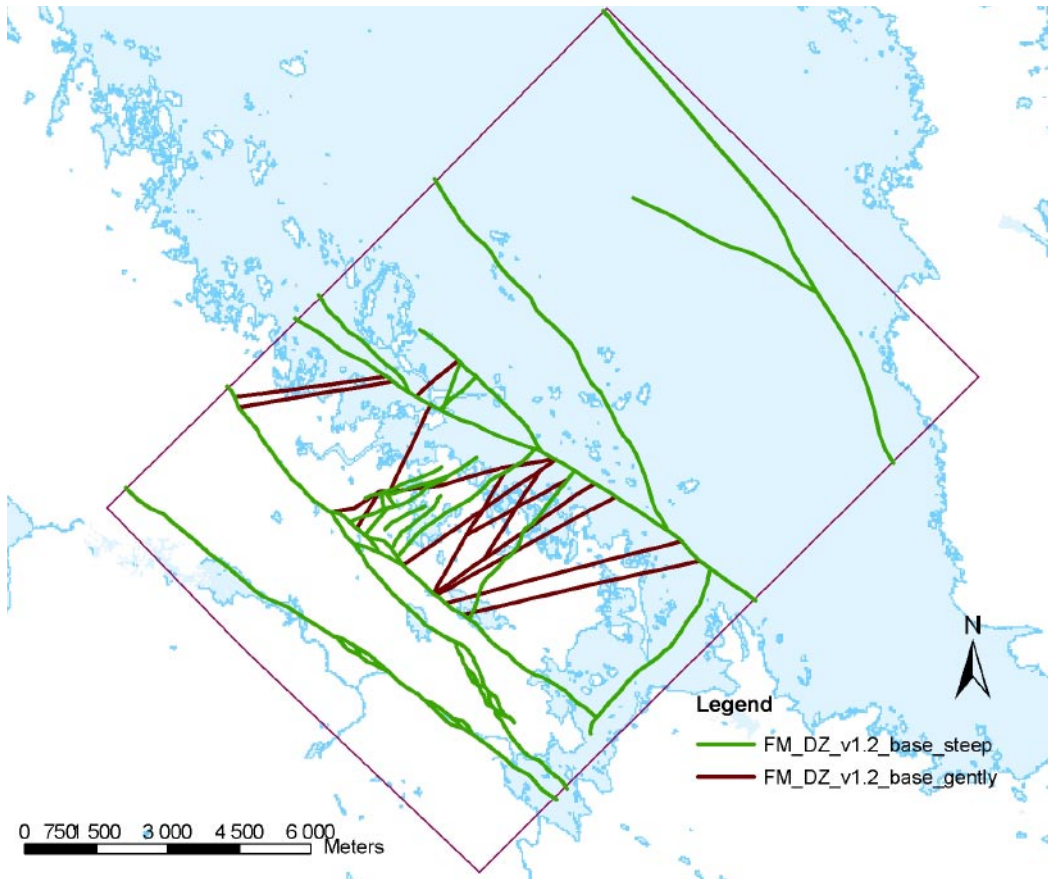


Figure 7-1. 2D section of the model for deformation zones, steeply and gently dipping structures.

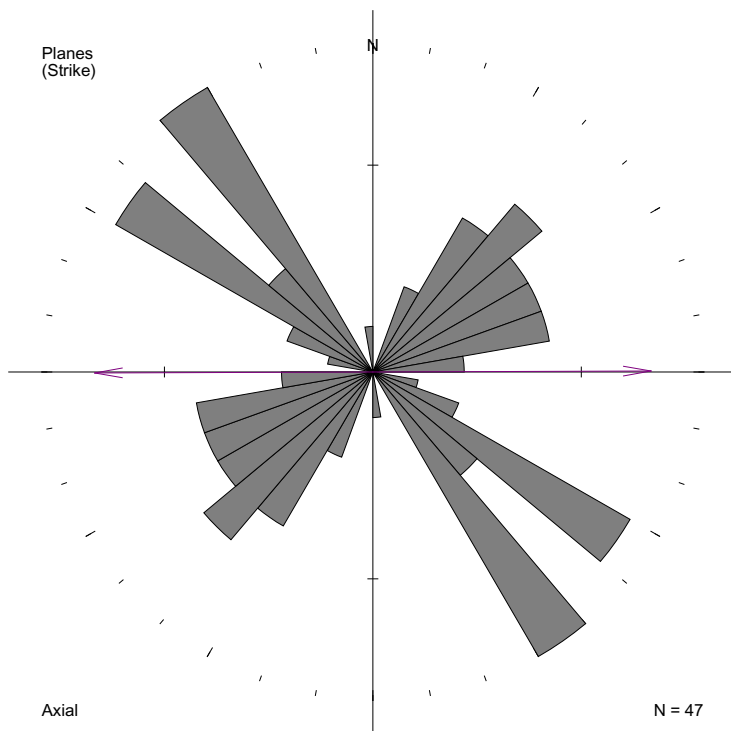


Figure 7-2. Rose diagrams for all structures in the model (equal area, angle 10°). The arrow represents the principal direction.

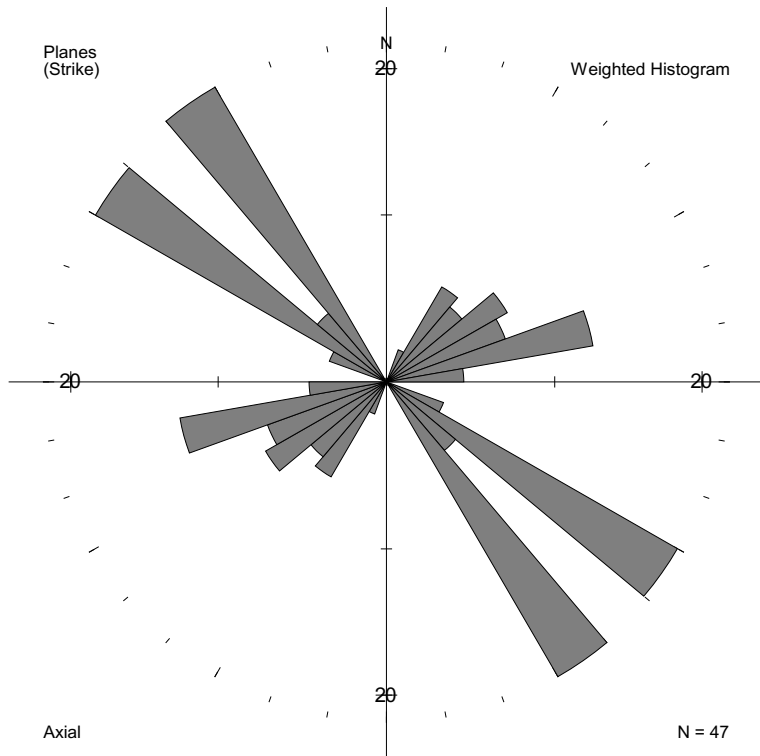


Figure 7-3. Weighted rose diagrams for all structures in the model (equal area, angle 10°). The arrow represents the principal direction.

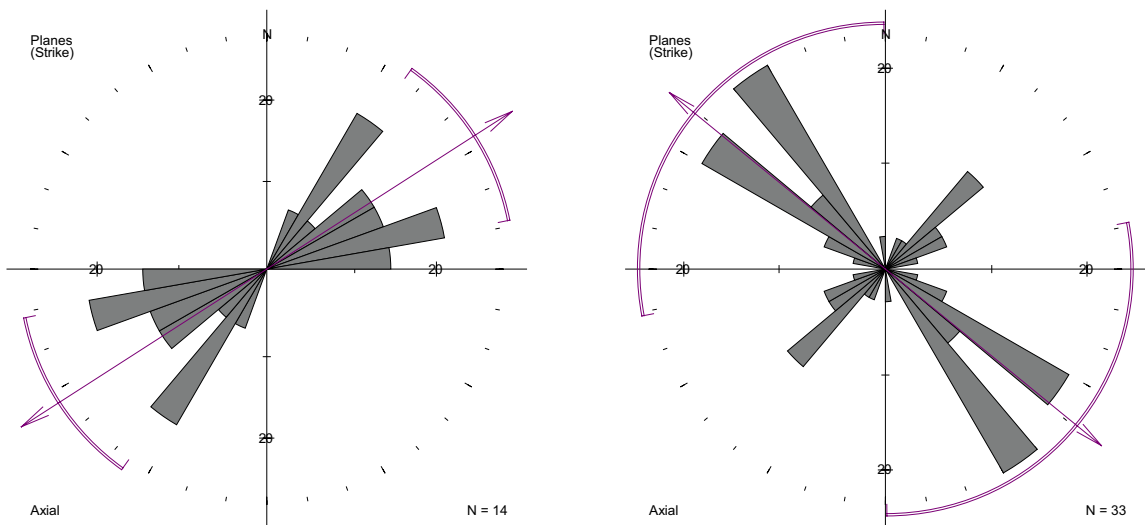


Figure 7-4. Rose diagrams for the a) gently dipping structures and b) steep dipping structures.

The principal directions identified are similar to those defined on all lineaments but because of the restricted amount of data the limit of sets is difficult to draw. The subvertical orientation sets identified in outcrops (Section 6.1) can be related to the orientation of the structures identified in the 2D deformation zone model.

Hence the orientation sets identified in Section 6.1.1 is valid also for this model.

7.3 Size of deformation zone traces

Relatively few deterministic deformation zones were identified in the 2D DZ model, which hinders calculating representative statistics for each orientation set. In fact most of the deformation zones have been identified in a quite small area inside of the local model volume, the remaining structures in the regional model volume are often regional deformation zones already identified. Almost all large deformation zones trending NW also terminate against the model boundary, which makes any size estimate highly biased.

The approach used has been to calculate the normalized number for each set of deformation zones identified in the 2D model and to plot this number on the normalization number plots presented in Section 6.2. However, the results show that the lengths of the deformation zones are on average longer than the lineaments. Including them in a powerlaw assumption with the outcrop data, and assuming that the minimum lengths are similar to the lineaments should produce a powerlaw size distribution with a k_t smaller than that for the lineaments. In practice it is impossible to quantify how much smaller k_t should be as the area that goes into the area renormalisation is difficult to estimate when deformation zones have only been recognized in a few spots over the local model domain, and are in many cases severely truncated

It is also likely that the identified deformation zones in the deformation zone model are the largest, most pronounced structures in the area together with a few localized smaller zones at specific locations where there have been drilling activities. To make statistics of this heterogeneous sub-sample of all possible deformation zones is risky as conclusions regarding their lengths can be highly over- or underestimated. In practice, the geologists are only able to confirm the position of the zones at discrete points, or in the best of cases over the length of a seismic reflector or similar. The modelled lengths of the deformation zones is a professional judgement based on all aggregated data sources to visually show the location and geological impact of the zone. However, this length is not intended to go into a statistical analysis of lengths to support the distribution of fractures over several scales.

It is also a matter of scale of observation; the deformation zone model is intended for illustrating the position of these zones at a regional scale and is in many cases simplified as single surfaces for modelling purposes. In reality these zones are possibly aggregates of many segments, splays etc. In contrast to the biased data from the deformation zones, it is actually an advantage to analyze the lineaments for statistical purposes, as this data set is at least treating all lineaments in an equal (but also biased) manner.

The conclusion of this analysis is that the lineament data still remains the best data set for analysing lengths of structures at a larger scale. The proposed size distribution estimation of the DFN model is therefore preferred.

7.4 Analysis of fracturing with lower truncation length (AFM100201)

The methodology used in the mapping of outcrop AFM100201 also provided an opportunity to assess the impact of a different mapping protocol on the derived DFN parameters. This analysis, although not an alternative model, can be found in Appendix 1, and assesses the impact of using fracture data of a much smaller truncation length. The conclusions of this analysis was that the orientation distribution did not change from previous analyses on truncated data. The size distribution parameters also remain valid. In conclusion fracture data with a smaller truncation length does not change the results of the analysis.

8 Evaluation of uncertainties

8.1 Quantification and propagation of uncertainty

Uncertainty in the model derives from several sources, including the uncertainty inherent in the data variability among the various outcrops and boreholes, as well as in the conceptual model in which the data is used to construct.

The uncertainty in fracture orientation has been quantified by calculating the orientation dispersion for each set at each of the five outcrops, as well as through the consideration of alternative dispersion models that are statistically significant.

The uncertainty in the fracture intensity has been quantified by calculating the mean and standard deviation for intensity, stratified by fracture type (open vs sealed), rock unit domain and depth. Users of this information may choose to propagate the uncertainty into their own models or calculations according to stratified Monte Carlo sampling or by analytical techniques as is appropriate and adequate for the intended purpose.

The uncertainty in size is quantified in two different ways. For the horizontal fracture set, the size model for the parent fracture radius distributions are based on aggregating all of the outcrop data for that set, and estimating a model for the distribution of fracture radii. There is also a conceptual uncertainty for this set, as its relation to other tectonic features is unknown, and the current method for calculating the size of the fractures assumes that it is not related to any other tectonic feature such as a lineament. For the lineament-related sets, three values are given: two bounding cases and a “best-guess”. Because of the artifacts having to do with censoring of trace length data, the trace length model fit to the normalized data is done visually rather than through non-linear regression. The “best-guess” is the best visual fit through all of the outcrop and lineament data. The two bounding cases are lines that approximate the shallowest and steepest lines that could be fit through the data. These represent the span of possible size variation given the existing data. As in the case of orientations, it is up to the user of this data to decide which parameter values to select.

Uncertainty in the spatial model is not completely specified except at the conceptual level. Because of current outcrop and borehole coverage, there is no fracture data for all specified rock domains, but it is possible that these unsampled domains have different spatial models than the sampled domains, as pointed out. Moreover, the mass fractal analysis showed a slight departure in the spatial model from Poissonian towards a slightly fractal spatial pattern. The conceptual uncertainty as to whether to specify the spatial model as Poissonian or slightly fractal will slightly impact the size calculations in a minor way, although the treatment of size uncertainty probably overshadows the impact, including the possibility to estimate the mass fractal dimension. It will also slightly impact the number of fractures in the larger scale models which extrapolate the P_{32} from small scales, like outcrops, to entire model regions. Depending upon whether the mass dimension is slightly below or above 2.0, the large scale model will overestimate or underestimate, respectively, the number of fractures that would be inferred from the Poissonian spatial model. However, the uncertainty inherent in the P_{32} intensity for the small domain probably has a far greater impact than the scaling uncertainty.

Overall, the uncertainty in the model has been reduced by stratifying the DFN geometry as a function of rock domain.

8.2 Unresolved aspects of uncertainty

The primary unresolved uncertainty that seems likely to have the largest impact on models is the intensity, and perhaps the fracture size, as a function of rock domain. The current outcrop and borehole data are very limited by the number of domains for which there is adequate data. Extrapolation of the values calculated for these few domains is a possible major uncertainty for site-scale modeling.

Another important unresolved uncertainty is the size model for the horizontal set. If these fractures are on the order of tens or hundreds of meters in radius, which is not possible to resolve from outcrop trace data for the current outcrop data sets, then this could have a major impact on flow and transport behavior of the rock mass.

A final unresolved uncertainty is the impact of intervals of high and low intensity in the boreholes, and how to incorporate this in site-scale models. The data and validation exercise showed that there were zones of open and sealed fracture intensity, extending from a few meters to a few hundred meters in vertical extent, where intensity is higher or lower. The changes in intensity within a single borehole often were associated with the consistent presence or absence of some of the fracture sets. Why these bands of high and low intensity occur, and why they are associated with the presence or absence of sets has not been resolved. They do not identify either to clusters in a Poissonian spatial model or clusters in a Fractal spatial model. Moreover, the impact on calculating a single intensity value from a borehole, or prescribing a single orientation model for a borehole, when in fact most boreholes do not follow this simplified conceptual model, is not known. Because the controls on these zones are not known, the manner to best propagate this uncertainty to a larger-scale model is not known.

9 Summary

9.1 Stochastic DFN model summary

Table 9-1 summarizes the parameters and their values derived for this model version. The derivation of the model parameters has been presented in Chapter 6.

The conceptual model consists of four subvertical sets and one subhorizontal set. Based upon their mineral fillings, orientations and structural geometry, it is suggested that the fractures in the different sets may have formed at different times, probably during the Proterozoic Phase 2 through Phase 4 tectonic periods, with an initial phase prior to 1.7 bybp. There is no evidence to suggest that recent processes, such as deglaciation and crustal unloading, have produced significant new fractures. Even the subhorizontal fractures appear to be as old as the vertical fractures, based upon their fillings with epidote and intensity patterns with depth that track the vertical set intensities. Intensity patterns do not show shallow zones of higher open fracture intensity, as might be expected if surficial stress relief had significantly produced new fractures or opened old ones. The relation of the subhorizontal fractures to tectonic fabric or processes is not known.

The four subvertical sets appear to be related to structural lineaments in terms of orientation, relative intensity and size. This relation suggests that each subvertical fracture set consists of a single population of fractures that varies in size from centimetres to kilometres. This model implies that there are fractures in the tens of meter to hundreds of meter size range that are not well represented in outcrop or in the lineament data, but do exist in the rock mass.

The intensity of the fractures does not appear to vary with depth in any systematic way that could be related to stress relief. Rather, the fracturing outside of identified deformation zones is often found in intervals hundreds of meters in extent with relatively constant intensity. However, the intensity among the intervals, even in the same borehole, rock domain and lithology can vary significantly, as can the presence or absence of any of the fracture sets. The reasons for this are not currently known, but it is clear that each domain consists of subdomains, often hundreds of meters in extent, with internally homogeneous fracture properties, and substantial variations between the subdomains.

Within each domain, the spatial pattern of fracturing is well-approximated by a Poissonian model in which there is no correlation in fracture intensity and the location of each fracture is independent of the location of other fractures.

In summary, the conceptual fracture model consists of five sets that probably formed during the early deformation stages of the craton. There is no need to call upon recent deglaciation to explain the generation of the fractures. The fractures show different intensity characteristics in different rock domains, and even within a single rock domain, there are subdomains of different intensity and orientation that show low variation within the subdomain, and large variation among subdomains. There is no variation of fracture intensity with depth that is consistent. The four subvertical sets are probably part of much larger fracture sets that also include structural lineaments.

Table 9-1. Summary of DFN model parameters.

Model Summary					
Number of sets	5	four subvertical associated with lineament trends; one subhorizontal			
Orientation of Sets	Name	Probability Distribution model	Mean Pole Trend/ Plunge	Dispersion	Major Axis Trend/ Plunge
	NS	Bivariate Fisher	92.4/5.9	19.31, 19.69	355.3/50.2
	NE	Bivariate Bingham	137.3/3.7	-17.09, -9.1	38.1/68.2
	NW	Fisher	40.6/2.2	23.9	
	EW	Fisher	190.4/0.7	30.63	
	HZ	Fisher	342.9/80.3	8.18	
Size	Name	Probability Distribution model	Exponent	Minimum Radius (m)	
	NS	Power Law	2.88	0.28	
	NE	Power Law	3.02	0.25	
	NW	Power Law	2.81	0.14	
	EW	Power Law	2.95	0.15	
	HZ	Power Law	2.92	0.25	
Spatial	Poissonian within each Rock Domain				
Intensity ($P_{32}-m^2/m^3$)	Name	Open	Partly Open	Sealed	Total
Domain 29	NS	0.12	0.01	0.47	0.60
	NE	0.46	0.05	1.56	2.07
	NW	0.16	0.01	0.27	0.45
	EW	0.05	0.00	0.17	0.23
	HZ	0.34	0.01	0.26	0.61
	All	1.13	0.09	2.73	3.95
Domain 18	NS	0.26	0.05	0.43	0.74
	NE	1.01	0.18	1.43	2.62
	NW	0.36	0.05	0.25	0.66
	EW	0.11	0.02	0.15	0.29
	HZ	0.73	0.04	0.24	1.01
	All	2.47	0.34	2.50	5.31
Domain 17	NS	0.01	0.01	0.51	0.53
	NE	0.02	0.04	1.70	1.77
	NW	0.01	0.01	0.30	0.32
	EW	0.00	0.00	0.18	0.19
	HZ	0.02	0.01	0.28	0.31
	All	0.06	0.08	2.98	3.12
Domain 12	NS	0.22	0.10	1.04	1.36
	NE	0.84	0.37	3.46	4.67
	NW	0.30	0.11	0.60	1.01
	EW	0.09	0.04	0.37	0.51
	HZ	0.61	0.09	0.57	1.27
	All	2.06	0.71	6.05	8.82

9.2 Conclusions

1. The geological data available in core and percussion boreholes, outcrops and lineament maps has proven adequate to calculate site-scale geometrical parameters for mechanical and fluid flow DFN models;
2. Major conceptual and data uncertainties have been quantified with the exception of uncertainties in how fracture intensity and size might vary by rock domain for all rock domains, and also why certain sets appear to be present or absent over specific intervals in the same borehole;
3. The fracturing, both open and sealed, outside of deformation zones, is characterized by four subvertical sets related to four lineament sets, and a subhorizontal set whose relation to other tectonic structures has not been identified;
4. The spatial model for distribution of fractures is Poissonian and has been estimated from mass dimension calculation and spatial correlation analyses among percussion boreholes. In some cases a low fractal pattern could be observed by the mass dimension calculation. Nevertheless the sharp contrast between the intervals of high or low fracture intensity does not support the definition of a spatial fractal pattern, but rather a series of domains within which the fractures conform to a Poissonian spatial model;
5. The fracture intensity of the DFN model is stratified by rock domains, both to reduce uncertainty and to reproduce the measured data with the most accuracy;
6. The orientations of the subvertical fractures rarely are constant with depth. Typically, they form vertically contiguous intervals from a few meters to a few hundred meters in extent, where specific sets are either present or absent relative to other zones in the borehole. The causes of this are not entirely clear, but seem to be a function of rock type and rock domain. However as the variation pattern and its constraints are still uncertain, the relative proportion of the orientation sets is kept constant in the DFN conceptual model;
7. There is no evidence for, and much evidence against, the hypothesis that there is recent fracturing within a few tens of meters of the surface due to causes such as glacial unloading, surficial stress relief or other mechanism. Rather, all evidence to date from the boreholes suggests that intervals of high and low fracture intensity do exist, but formed at a much older time, probably at least in part prior to 1.7 bypb. However the fracture pattern mapped on outcrop AFM100201 includes a higher proportion of glacial fractures in proportions that were not observed in other outcrops in the area /Hansen et al. 2004/; and
8. Future work directed at better quantifying the size of the horizontal fracture set, and the fracture characteristics of unsampled rock domains, would probably be the most useful in reducing model uncertainty.

10 References

Analyses-It Software LTD, 2003. Analyse-It Software, ltd. PO Box 77, Leeds LS12 5XA, England, UK.

Hansen L, Hermanson J, Vestgård J, Leiner P, 2004. Detailed fracture mapping of excavated rock outcrop at drilling site 5, AFM100201. Forsmark site investigation. SKB P-04-90. Svensk Kärnbränslehantering AB.

Isaksson H, Thunehed H, Mattsson H, Keisu M, 2004. Interpretation of airborne geophysics and integration with topography. Stage 1 (2002). SKB P-04-29, Svensk Kärnbränslehantering AB.

La Pointe P R, 2001. Scaling analysis of natural fracture system in support for fluid modeling and seismic risk assessment (abstr.). Annual Meeting, American Geophysical Union, December 14, 2001, San Francisco, CA.

La Pointe P R, 2002. Derivation of parent fracture population statistics from trace length measurements for fractal fracture populations. International Journal of Rock Mechanics and Mining Sciences, Vol. 39, 381–388.

Microsoft Corporation, 2000. Excel 2002, Version (10.5815.4219) SP-2, MicroSoft Corp. www.microsoft.com

Munier R, 2004. Statistical analysis of fracture data, adapted for modeling Discrete Fracture Networks – Version 2. SKB R-04-66. Svensk Kärnbränslehantering AB.

Munier R, 1989. Brittle tectonics on Äspö, SE Sweden. SKB HRL Progress report 25-89-15. Svensk Kärnbränslehantering AB.

Press W H, Teukolsky S A, Vetterling W T, Flannery B P, 1992. Numerical Recipes in FORTRAN: The Art of Scientific Computing (second edition). Cambridge University Press, Cambridge.

SKB, 2004. Preliminary Site Description – Forsmark area – version 1.1. SKB R-04-15. Svensk Kärnbränslehantering AB. Preliminary Site Description – Forsmark area – version 1.2. SKB R-05-18. Svensk Kärnbränslehantering AB.

Tullborg E-L, Larsson S Å, Stiberg J-P, 1996. Subsidence and uplift of the present land surface in the southeastern part of the Fennoscandian Shield. GFF, 118: 126–128.

Sensitivity analysis

1 Influence of the truncation length for mapping on outcrops

1.1 Influence on fracture orientation

The total amount of fractures and the amount of fractures shorter than 0.5 m that have been mapped per outcrop is presented in Table 1. The amount of open and closed fractures is also given. In all cases except AFM100201 fractures shorter than 0.5 m that have been mapped are sealed fractures which might indicate a bias in the measurements. However the proportion of fractures shorter than 0.5 m is most often low enough not to influence the orientation density distribution.

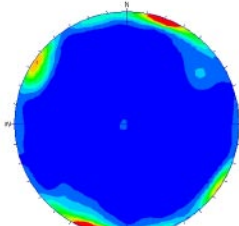
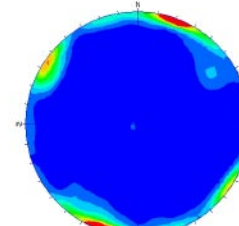
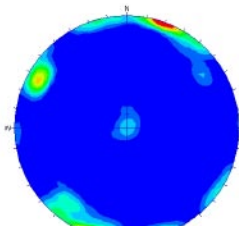
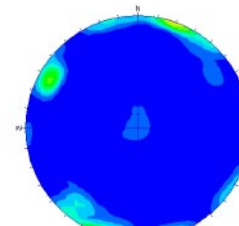
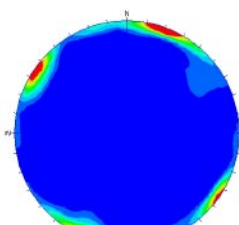
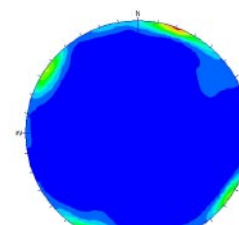
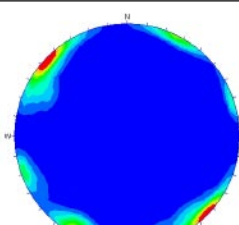
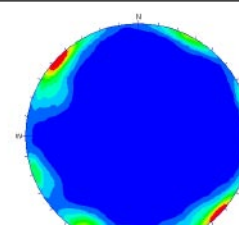
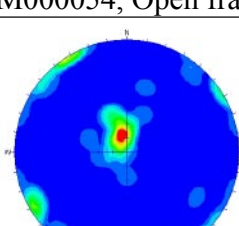
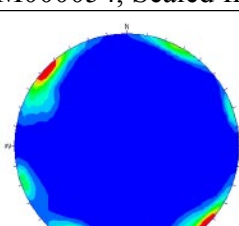
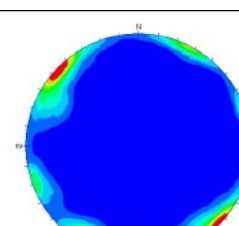
In all cases except AFM100201 data for fractures shorter than 0.5 m are available as a result of mapping procedure in the field. The amount of fractures shorter than 0.5 m that is mapped is not representative of the amount of fractures shorter than 0.5 m on the same outcrop. Concerning AFM100201 no minimal truncation length was applied and all fractures visible on outcrop were mapped. In this case the amount of fractures shorter than 0.5 m mapped should be representative of this outcrop.

Table 1. Amount of fractures mapped on outcrops.

	Amount of fractures			Amount of fractures, L < 0.5 m		
	Total	Open	Sealed	Total	Open	Sealed
AFM000053	980 ⁽¹⁾	248	730	12	2	10
AFM000054	1,234	44	1,190	52	0	52
AFM001097	1,195	68	1,127	7	0	7
AFM001098	1,201	23	1,178	71	0	71
AFM100201	1,280	932	348	411	380	31

⁽¹⁾ Two undetermined apertures

Figure 1 illustrates the impact of the traces shorter than 0.5 m on the orientation sets identified from outcrop data. Even in the case of AFM100201 the presence of shorter trace lengths does not have a significant influence on the stereoplots.

All fracture length in data set	Longer or equal to 0.5m
<p>AFM000053, all fractures</p>  <p>Fisher Concentration % of total per 1.0 % area</p> <ul style="list-style-type: none"> 0.00 - 1.00 % 1.00 - 2.13 % 2.13 - 3.25 % 3.25 - 4.38 % 4.38 - 5.50 % 5.50 - 6.63 % 6.63 - 7.75 % 7.75 - 8.88 % 8.88 - 10.00 % >10.00 % <p>No Bias Correction Max. Conc. = 14.7942%</p> <p>Equal Area Lower Hemisphere 500 Poles 500 Entries</p>	 <p>Fisher Concentration % of total per 1.0 % area</p> <ul style="list-style-type: none"> 0.00 - 1.00 % 1.00 - 2.13 % 2.13 - 3.25 % 3.25 - 4.38 % 4.38 - 5.50 % 5.50 - 6.63 % 6.63 - 7.75 % 7.75 - 8.88 % 8.88 - 10.00 % >10.00 % <p>No Bias Correction Max. Conc. = 14.0422%</p> <p>Equal Area Lower Hemisphere 500 Poles 500 Entries</p>
<p>AFM000053, Open fractures</p>  <p>Fisher Concentration % of total per 1.0 % area</p> <ul style="list-style-type: none"> 0.00 - 1.50 % 1.50 - 2.50 % 2.50 - 3.50 % 3.50 - 4.50 % 4.50 - 5.75 % 5.75 - 6.91 % 6.91 - 7.98 % 7.98 - 9.04 % 9.04 - 10.00 % >10.00 % <p>No Bias Correction Max. Conc. = 12.5967%</p> <p>Equal Area Lower Hemisphere 240 Poles 240 Entries</p>	 <p>Fisher Concentration % of total per 1.0 % area</p> <ul style="list-style-type: none"> 0.00 - 1.50 % 1.50 - 2.50 % 2.50 - 3.50 % 3.50 - 4.50 % 4.50 - 5.75 % 5.75 - 6.91 % 6.91 - 7.98 % 7.98 - 9.04 % 9.04 - 10.00 % >10.00 % <p>No Bias Correction Max. Conc. = 12.4867%</p> <p>Equal Area Lower Hemisphere 240 Poles 240 Entries</p>
<p>AFM000053, Sealed fractures</p>  <p>Fisher Concentration % of total per 1.0 % area</p> <ul style="list-style-type: none"> 0.00 - 1.50 % 1.50 - 2.50 % 2.50 - 3.50 % 3.50 - 4.50 % 4.50 - 5.75 % 5.75 - 6.91 % 6.91 - 7.98 % 7.98 - 9.04 % 9.04 - 10.00 % >10.00 % <p>No Bias Correction Max. Conc. = 15.6167%</p> <p>Equal Area Lower Hemisphere 730 Poles 730 Entries</p>	 <p>Fisher Concentration % of total per 1.0 % area</p> <ul style="list-style-type: none"> 0.00 - 1.50 % 1.50 - 2.50 % 2.50 - 3.50 % 3.50 - 4.50 % 4.50 - 5.75 % 5.75 - 6.91 % 6.91 - 7.98 % 7.98 - 9.04 % 9.04 - 11.03 % 11.03 - 13.31 % 13.31 - 15.00 % >15.00 % <p>No Bias Correction Max. Conc. = 15.3069%</p> <p>Equal Area Lower Hemisphere 730 Poles 730 Entries</p>
<p>AFM000054, all fractures</p>  <p>Fisher Concentration % of total per 1.0 % area</p> <ul style="list-style-type: none"> 0.00 - 1.50 % 1.50 - 2.50 % 2.50 - 3.50 % 3.50 - 4.50 % 4.50 - 5.75 % 5.75 - 6.91 % 6.91 - 7.98 % 7.98 - 9.04 % 9.04 - 10.00 % >10.00 % <p>No Bias Correction Max. Conc. = 12.5151%</p> <p>Equal Area Lower Hemisphere 1224 Poles 1224 Entries</p>	 <p>Fisher Concentration % of total per 1.0 % area</p> <ul style="list-style-type: none"> 0.00 - 1.00 % 1.00 - 2.13 % 2.13 - 3.25 % 3.25 - 4.38 % 4.38 - 5.50 % 5.50 - 6.63 % 6.63 - 7.75 % 7.75 - 8.88 % 8.88 - 10.00 % >10.00 % <p>No Bias Correction Max. Conc. = 12.7514%</p> <p>Equal Area Lower Hemisphere 1102 Poles 1102 Entries</p>
<p>AFM000054, Open fractures</p>  <p>Fisher Concentration % of total per 1.0 % area</p> <ul style="list-style-type: none"> 0.00 - 1.50 % 1.50 - 2.50 % 2.50 - 3.50 % 3.50 - 4.50 % 4.50 - 5.75 % 5.75 - 6.91 % 6.91 - 8.25 % 8.25 - 9.91 % 9.91 - 11.03 % 11.03 - 13.31 % 13.31 - 15.00 % >15.00 % <p>No Bias Correction Max. Conc. = 16.8519%</p> <p>Equal Area Lower Hemisphere 44 Poles 44 Entries</p>	
<p>AFM000054, Sealed fractures</p>  <p>Fisher Concentration % of total per 1.0 % area</p> <ul style="list-style-type: none"> 0.00 - 1.50 % 1.50 - 2.50 % 2.50 - 3.50 % 3.50 - 4.50 % 4.50 - 5.75 % 5.75 - 6.91 % 6.91 - 7.98 % 7.98 - 9.04 % 9.04 - 10.00 % >10.00 % <p>No Bias Correction Max. Conc. = 13.8026%</p> <p>Equal Area Lower Hemisphere 1190 Poles 1190 Entries</p>	 <p>Fisher Concentration % of total per 1.0 % area</p> <ul style="list-style-type: none"> 0.00 - 1.00 % 1.00 - 2.13 % 2.13 - 3.25 % 3.25 - 4.38 % 4.38 - 5.50 % 5.50 - 6.63 % 6.63 - 7.75 % 7.75 - 8.88 % 8.88 - 10.00 % >10.00 % <p>No Bias Correction Max. Conc. = 13.0376%</p> <p>Equal Area Lower Hemisphere 1130 Poles 1130 Entries</p>
<p>AFM001098, all fractures</p>	

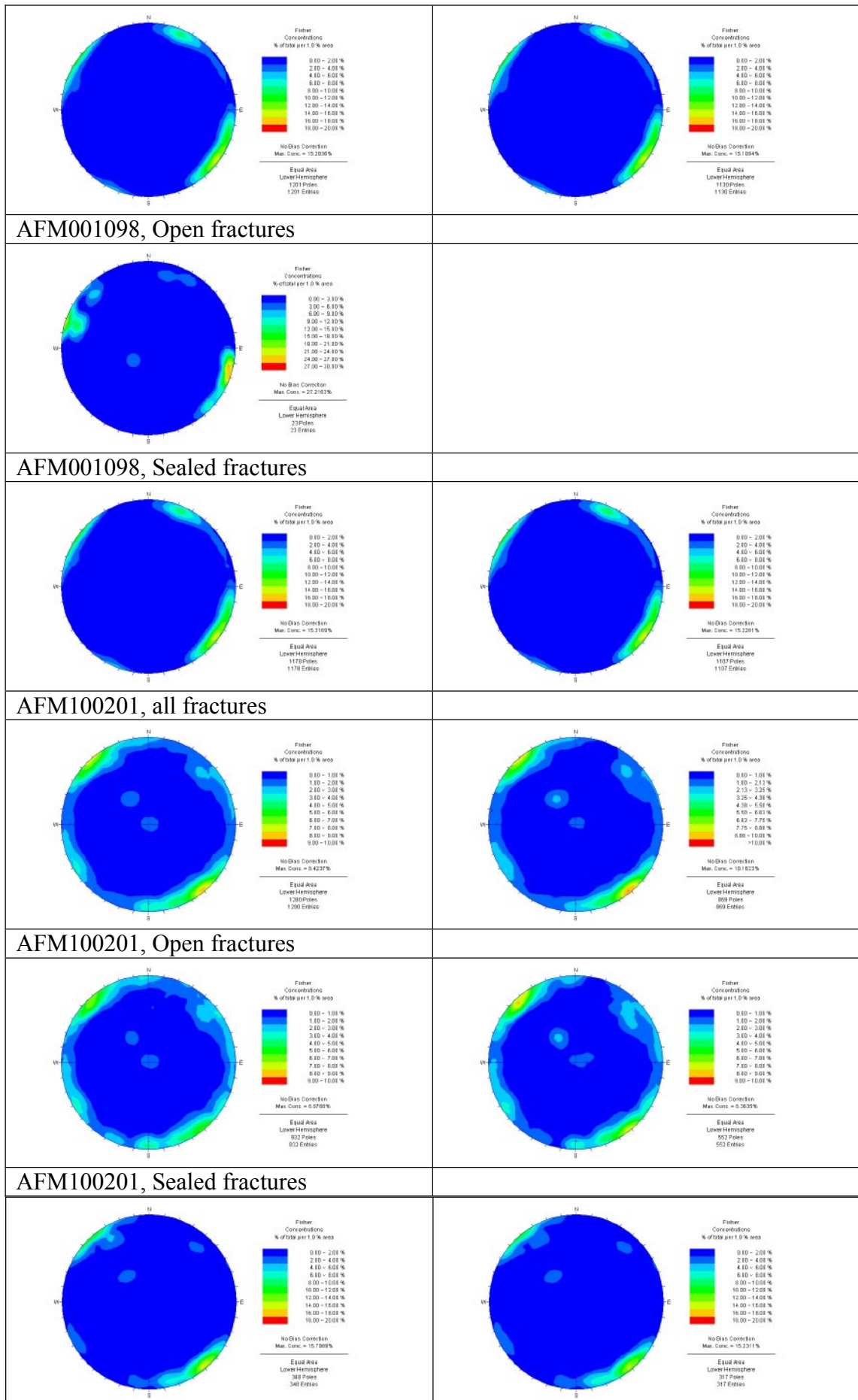


Figure 1. Stereoplots of poles to fracture planes on outcrops, for all trace lengths and for traces longer than 0.5 m.

1.2 Influence on fracture size distribution

The influence on fracture size distribution has been estimated using the same approach as presented in section 6.2. In this section all fractures were used for the calculations. Figure 2 and Figure 3 illustrates the normalization plot for the NS orientation set, truncated at 0.5 m and including all mapped fractures. The presence of shorter fractures does not influence the best fit curve for the Power law distribution.

However studying data sets without any truncation might be a good way to validate the choice of a Power law distribution for all fractures.

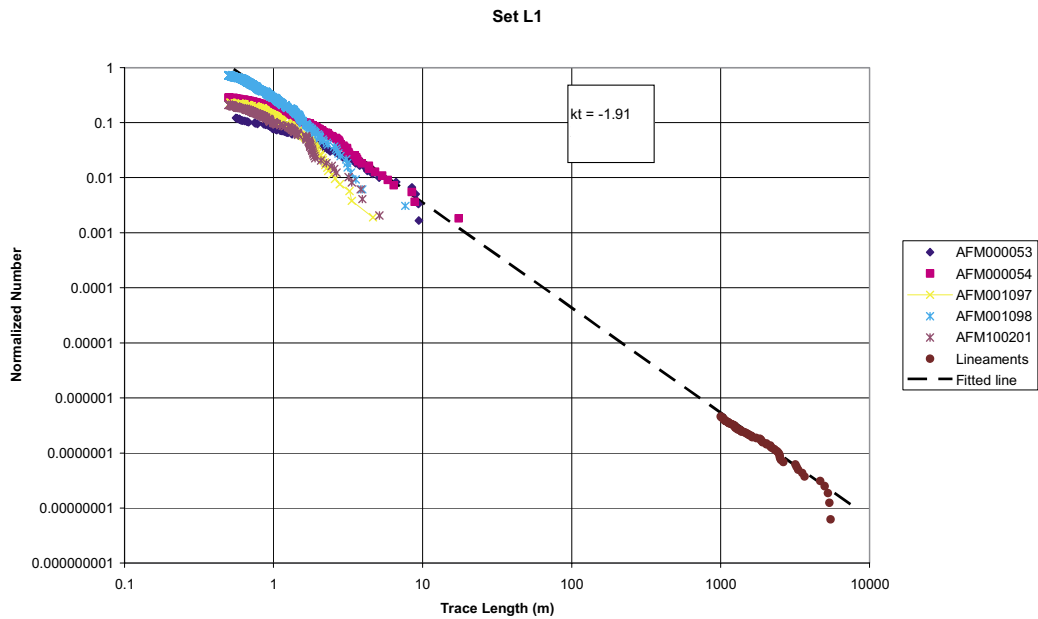


Figure 2. Normalization plot for the NS set, trace length longer than 0.5 m.

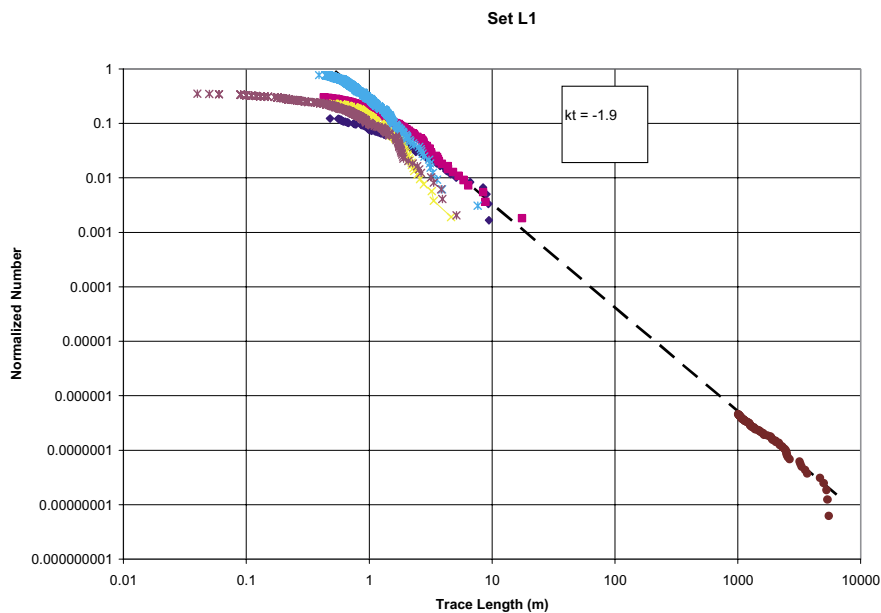


Figure 3. Normalization plot for the NS set, all trace lengths.

2 Influence of the truncation of lineaments

The main issues are:

- 1) The influence of offshore lineaments on the analysis. In the DFN analysis only lineaments onshore are studied. Based on Table 2 (amount of lineaments compared to the area of the volume) it is obvious that the density of lineaments onshore (SW box model) is higher than the density of lineaments offshore (NE box model). Nevertheless removing the data set from the NE box model from the DFN analysis might influence the rosette and the size distribution. In order to catch this impact, data from the SW box model were compared to data from the regional volume.
- 2) The influence of lineaments truncated at the border of the model volume on the size distribution. Several regional lineaments and a significant amount of local lineaments are truncated at the border of the regional volume. In order to study the impact of these truncated lineaments on the size distribution all truncated lineaments were removed from the data set and a new size distribution analysis was conducted.

Table 2. Length of the lineaments in the different boxes.

	n	Area, km ²	Mean	Std Dev.	Min	Max	Median
Regional box model, all	1,169	162	851	1,139	16	11,445	500
Regional box model, non truncated	1,042	162	738	827	16	7,970	466
SW box model, all	981	78	734	1,010	16	11,445	439
NE box model, all	188	84	1,461	1,518	125	11,389	1,017

2.1 Influence on orientation sets

Table 3 presents the relative proportion of lineament sets in the different model volumes. The rosettes for the three model volumes are presented in Figure 4 and Figure 5. The main discrepancy is observed in the occurrence of the NW lineament set. This difference is smoothed when weighting the lineament orientation with their length. The explanation is that the NW set is represented mostly by long and persistent lineaments, and are mostly located in the NE part of the regional model.

Table 3. Repartition of the lineaments in the 4 identified sets in the different boxes.

		L1 (NS)	L2 (NE)	L3 (NW)	L4 (EW)
Regional box model,	n	315	363	335	156
all	%	26.95	31.05	28.66	13.34
Regional box model,	n	280	334	291	137
non truncated	%	26.87	32.05	27.93	13.15
SW box model, all	n	267	313	269	132
	%	27.22	31.91	27.42	13.46
NE box model, all	n	48	50	66	24
	%	25.53	26.6	35.11	12.77

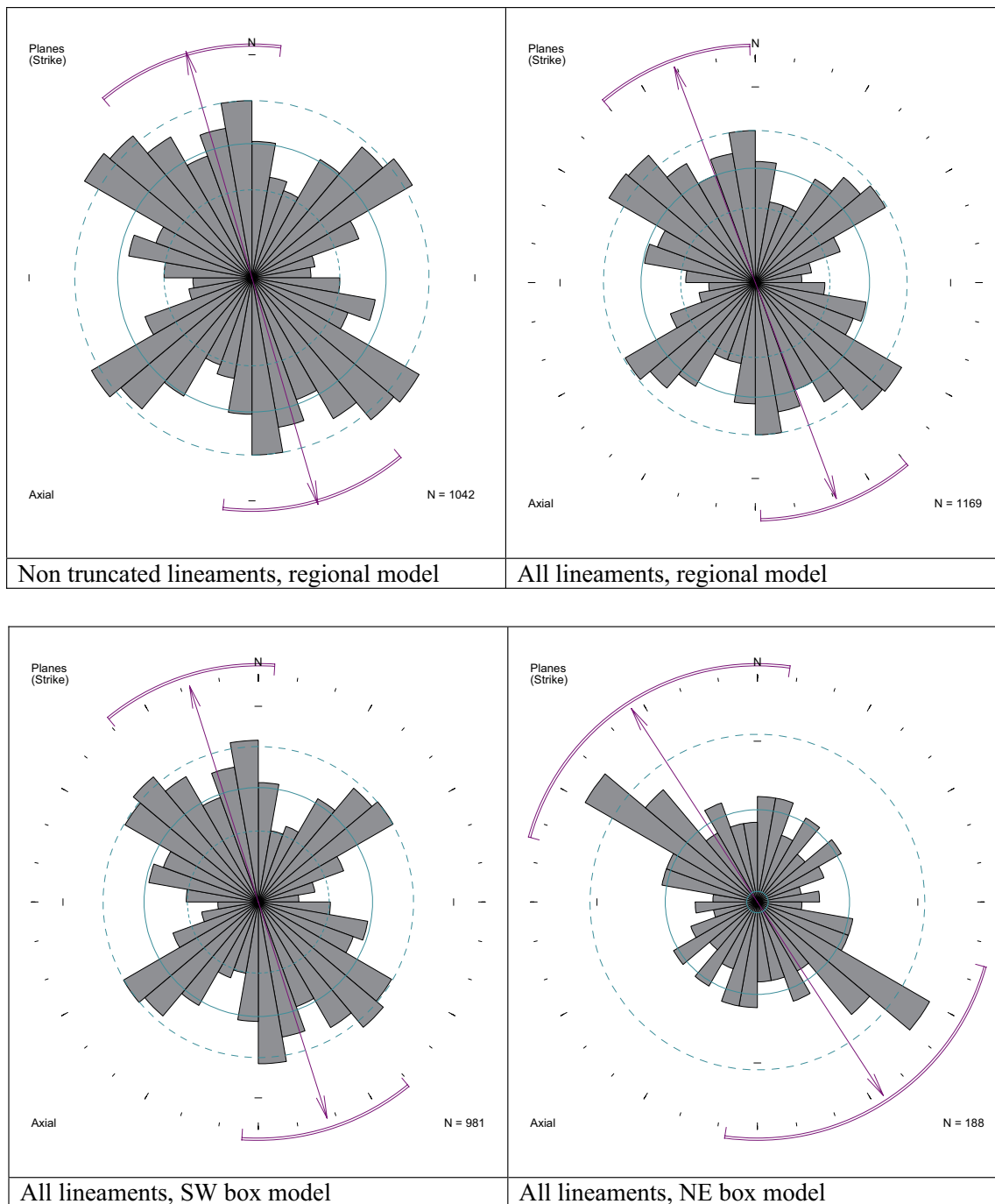


Figure 4. Rosette diagrams (non weighted) for lineaments in the different model volumes.

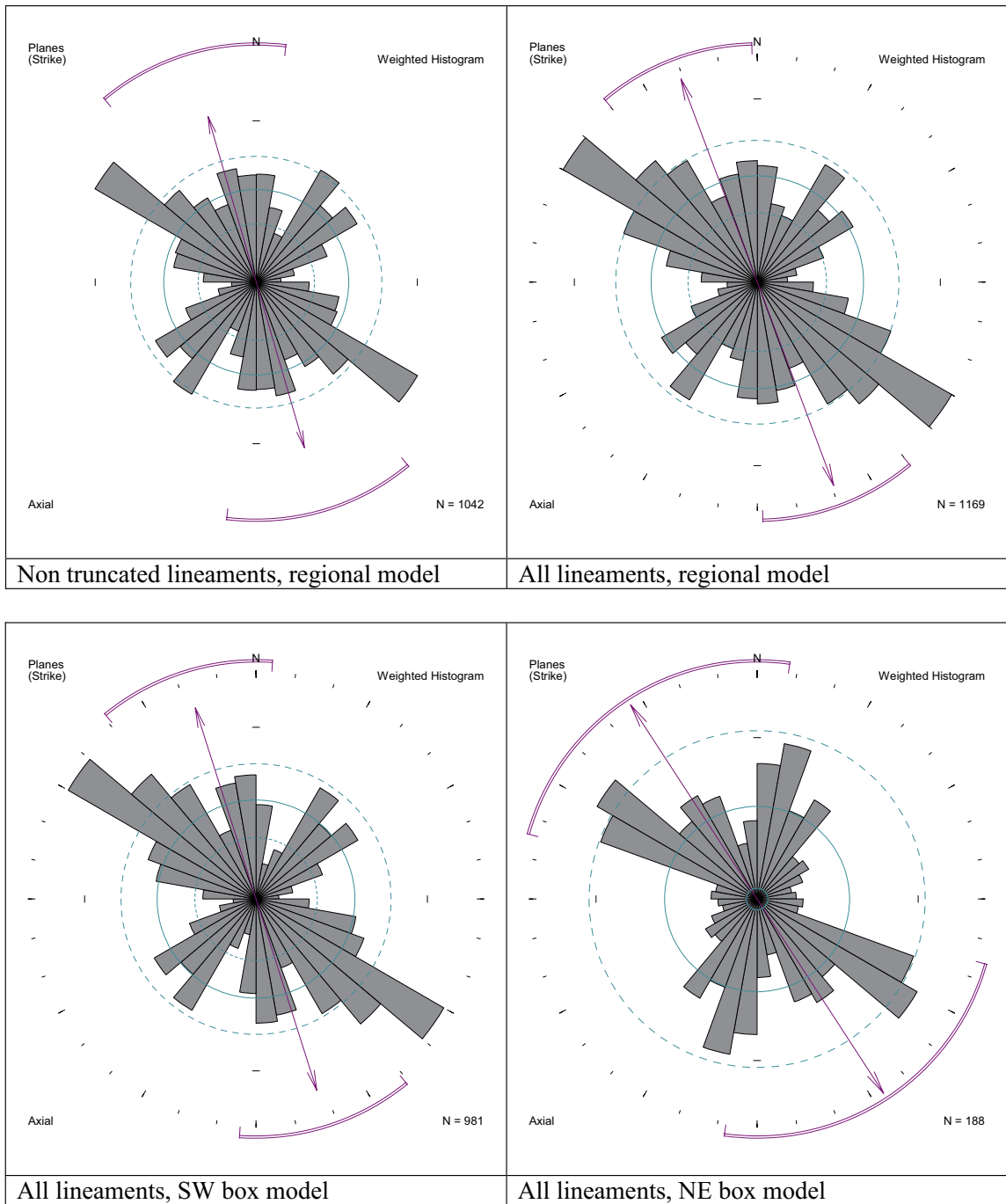


Figure 5. Rosette diagrams (weighted with length) for lineaments in the different model volumes.

2.2 Influence on the size distribution

While outcrop data is still the same (no fractures shorter than 0.5 m, selection per set) the different sets of lineament data are plotted and the parameters of the Power law median fit are calculated. The parameters of the fit are presented in Table 4.

The truncation of the lineaments data sets towards shorter lineaments (less than 1,000 m) does not affect the normalization plots or the regression lines as they most often fall out of the linear part of the plot which is used to fit the Power law distribution. However the identification of lineaments in different model areas might change the plots significantly.

Table 4. Parameters for the power law size distribution of the parent population.

	L1 (NS) K_t	L2 (NE) K_t	L3 (NW) K_t	L4 (EW) K_t
Regional box model, all	1.88	2.03	1.82	1.95
Regional box model, longer than 1,000 m	1.88	2.02	1.81	1.95
Regional box model, non truncated	1.9	2.07	1.96	2.02
SW box model, all	1.89	2.04	1.83	1.92
SW box model, longer than 1,000 m	1.89	2.04	1.83	1.92

The most significant variations are noticed for the NW and EW sets but the parameters are still in the span of the lower and upper bounds defined in the main analysis. The overall variations are estimated to be less than the “user-dependent” variation.

Cross tabulation tables from statistical analyses

Table 1. Contingency table of lithology vs fracture intensity.

Crosstab

		ROCK_TYP								Total	
		101051.00	101054.00	101056.00	101057.00	101061.00	102017.00	103076.00	111058.00		
SHIZ	.0	Count	773	70	0	5644	185	271	26	148	7117
		Expected Count	744.8	46.4	313.0	5432.4	151.9	236.8	85.6	106.1	7117.0
		% within SHIZ	10.9%	1.0%	.0%	79.3%	2.6%	3.8%	.4%	2.1%	100.0%
		% within ROCK_TYP	68.8%	100.0%	.0%	68.9%	80.8%	75.9%	20.2%	92.5%	66.3%
1.0		Count	350	0	472	2547	44	86	103	12	3614
		Expected Count	378.2	23.6	159.0	2758.6	77.1	120.2	43.4	53.9	3614.0
		% within SHIZ	9.7%	.0%	13.1%	70.5%	1.2%	2.4%	2.9%	.3%	100.0%
		% within ROCK_TYP	31.2%	.0%	100.0%	31.1%	19.2%	24.1%	79.8%	7.5%	33.7%
Total		Count	1123	70	472	8191	229	357	129	160	10731
		Expected Count	1123.0	70.0	472.0	8191.0	229.0	357.0	129.0	160.0	10731.0
		% within SHIZ	10.5%	.7%	4.4%	76.3%	2.1%	3.3%	1.2%	1.5%	100.0%
		% within ROCK_TYP	100.0%	100.0%	100.0%	100.0%	100.0%	100.0%	100.0%	100.0%	100.0%
	% of Total	10.5%	.7%	4.4%	76.3%	2.1%	3.3%	1.2%	1.5%	100.0%	

Table 2. Statistical test results for crosstabulation of lithology vs fracture intensity

Chi-Square Tests

	Value	df	Asymp. Sig. (2-sided)
Pearson Chi-Square	1201.019 ^a	7	.000
Likelihood Ratio	1330.360	7	.000
Linear-by-Linear Association	30.021	1	.000
N of Valid Cases	10731		

a. 0 cells (.0%) have expected count less than 5. The minimum expected count is 23.57.

Directional Measures

			Value	Asymp. Std. Error ^a	Approx. T ^b	Approx. Sig.
Nominal by Nominal	Lambda	Symmetric	.089	.004	22.937	.000
		SHIZ Dependent	.152	.006	22.937	.000
		ROCK_TYP Dependent	.000	.000	. ^c	. ^c
Goodman and Kruskal tau		SHIZ Dependent	.112	.003		.000 ^d
		ROCK_TYP Dependent	.015	.001		.000 ^d
Uncertainty Coefficient		Symmetric	.079	.003	24.289	.000 ^e
		SHIZ Dependent	.097	.004	24.289	.000 ^e
		ROCK_TYP Dependent	.067	.002	24.289	.000 ^e

- a. Not assuming the null hypothesis.
- b. Using the asymptotic standard error assuming the null hypothesis.
- c. Cannot be computed because the asymptotic standard error equals zero.
- d. Based on chi-square approximation
- e. Likelihood ratio chi-square probability.

Table 3. Contingency table of primary mineral filing (MIN1) vs fracture intensity.

Crosstab

		SHIZ										Total				
		.0					1.0					Count	Expected Count	% within SHIZ	% within MIN_1	% of Total
		Count	Expected Count	% within SHIZ	% within MIN_1	% of Total	Count	Expected Count	% within SHIZ	% within MIN_1	% of Total					
MIN_1	Biotite	10	10.0	.2%	100.0%	.1%	0	3.4	.0%	.0%	.0%	10	10.0	.1%	100.0%	.1%
	Calcite	1198	1322.0	16.8%	60.1%	11.2%	795	671.0	22.0%	39.9%	7.4%	1993	1993.0	18.6%	100.0%	18.6%
	Chlorite	2076	2154.4	29.2%	63.9%	19.3%	1172	1093.6	32.4%	36.1%	10.9%	3248	3248.0	30.3%	100.0%	30.3%
	Clay Minerals	22	38.5	.3%	37.9%	.2%	36	19.5	1.0%	62.1%	.3%	58	58.0	.5%	100.0%	.5%
	Epidote	97	138.0	1.4%	46.6%	.9%	111	70.0	3.1%	53.4%	1.0%	208	208.0	1.9%	100.0%	1.9%
	Goethite	3	2.7	.0%	75.0%	.0%	1	1.3	.0%	25.0%	.0%	4	4.0	.0%	100.0%	.0%
	Hematite	478	453.0	6.7%	70.0%	4.5%	205	230.0	5.7%	30.0%	1.9%	683	683.0	6.4%	100.0%	6.4%
	Hornblende	1	.7	.0%	100.0%	.0%	0	.3	.0%	.0%	.0%	1	1.0	.0%	100.0%	.0%
	Hypersthene	2	1.3	.0%	100.0%	.0%	0	.7	.0%	.0%	.0%	2	2.0	.0%	100.0%	.0%
	Laumontite	740	707.8	10.4%	69.4%	6.9%	327	359.2	9.0%	30.6%	3.0%	1067	1067.0	9.9%	100.0%	9.9%
	Malachite	1	.7	.0%	100.0%	.0%	0	.3	.0%	.0%	.0%	1	1.0	.0%	100.0%	.0%
	None	781	863.6	11.0%	60.0%	7.3%	521	438.4	14.4%	40.0%	4.9%	1302	1302.0	12.1%	100.0%	12.1%
	Oxidized Walls	769	607.6	10.8%	84.0%	7.2%	147	308.4	4.1%	16.0%	1.4%	916	916.0	8.5%	100.0%	8.5%
	Potash Feldspar	8	7.3	.1%	72.7%	.1%	3	3.7	.1%	27.3%	.0%	11	11.0	.1%	100.0%	.1%
	Prehnite	288	291.2	4.0%	65.6%	2.7%	151	147.8	4.2%	34.4%	1.4%	439	439.0	4.1%	100.0%	4.1%
	Pyrite	16	29.8	.2%	35.6%	.1%	29	15.2	.8%	64.4%	.3%	45	45.0	.4%	100.0%	.4%
	Pyrrhotite	2	2.0	.0%	66.7%	.0%	1	1.0	.0%	33.3%	.0%	3	3.0	.0%	100.0%	.0%
	Quartz	414	307.8	5.8%	89.2%	3.9%	50	156.2	1.4%	10.8%	.5%	464	464.0	4.3%	100.0%	4.3%
	Red Feldspar	34	23.9	.5%	94.4%	.3%	2	12.1	.1%	5.6%	.0%	36	36.0	.3%	100.0%	.3%
	Sericite	0	.7	.0%	.0%	.0%	1	.3	.0%	100.0%	.0%	1	1.0	.0%	100.0%	.0%
	Sulfides	0	.7	.0%	.0%	.0%	1	.3	.0%	100.0%	.0%	1	1.0	.0%	100.0%	.0%
	Unknown mineral	140	132.0	2.0%	70.4%	1.3%	59	67.0	1.6%	29.6%	.5%	199	199.0	1.9%	100.0%	1.9%
	White Feldspar	2	1.3	.0%	100.0%	.0%	0	.7	.0%	.0%	.0%	2	2.0	.0%	100.0%	.0%
	X1	2	1.3	.0%	100.0%	.0%	0	.7	.0%	.0%	.0%	2	2.0	.0%	100.0%	.0%
	X9	23	15.3	.3%	100.0%	.2%	0	7.7	.0%	.0%	.0%	23	23.0	.2%	100.0%	.2%
	Zeolites	7	6.0	.1%	77.8%	.1%	2	3.0	.1%	22.2%	.0%	9	9.0	.1%	100.0%	.1%
Total		7120	7120.0	100.0%	66.3%	66.3%	3614	3614.0	100.0%	33.7%	33.7%	10734	10734.0	100.0%	100.0%	100.0%

Table 4. Statistical test results for crosstabulation of primary mineral filling (MIN1) vs fracture intensity.

Chi-Square Tests

	Value	df	Asymp. Sig. (2-sided)
Pearson Chi-Square	430.294 ^a	25	.000
Likelihood Ratio	482.812	25	.000
N of Valid Cases	10734		

a. 20 cells (38.5%) have expected count less than 5. The minimum expected count is .34.

Directional Measures

			Value	Asymp. Std. Error ^a	Approx. T ^b	Approx. Sig.
Nominal by Nominal	Lambda	Symmetric	.004	.002	2.431	.015
		SHIZ Dependent	.012	.005	2.431	.015
		MIN_1 Dependent	.000	.000	. ^c	. ^c
Goodman and Kruskal tau		SHIZ Dependent	.040	.003		.000 ^d
		MIN_1 Dependent	.003	.000		.000 ^d
Uncertainty Coefficient		Symmetric	.017	.001	12.195	.000 ^e
		SHIZ Dependent	.035	.003	12.195	.000 ^e
		MIN_1 Dependent	.011	.001	12.195	.000 ^e

- a. Not assuming the null hypothesis.
- b. Using the asymptotic standard error assuming the null hypothesis.
- c. Cannot be computed because the asymptotic standard error equals zero.
- d. Based on chi-square approximation
- e. Likelihood ratio chi-square probability.

Symmetric Measures

		Value	Approx. Sig.
Nominal by Nominal	Phi	.200	.000
	Cramer's V	.200	.000
	Contingency Coefficient	.196	.000
N of Valid Cases		10734	

- Not assuming the null hypothesis.
- Using the asymptotic standard error assuming the null hypothesis.

Table 5. Contingency table of secondary mineral filing (MIN2) vs fracture intensity.

Crosstab

		SHIZ										Total				
		.0					1.0									
		Count	Expected Count	% within SHIZ	% within MIN_2	% of Total	Count	Expected Count	% within SHIZ	% within MIN_2	% of Total	Count	Expected Count	% within SHIZ	% within MIN_2	% of Total
MIN_2	Asphalt	1	.7	.0%	100.0%	.0%	0	.3	.0%	.0%	.0%	1	1.0	.0%	100.0%	.0%
	Biotite	5	3.3	.1%	100.0%	.1%	0	1.7	.0%	.0%	.0%	5	5.0	.1%	100.0%	.1%
	Calcite	1067	989.0	29.0%	70.8%	19.1%	440	518.0	22.9%	29.2%	7.9%	1507	1507.0	26.9%	100.0%	26.9%
	Chalcopy	1	.7	.0%	100.0%	.0%	0	.3	.0%	.0%	.0%	1	1.0	.0%	100.0%	.0%
	Chlorite	553	619.5	15.1%	58.6%	9.9%	391	324.5	20.3%	41.4%	7.0%	944	944.0	16.9%	100.0%	16.9%
	Clay Min	81	117.5	2.2%	45.3%	1.4%	98	61.5	5.1%	54.7%	1.8%	179	179.0	3.2%	100.0%	3.2%
	Epidote	23	21.7	.6%	69.7%	.4%	10	11.3	.5%	30.3%	.2%	33	33.0	.6%	100.0%	.6%
	Goethite	9	11.2	.2%	52.9%	.2%	8	5.8	.4%	47.1%	.1%	17	17.0	.3%	100.0%	.3%
	Hematite	284	378.7	7.7%	49.2%	5.1%	293	198.3	15.2%	50.8%	5.2%	577	577.0	10.3%	100.0%	10.3%
	Hornblen	1	.7	.0%	100.0%	.0%	0	.3	.0%	.0%	.0%	1	1.0	.0%	100.0%	.0%
	Hypersth	2	2.0	.1%	66.7%	.0%	1	1.0	.1%	33.3%	.0%	3	3.0	.1%	100.0%	.1%
	Laumonti	128	190.3	3.5%	44.1%	2.3%	162	99.7	8.4%	55.9%	2.9%	290	290.0	5.2%	100.0%	5.2%
	Magnetit	1	.7	.0%	100.0%	.0%	0	.3	.0%	.0%	.0%	1	1.0	.0%	100.0%	.0%
	Malachit	1	.7	.0%	100.0%	.0%	0	.3	.0%	.0%	.0%	1	1.0	.0%	100.0%	.0%
	Muscovit	0	.7	.0%	.0%	.0%	1	.3	.1%	100.0%	.0%	1	1.0	.0%	100.0%	.0%
	Oxidized	1218	968.6	33.2%	82.5%	21.8%	258	507.4	13.4%	17.5%	4.6%	1476	1476.0	26.4%	100.0%	26.4%
	Potash F	6	3.9	.2%	100.0%	.1%	0	2.1	.0%	.0%	.0%	6	6.0	.1%	100.0%	.1%
	Prehnite	97	91.9	2.6%	69.3%	1.7%	43	48.1	2.2%	30.7%	.8%	140	140.0	2.5%	100.0%	2.5%
	Pyrite	55	142.4	1.5%	25.3%	1.0%	162	74.6	8.4%	74.7%	2.9%	217	217.0	3.9%	100.0%	3.9%
	Pyrrhoti	1	1.3	.0%	50.0%	.0%	1	.7	.1%	50.0%	.0%	2	2.0	.0%	100.0%	.0%
	Quartz	74	68.9	2.0%	70.5%	1.3%	31	36.1	1.6%	29.5%	.6%	105	105.0	1.9%	100.0%	1.9%
	Red Feld	19	15.1	.5%	82.6%	.3%	4	7.9	.2%	17.4%	.1%	23	23.0	.4%	100.0%	.4%
	Sericite	0	.7	.0%	.0%	.0%	1	.3	.1%	100.0%	.0%	1	1.0	.0%	100.0%	.0%
	Sulfides	1	.7	.0%	100.0%	.0%	0	.3	.0%	.0%	.0%	1	1.0	.0%	100.0%	.0%
	Unknown	34	33.5	.9%	66.7%	.6%	17	17.5	.9%	33.3%	.3%	51	51.0	.9%	100.0%	.9%
	White Fe	6	5.9	.2%	66.7%	.1%	3	3.1	.2%	33.3%	.1%	9	9.0	.2%	100.0%	.2%
	Zeolites	5	3.3	.1%	100.0%	.1%	0	1.7	.0%	.0%	.0%	5	5.0	.1%	100.0%	.1%
Total		3673	3673.0	100.0%	65.6%	65.6%	1924	1924.0	100.0%	34.4%	34.4%	5597	5597.0	100.0%	100.0%	100.0%

Table 6. Statistical test results for crosstabulation of secondary mineral filling (MIN2) vs fracture intensity.

Chi-Square Tests

	Value	df	Asymp. Sig. (2-sided)
Pearson Chi-Square	564.547 ^a	26	.000
Likelihood Ratio	576.052	26	.000
N of Valid Cases	5597		

- a. 27 cells (50.0%) have expected count less than 5. The minimum expected count is .34.

Directional Measures

			Value	Asymp. Std. Error ^a	Approx. T ^b	Approx. Sig.
Nominal by Nominal	Lambda	Symmetric	.053	.010	5.385	.000
		SHIZ Dependent	.088	.018	4.761	.000
		MIN_2 Dependent	.037	.011	3.162	.002
	Goodman and Kruskal tau	SHIZ Dependent	.101	.008		.000 ^c
		MIN_2 Dependent	.016	.001		.000 ^c
	Uncertainty Coefficient	Symmetric	.040	.003	12.577	.000 ^d
SHIZ Dependent		.080	.006	12.577	.000 ^d	
MIN_2 Dependent		.026	.002	12.577	.000 ^d	

- a. Not assuming the null hypothesis.
- b. Using the asymptotic standard error assuming the null hypothesis.
- c. Based on chi-square approximation
- d. Likelihood ratio chi-square probability.

Symmetric Measures

		Value	Approx. Sig.
Nominal by Nominal	Phi	.318	.000
	Cramer's V	.318	.000
	Contingency Coefficient	.303	.000
N of Valid Cases		5597	

- a. Not assuming the null hypothesis.
- b. Using the asymptotic standard error assuming the null hypothesis.

Table 7. Contingency table of fracture roughness vs fracture intensity.

Crosstab

			ROUGHNES				Total
			Irregula	Planar	Stepped	Undulati	
SHIZ	.0	Count	545	1809	208	420	2982
		Expected Count	556.3	1809.7	198.0	418.0	2982.0
		% within SHIZ	18.3%	60.7%	7.0%	14.1%	100.0%
		% within ROUGHNES	59.7%	60.9%	64.0%	61.2%	60.9%
		% of Total	11.1%	37.0%	4.3%	8.6%	60.9%
1.0		Count	368	1161	117	266	1912
		Expected Count	356.7	1160.3	127.0	268.0	1912.0
		% within SHIZ	19.2%	60.7%	6.1%	13.9%	100.0%
		% within ROUGHNES	40.3%	39.1%	36.0%	38.8%	39.1%
		% of Total	7.5%	23.7%	2.4%	5.4%	39.1%
Total		Count	913	2970	325	686	4894
		Expected Count	913.0	2970.0	325.0	686.0	4894.0
		% within SHIZ	18.7%	60.7%	6.6%	14.0%	100.0%
		% within ROUGHNES	100.0%	100.0%	100.0%	100.0%	100.0%
		% of Total	18.7%	60.7%	6.6%	14.0%	100.0%

Table 8. Statistical test results for crosstabulation of fracture roughness vs fracture intensity.

Chi-Square Tests

	Value	df	Asymp. Sig. (2-sided)
Pearson Chi-Square	1.899 ^a	3	.594
Likelihood Ratio	1.910	3	.591
N of Valid Cases	4894		

a. 0 cells (.0%) have expected count less than 5. The minimum expected count is 126.97.

Directional Measures

			Value	Asymp. Std. Error ^a	Approx. T ^b	Approx. Sig.
Nominal by Nominal	Lambda	Symmetric	.000	.000	. ^c	. ^c
		SHIZ Dependent	.000	.000	. ^c	. ^c
		ROUGHNES Dependent	.000	.000	. ^c	. ^c
Goodman and Kruskal tau		SHIZ Dependent	.000	.001		.594 ^d
		ROUGHNES Dependent	.000	.000		.791 ^d
Uncertainty Coefficient		Symmetric	.000	.000	.693	.591 ^e
		SHIZ Dependent	.000	.000	.693	.591 ^e
		ROUGHNES Dependent	.000	.000	.693	.591 ^e

- a. Not assuming the null hypothesis.
- b. Using the asymptotic standard error assuming the null hypothesis.
- c. Cannot be computed because the asymptotic standard error equals zero.
- d. Based on chi-square approximation
- e. Likelihood ratio chi-square probability.

Symmetric Measures

		Value	Approx. Sig.
Nominal by Nominal	Phi	.020	.594
	Cramer's V	.020	.594
	Contingency Coefficient	.020	.594
N of Valid Cases		4894	

- a. Not assuming the null hypothesis.
- b. Using the asymptotic standard error assuming the null hypothesis.

Table 9. Contingency table of alteration degree vs fracture intensity.

Crosstab

			ALTERATI				Total	
			Fresh	Gouge	Moderately Alter	Slightly Altered		
SHIZ	.0	Count	163	5872	8	35	1042	7120
		Expected Count	175.1	5768.2	6.0	37.8	1132.9	7120.0
		% within SHIZ	2.3%	82.5%	.1%	.5%	14.6%	100.0%
		% within ALTERATI	61.7%	67.5%	88.9%	61.4%	61.0%	66.3%
		% of Total	1.5%	54.7%	.1%	.3%	9.7%	66.3%
1.0	Count	101	2824	1	22	666	3614	
	Expected Count	88.9	2927.8	3.0	19.2	575.1	3614.0	
	% within SHIZ	2.8%	78.1%	.0%	.6%	18.4%	100.0%	
	% within ALTERATI	38.3%	32.5%	11.1%	38.6%	39.0%	33.7%	
	% of Total	.9%	26.3%	.0%	.2%	6.2%	33.7%	
Total	Count	264	8696	9	57	1708	10734	
	Expected Count	264.0	8696.0	9.0	57.0	1708.0	10734.0	
	% within SHIZ	2.5%	81.0%	.1%	.5%	15.9%	100.0%	
	% within ALTERATI	100.0%	100.0%	100.0%	100.0%	100.0%	100.0%	
	% of Total	2.5%	81.0%	.1%	.5%	15.9%	100.0%	

Table 10. Statistical test results for crosstabulation of alteration degree vs fracture intensity.

Chi-Square Tests

	Value	df	Asymp. Sig. (2-sided)
Pearson Chi-Square	32.391 ^a	4	.000
Likelihood Ratio	32.277	4	.000
N of Valid Cases	10734		

a. 1 cells (10.0%) have expected count less than 5. The minimum expected count is 3.03.

Directional Measures

			Value	Asymp. Std. Error ^a	Approx. T ^b	Approx. Sig.
Nominal by Nominal	Lambda	Symmetric	.000	.000	. ^c	. ^c
		SHIZ Dependent	.000	.000	. ^c	. ^c
		ALTERATI Dependent	.000	.000	. ^c	. ^c
Goodman and Kruskal tau		SHIZ Dependent	.003	.001		.000 ^d
		ALTERATI Dependent	.002	.001		.000 ^d
Uncertainty Coefficient		Symmetric	.002	.001	2.844	.000 ^e
		SHIZ Dependent	.002	.001	2.844	.000 ^e
		ALTERATI Dependent	.003	.001	2.844	.000 ^e

- a. Not assuming the null hypothesis.
- b. Using the asymptotic standard error assuming the null hypothesis.
- c. Cannot be computed because the asymptotic standard error equals zero.
- d. Based on chi-square approximation
- e. Likelihood ratio chi-square probability.

Table 11. Contingency table of ISRM alteration class vs fracture intensity.

Crosstab

		ALT ISRM							Total		
		0.8	1	2	3	4	6	8		none	
SHIZ	.0	Count	0	1637	601	326	195	4	1	474	3238
		Expected Count	.6	1382.9	611.3	373.7	137.9	7.9	.6	723.2	3238.0
		% within SHIZ	.0%	50.6%	18.6%	10.1%	6.0%	.1%	.0%	14.6%	100.0%
		% within ALT_ISRM	.0%	71.6%	59.4%	52.8%	85.5%	30.8%	100.0%	39.6%	60.5%
	% of Total	.0%	30.6%	11.2%	6.1%	3.6%	.1%	.0%	8.9%	60.5%	
	1.0	Count	1	650	410	292	33	9	0	722	2117
		Expected Count	.4	904.1	399.7	244.3	90.1	5.1	.4	472.8	2117.0
		% within SHIZ	.0%	30.7%	19.4%	13.8%	1.6%	.4%	.0%	34.1%	100.0%
		% within ALT_ISRM	100.0%	28.4%	40.6%	47.2%	14.5%	69.2%	.0%	60.4%	39.5%
	% of Total	.0%	12.1%	7.7%	5.5%	.6%	.2%	.0%	13.5%	39.5%	
Total		Count	1	2287	1011	618	228	13	1	1196	5355
		Expected Count	1.0	2287.0	1011.0	618.0	228.0	13.0	1.0	1196.0	5355.0
		% within SHIZ	.0%	42.7%	18.9%	11.5%	4.3%	.2%	.0%	22.3%	100.0%
		% within ALT_ISRM	100.0%	100.0%	100.0%	100.0%	100.0%	100.0%	100.0%	100.0%	100.0%
	% of Total	.0%	42.7%	18.9%	11.5%	4.3%	.2%	.0%	22.3%	100.0%	

Table 12. Statistical test results for crosstabulation of ISRM alteration class vs fracture intensity.

Chi-Square Tests

	Value	df	Asymp. Sig. (2-sided)
Pearson Chi-Square	418.019 ^a	7	.000
Likelihood Ratio	426.119	7	.000
N of Valid Cases	5355		

a. 4 cells (25.0%) have expected count less than 5. The minimum expected count is .40.

Directional Measures

			Value	Asymp. Std. Error ^a	Approx. T ^b	Approx. Sig.
Nominal by Nominal	Lambda	Symmetric	.063	.012	5.151	.000
		SHIZ Dependent	.120	.015	7.339	.000
		ALT_ISRM Dependent	.023	.012	1.945	.052
Goodman and Kruskal tau		SHIZ Dependent	.078	.007		.000 ^c
		ALT_ISRM Dependent	.027	.003		.000 ^c
Uncertainty Coefficient		Symmetric	.038	.004	10.637	.000 ^d
		SHIZ Dependent	.059	.006	10.637	.000 ^d
		ALT_ISRM Dependent	.028	.003	10.637	.000 ^d

- a. Not assuming the null hypothesis.
- b. Using the asymptotic standard error assuming the null hypothesis.
- c. Based on chi-square approximation
- d. Likelihood ratio chi-square probability.

Symmetric Measures

		Value	Approx. Sig.
Nominal by Nominal	Phi	.279	.000
	Cramer's V	.279	.000
	Contingency Coefficient	.269	.000
N of Valid Cases		5355	

- a. Not assuming the null hypothesis.
- b. Using the asymptotic standard error assuming the null hypothesis.

Table 13. Contingency table of fracture set vs fracture intensity.

Crosstab

		SET					Total	
		H	L1	L2	L3	L4		
SHIZ	.0	Count	1269	1555	2582	1079	635	7120
		Expected Count	1394.3	1289.5	2340.2	1440.1	656.0	7120.0
		% within SHIZ	17.8%	21.8%	36.3%	15.2%	8.9%	100.0%
		% within SET	60.4%	80.0%	73.2%	49.7%	64.2%	66.3%
		% of Total	11.8%	14.5%	24.1%	10.1%	5.9%	66.3%
1.0		Count	833	389	946	1092	354	3614
		Expected Count	707.7	654.5	1187.8	730.9	333.0	3614.0
		% within SHIZ	23.0%	10.8%	26.2%	30.2%	9.8%	100.0%
		% within SET	39.6%	20.0%	26.8%	50.3%	35.8%	33.7%
		% of Total	7.8%	3.6%	8.8%	10.2%	3.3%	33.7%
Total		Count	2102	1944	3528	2171	989	10734
		Expected Count	2102.0	1944.0	3528.0	2171.0	989.0	10734.0
		% within SHIZ	19.6%	18.1%	32.9%	20.2%	9.2%	100.0%
		% within SET	100.0%	100.0%	100.0%	100.0%	100.0%	100.0%
		% of Total	19.6%	18.1%	32.9%	20.2%	9.2%	100.0%

Table 14. Statistical test results for crosstabulation of fracture set vs fracture intensity.

Chi-Square Tests

	Value	df	Asymp. Sig. (2-sided)
Pearson Chi-Square	540.914 ^a	4	.000
Likelihood Ratio	543.011	4	.000
N of Valid Cases	10734		

a. 0 cells (.0%) have expected count less than 5. The minimum expected count is 332.98.

Directional Measures

			Value	Asymp. Std. Error ^a	Approx. T ^b	Approx. Sig.
Nominal by Nominal	Lambda	Symmetric	.015	.007	1.989	.047
		SHIZ Dependent	.004	.013	.279	.780
		SET Dependent	.020	.006	3.236	.001
	Goodman and Kruskal tau	SHIZ Dependent	.050	.004		.000 ^c
		SET Dependent	.014	.001		.000 ^c
	Uncertainty Coefficient	Symmetric	.023	.002	11.814	.000 ^d
SHIZ Dependent		.040	.003	11.814	.000 ^d	
SET Dependent		.016	.001	11.814	.000 ^d	

- a. Not assuming the null hypothesis.
- b. Using the asymptotic standard error assuming the null hypothesis.
- c. Based on chi-square approximation
- d. Likelihood ratio chi-square probability.

Symmetric Measures

		Value	Approx. Sig.
Nominal by	Phi	.224	.000
Nominal	Cramer's V	.224	.000
	Contingency Coefficient	.219	.000
N of Valid Cases		10734	

- a. Not assuming the null hypothesis.
- b. Using the asymptotic standard error assuming the null hypothesis.

Plots of TVDSS vs fracture strike

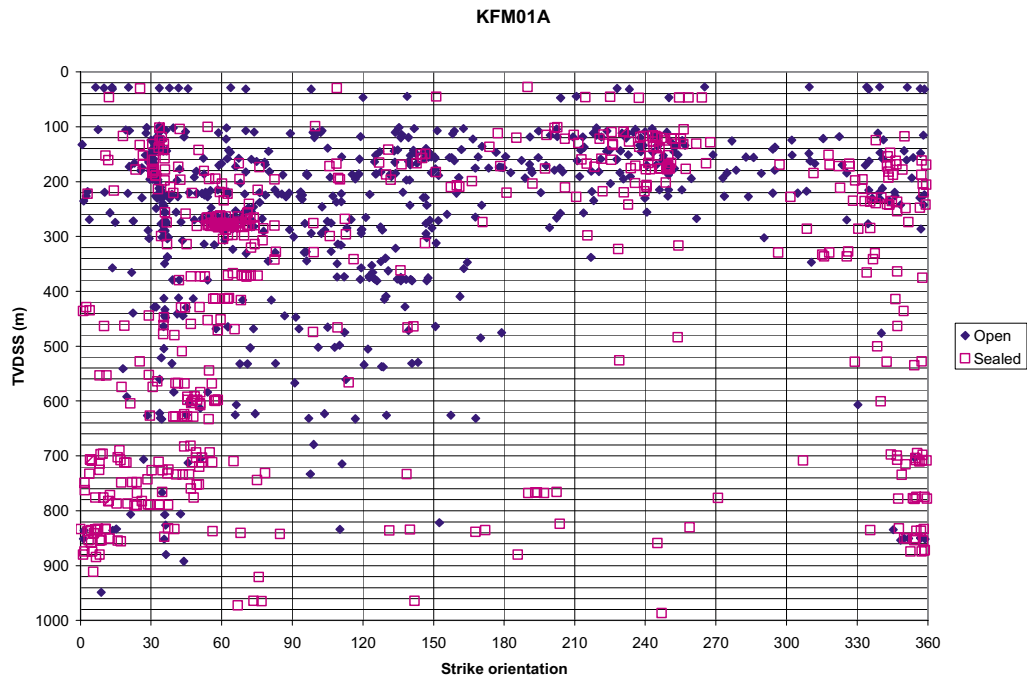


Figure 1. Variation of fracture strike with TVDSS, cored borehole KFM01A, open and sealed fractures.

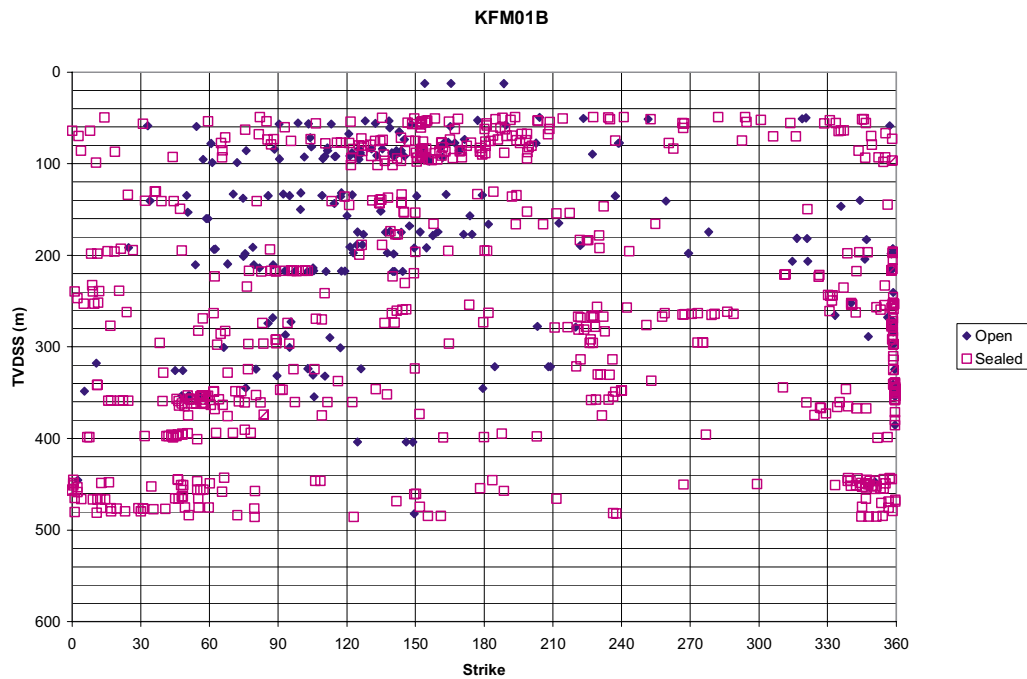


Figure 2. Variation of fracture strike with TVDSS, cored borehole KFM01B, open and sealed fractures.



Figure 3. Variation of fracture strike with TVDSS, cored borehole KFM02A, open and sealed fractures.

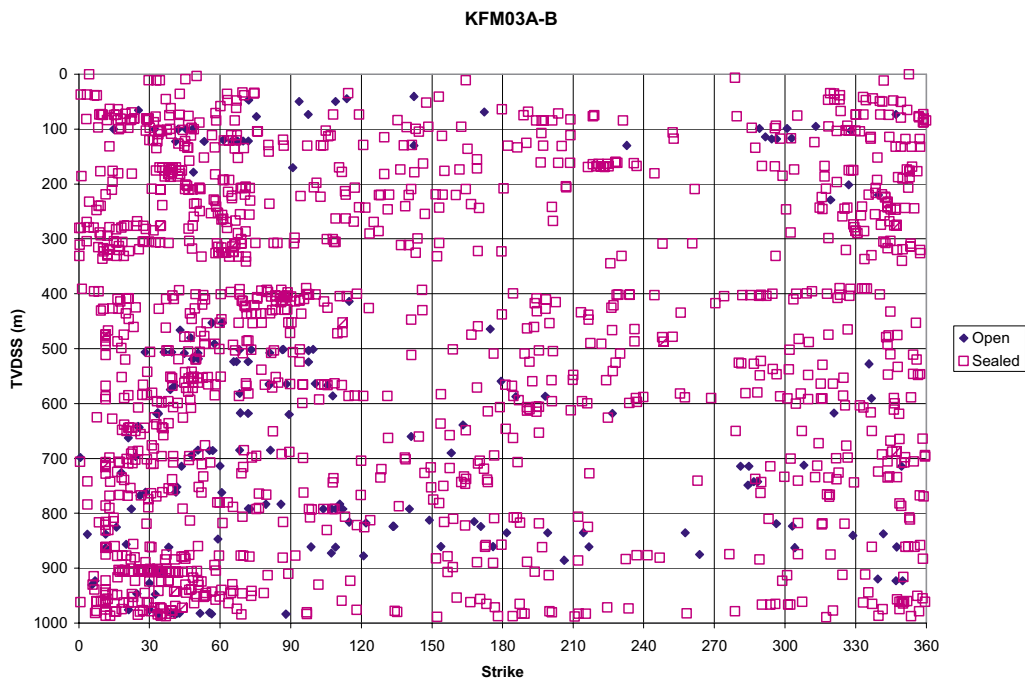


Figure 4. Variation of fracture strike with TVDSS, cored borehole KFM03A-B, open and sealed fractures.

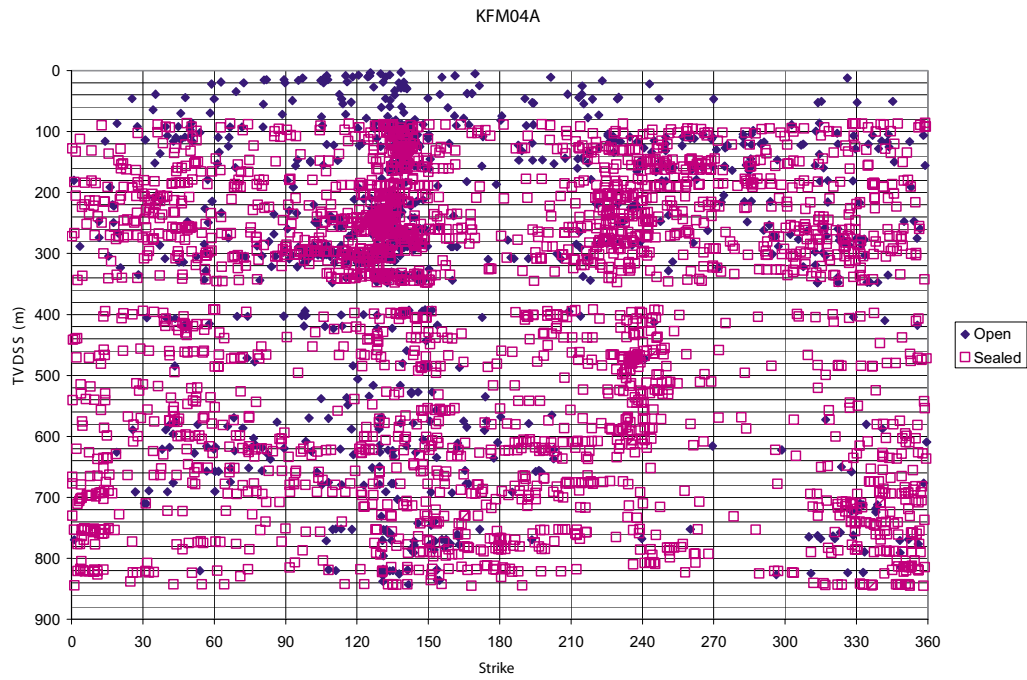


Figure 5. Variation of fracture strike with TVDSS, cored borehole KFM04A, open and sealed fractures.

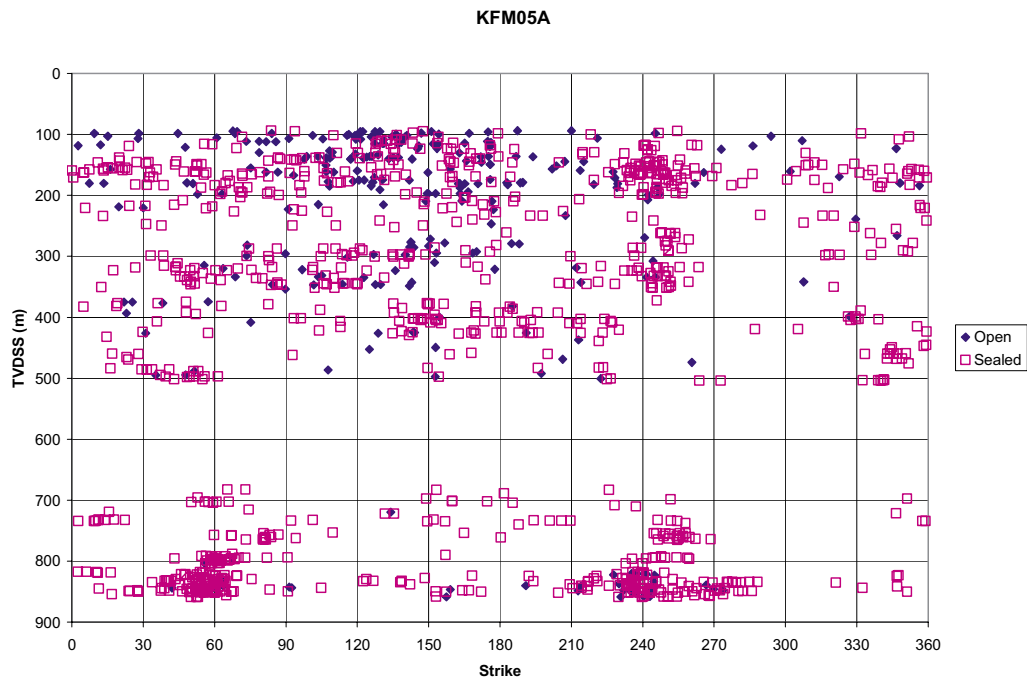


Figure 6. Variation of fracture strike with TVDSS, cored borehole KFM05A, open and sealed fractures.

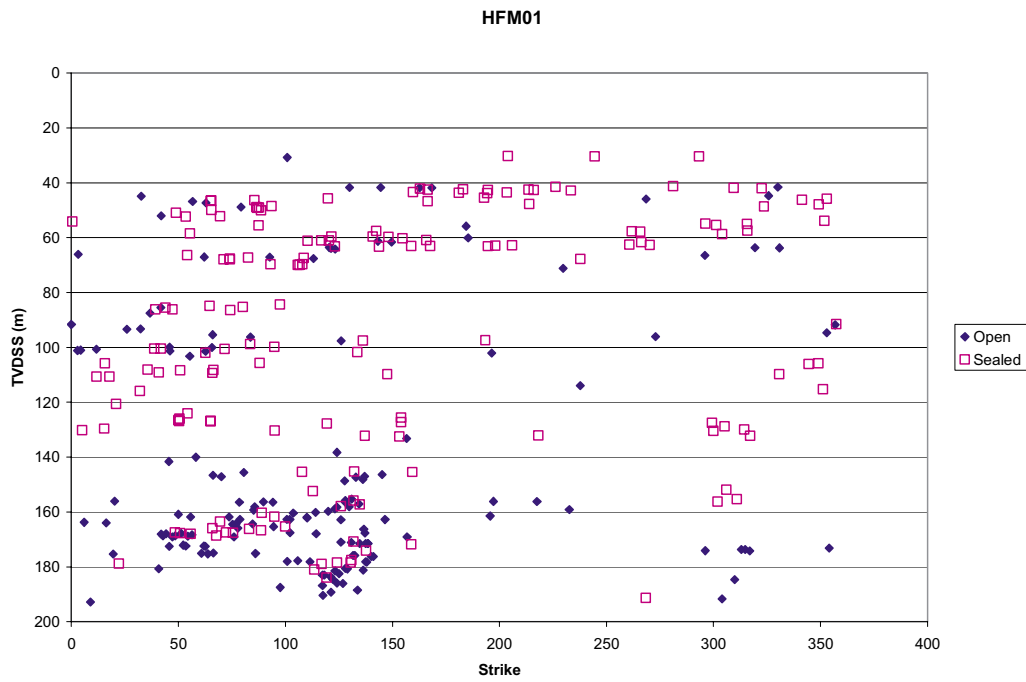


Figure 7. Variation of fracture strike with TVDSS, percussion borehole HFM01, open and sealed fractures.

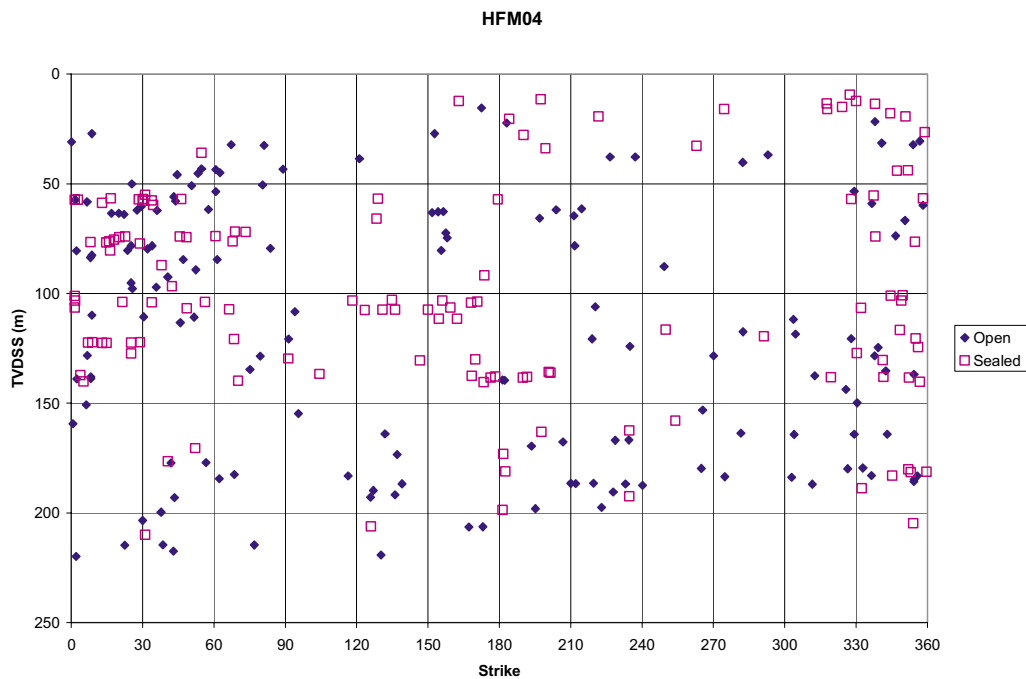


Figure 8. Variation of fracture strike with TVDSS, percussion borehole HFM04, open and sealed fractures.